Charles University in Prague
Faculty of Mathematics and Physics

DOCTORAL THESIS

Petra Adamová

Earthquake source models

Department of Geophysics
Supervisor of the doctoral thesis: RNDr. Jan Šílený, CSc.

Study programm: Physics
Specialization: Geophysics

Prague 2013

Acknowledgements

First of all, I would like to thank Jan Šílený, the supervisor of the thesis, for inspiring leadership and valuable comments that helped me solve many problems. Further, I would like to thank all my colleagues from the Department of Seismology, Institute of Geophysics, Academy of Sciences of the Czech Republic, for friendly atmosphere and help. Special thanks are due to prof. Jiří Zahradník for interesting discussions. Jan Burjánek helped me with preparing synthetic data for finete-extent fault. I would like to thank all staff from Institute of Mine Seismology for help with mining data and for providing programs for visualization mining events. Last but not at least, I am very grateful to my parents for their support and patience during my studies.

The research was financially supported by The Czech Republic Grant Agency under grant numbers 205/09/0724, P210/10/0296 and P210/10/1728, The Grant Agency of the Academy of Sciences by grant IAA300120502 and by EU project No. FP7-PEOPLE-IAPP-2009-230669.

Prohlašuji, že jsem tuto disertační práci vypracovala samostatně a výhradně s použitím citovaných pramenů, literatury a dalších odborných zdrojů.

Beru na vědomí, že se na moji práci vztahují práva a povinnosti vyplývající ze zákona č. 121/2000 Sb., autorského zákona v platném znění, zejména skutečnost, že Univerzita Karlova v Praze má právo na uzavření licenční smlouvy o užití této práce jako školního díla podle § 60 odst. 1 autorského zákona.

V Praze dne..... podpis

Název práce: Modely zemětřesného ohniska
Autor: Petra Adamová
Katedra/Ústav: Katedra geofyziky MFF UK
Vedoucí: RNDr. Jan Šílený, CSc., Geofyzikální ústav, v.v.i AV ČR
Konzultant: RNDr. Aleš Špičák, CSc., Geofyzikální ústav, v.v.i AV ČR
Abstrakt: Zemětřesné ohnisko je standardně popisováno pomocí momentového tenzoru. V mnoha případech potřebujeme více informací o seismickém zdroji a proto se zabýváme vyššími momenty. Tento přístup nám umožňuje odhadnout nebodové veličiny včetně některých dynamických parametrů (geometrie zdroje, trvání zdrojového procesu, průměrný skluz na zlomu, prostorový a časový centroid a průměrnou rychlost rozrušování) z aproximace bodovým zdrojem. Tento popis zahrnuje celkem 20 parametrů: 6 pro standardní momentový tenzor a 14 pro momenty druhého řádu. Nejdříve aplikujeme metodu na syntetická data. Mnoho velkých zemětřesení na výrazných zlomech vykazuje falešnou nesmykovou složkou, která může být způsobena aproximací konečného zdroje zdrojem bodovým. Tato hypotéza byla ověřena na případu jednostranně se šířící trhliny kde klasický momentový tenzor obsahoval více než 20 % nesmykových složek a po odečtení vyšších momentů tato složka klesla na 6 %. V další části byla metoda aplikovaná na reálná data. Vybrali jsme velké jevy (Mw>6) s výraznou nesmykovou složkou. Určili jsme pro ně vyšší momenty a potvrdili falešné nesmykové složky způsobené konečností zdroje. V poslední části jsme aplikovali metodu na důlní data a určili rovinu zlomu.
Klíčová slova: mechanismus ohniska, momenty vyššího řádu, nesmykové složky.

Title: Earthquake source models
Author: Petra Adamová
Department: Department of Geophysics
Supervisor: RNDr. Jan Šílený, CSc., Institute of Geophysics AS CR
Consultant: RNDr. Aleš Špičák, CSc., Institute of Geophysics AS CR
Abstract: The earthquake source is routinely modeled by moment tensor description. In many cases we need more information about the source process and for that reason we occupy with higher degree moments. This approach allows us to estimate non-point characteristics (including some dynamic parameters): geometry of the source, duration of the source process, average slip on the fault, spatial and temporal centroid and rupture velocity vector within the point source approach. This description includes 20 parameters – 6 parameters for standard moment tensor (MT) and 14 parameters for second degree moments (SDM). First, we studied synthetic tests. Large amount of significant earthquakes contains false non-DC component which can be caused by approximation finite source by point source. This hypothesis was proved on the case of unilateral rupture. Standard MT contains more than 20 % non-DC components which was reduced to 6 %. In the second part we applied this procedure to real data. We chose large earthquakes (Mw>6) with large non-DC component. We estimated second degree moments for them and compared them with previous studies. Moreover we restitute higher degree moments from data and proved that false non-DC component were caused by source finiteness. In the last part we applied this method to mining data and identified the fault plane.
Key words: source mechanism, higher degree moments, non-DC components

Contents

Chapter 1

Introduction

Earthquake source modelling is a broad topic with different applications. These applications range from the earthquake mechanism retrievals mostly for needs of geologists inferring tectonics and its evolution in time, through modelling of fault slip history during significant and well monitored earthquakes, to investigation of the earthquake physics. In such a way it is possible to study the dynamics of rupture process in complexities of non-elastic rheology and examine constitutive laws ruling the phenomena on the crack edges and on the fault surface.

In our study we aimed at applications of the earthquake mechanism retrievals dealing with the mechanism of a seismic event but in a generalized way. This approach allowed us to extend the concept of the mechanism from a point source quantity towards the finite extent sources. The finiteness is treated in a simplified way, of course, aiming to keep the applicability of the method to events with a limited amount of data which excludes the reconstruction of slip history. The source finiteness in our approach means the determination of several integral parameters over the focus which provide rough information on its orientation, shape, average rupture velocity etc. When these parameters have been obtained, an implicit benefit can be seen in the identification of the fault plane from the couple of the nodal planes. Decreasing the ambiguity in the fault plane solution may be a major help for geologists who use seismic investigation and represent a bridge towards tectonic interpretations.

Knowledge of a mechanism of seismic wave generation is important because it provides the first insight into source physics and the processes inside. The process of rupturing of geological material is obviously very complex. Its study is indirect, from data which are necessarily limited due to technical aspects of data collection, and needs prior simplification. It means that we cannot study the physics of the process in a straightforward way as physicists do in their labs, but we are constrained to a phenomenological description of the source.

The moment tensor is the general dipole source (Backus and Mulcahy 1976a, b). It

is the second-rank tensor, which describes a superposition of nine elementary dipoles: the diagonal components correspond to linear dipoles without torque, and the non-diagonal elements correspond to force couples. For the sake of interpretation it is usually decomposed into several "elementary mechanisms". Apart from the separation of the isotropic part (ISO), the decomposition is not unique. The most common decomposition is separating the deviatoric part into the double couple (DC) and compensated linear vector dipole (CLVD) with the same P or T axis. Usually the moment tensor (MT) is not retrieved in the full complexity, but for the sake of increasing the stability of the waveform inversion, it is assumed to be deviatoric, i.e. without the ISO part.

Non-DC components (CLVD and ISO) have been widely studied during last years. Their occurrence can have many reasons (Julian et al., 1998; Miller et al., 1998). Let's note the following: 1. Complex shear faulting: multiple shear events, volcanic ring faults or Ortlepp shear fault (Ortlepp, 1984); 2. Tensile faulting: opening tensile faults, effects of fluids, combined tensile and shear faulting, shear faulting in an anisotropic or heterogeneous medium.

The higher degree moment tensor representation was suggested by Backus (1977a, b). His formalism initiated the effort to determine finite extent source parameters described by higher degree moments from the inverse problem. Doornbos (1982) designed the source model based on second degree moments consisting of 20 parameters, which he related to Haskell (1964) and Savage (1966) finite extent fault models. Stump and Johnson (1982) related higher-degree moments with 19 parameters of plane rectangular shear source where the rupture propagates unilaterally with constant velocity and rise time. They found the convergence of the moment series to be frequency dependent with the higher frequencies being emphasized in the higher degree moment tensors. The convergence is also a function of azimuth and fault model. Das and Kostrov (1997) formulated the inverse problem of determining the temporal and spatial power moments of the seismic source moment rate density distribution. In numerical experiments, they demonstrated the necessity of the positivity constraints (in their formalism the absence of back-slip on the fault), which they enforced through a set of linear equations. They suggested to proceed from low degree moments (zero and first degree moments specifying the size and duration) retrieved from long periods to higher degree moments estimated from high frequencies. They stress the necessity to subdivide the source region to achieve a low approximation error of the Green's functions. Similarly, Dahm and Krüger (1999) pointed out that for inversion of seismic waves with periods and wavelengths in the range of the rupture duration and spatial extent of the fault, respectively, a single centroid is not sufficient for the Green's function approximation to be accurate enough. Therefore, they developed a method to estimate the extended source parameters by using higher degree moments at 27 centroid locations (3 along the time duration of the rupture and 9 centroids covering the rupture area). They developed an iterative scheme to estimate the higher degree moments related to uni-

and bi-directional finite source model of Haskell, and showed that the rupture model can be distinguished, fault and auxiliary plane resolved and the rupture direction estimated. The higher degree moments approach has particular importance if applied to studying the foci of deep earthquakes because these seismic events usually have few aftershocks, from which extension of active fault area is usually estimated (the couple of papers listed above; Gusev and Pavlov 1986, 1988). However, it has been used to study the spatial-temporal characteristics of sources of shallow earthquakes as well (e.g., Silver and Masuda 1985, Bukchin et al. 1992).

From all the approaches listed we focused on the representation by Doornbos (1982) for its clarity and straightforward relation of its parameters to quantities describing the rupturing along a simple finite-extent fault.

Higher degree moments represent an advantageous formalism for description of the temporal and geometrical characteristics of extended seismic source from the point source approximation. It means that it is not necessary to specify ad hoc a finite extent focus (e.g., the fault plane orientation and size) and solve for the rupture propagation in a tomographic inverse problem. Of course, these two approaches are not equivalent: higher degree moments provide averaged parameters only while computing rupture propagation is performed to obtain a detailed insight into the kinematics of the rupturing. However, the approach of higher degree moments is less laborious and can be applied even when only low period data are available in a particular site. Thus, it is anticipated to be a next step following the standard retrievals of the seismic moment tensor. Then, we may ask a similar question which is vital in the routine of the MT determination, namely how reliably it is reconstructed when the response of the earth structure, the Green's function, is not known accurately. Apart from the global studies where extremely long waves are used, in local and frequently also regional studies, we rarely know the medium sufficiently well to model successfully the details of the waveforms. The poor knowledge about the medium in this frequency band is rather a rule than the exception. Therefore, it is important to investigate how the resolution of the parameters of the finite extent source, described by the higher-degree moments, is limited by the unfamiliarity with the medium. In configurations of several case studies, we intend to simulate mislocation of the hypocenter and mismodeling of the structure of the earth crust/mantle and test how successfully the finite source parameters are reconstructed.

We will apply this methodology to two applications. First, we apply second degree moments to large non-DC earthquake and show that these non-DC components can be caused by neglecting source finiteness. Second application will be determination of second degree moments for mining events where we can identify the fault plane from two nodal planes.

Chapter 2

Theory

2.1 Second degree moments

If we have enough data available for the detailed modeling of the rupture history along the fault, we can use the second degree moment approach and obtain at least average values of parameters of the fault like geometry, orientation, slip velocity, etc. we can use second degree moment tensor. The standard moment tensor does not contain spatial information, and cannot be related to finite-extent source parameters like fault geometry, average velocity at the fault, etc. The information on geometry of the focus and simplified insight into the dynamics of the source process are contained in quantities called second degree moments (SDM). We follow the approach developed by Doornbos (1982). In his approach he starts from the relation of the displacement with moment tensor density

$$u_i(\mathbf{x},t) = \int_{-\infty}^{t}\int_{V} \partial\xi_k G_{ij}(\boldsymbol{\xi}, t-\tau) m_{jk}(\boldsymbol{\xi},\tau) dV d\tau \tag{2.1}$$

derived from the representation theorem. The elementary source substituted by the $m_{jk}(\xi,\tau)$ is applied at position $\boldsymbol{\xi}$ and in time τ; G_{ij} is Green's function tensor. In the following text (from the equation 2.2) we use notation $\partial\xi_k G_{ij} \equiv G_{ij,k}$. Equation (2.1) can be replaced by a point source representation by expanding $G_{ij,k}$ about a reference source point $\boldsymbol{\xi_0}$ using Taylor expansion up to degree two. The expansion of the Green's function can be written as

$$G_{ij,k}(\mathbf{x},\boldsymbol{\xi},t,\tau) = G_{ij,k}(\mathbf{x},\boldsymbol{\xi}_0,t,\tau) + G_{ij,kl}(\mathbf{x},\boldsymbol{\xi}_0,t,\tau)(\xi_l - \xi_l^0) \tag{2.2}$$

$$+\frac{1}{2} G_{ij,klm}(\mathbf{x},\boldsymbol{\xi}_0,t,\tau)(\xi_l - \xi_l^0)(\xi_m - \xi_m^0)$$

We neglect terms of degree three and higher. The displacement can be now written as

$$u_i(\mathbf{x},t) = G_{ij,k}(\boldsymbol{\xi_o},\mathbf{x},t,\tau) * M_{jk}(t) + G_{ij,kl}(\boldsymbol{\xi_0},\mathbf{x},t,\tau) * M_{jk,l}(\boldsymbol{\xi_0},t) + \\ + G_{ij,klm}(\boldsymbol{\xi_0},\mathbf{x},t,\tau) * M_{jk,lm}(\boldsymbol{\xi_0},t) \tag{2.3}$$

where

$$M_{jk}(t) = \int_V m_{jk}(\boldsymbol{\xi},\tau)dV \tag{2.4}$$

$$M_{jk,l}(\boldsymbol{\xi_0},t) = \int_V (\xi_l - \xi_l^0) m_{jk}(\boldsymbol{\xi},\tau)dV \tag{2.5}$$

$$M_{jk,lm}(\boldsymbol{\xi_0},t) = \int_V (\xi_l - \xi_l^0)(\xi_m - \xi_m^0) m_{jk}(\boldsymbol{\xi},\tau)dV \tag{2.6}$$

We expand the convolution into series of time moments of degree less than three (Doornbos, 1981)

$$u(t) = G(t) * \dot{F}(t) = G(t-\tau_0)F^{(0)} - \dot{G}(t-\tau_0)F^{(1)}(\tau_0) + \frac{1}{2}\ddot{G}(t-\tau_0)F^{(2)}(\tau_0) + \dots \tag{2.7}$$

where $F^{(n)}(\tau_0)$ is n-th moment of the function F aroundτ_0

$$F^{(n)}(\tau_0) = \int_{-\infty}^{\infty} (t-\tau_0)^n \dot{F}(\tau)d\tau \tag{2.8}$$

Then, we obtain formula for displacement in this form:

$$
\begin{aligned}
u_i(\mathbf{x},t) = {} & G_{ij,k}(\boldsymbol{\xi_0},\mathbf{x},t-\tau_0)\int_{-\infty}^{\infty}\dot{M}_{jk}(\tau)d\tau - \\
& -\dot{G}_{ij,k}(\boldsymbol{\xi_0},\mathbf{x},t-\tau_0)\int_{-\infty}^{\infty}(\tau-\tau_0)\dot{M}_{jk}(\tau)d\tau + \\
& +\frac{1}{2}\ddot{G}_{ij,k}(\boldsymbol{\xi_0},\mathbf{x},t-\tau_0)\int_{-\infty}^{\infty}(\tau-\tau_0)^2\dot{M}_{jk}(\tau)d\tau + \\
& +G_{ij,kl}(\boldsymbol{\xi_0},\mathbf{x},t-\tau_0)M_{jk,l}(\boldsymbol{\xi_0}) - \\
& -\dot{G}_{ij,kl}(\boldsymbol{\xi_0},\mathbf{x},t-\tau_0)\int_{-\infty}^{\infty}\int_V(\tau-\tau_0)(\xi_l-\xi_l^0)\dot{m}_{jk}(\boldsymbol{\xi},\tau)dVd\tau + \\
& +\frac{1}{2}G_{ij,klm}(\boldsymbol{\xi_0},\mathbf{x},t-\tau_0)M_{jk,lm}(\boldsymbol{\xi_0}) \\
& +\frac{1}{2}\ddot{G}_{ij,kl}(\boldsymbol{\xi_0},\mathbf{x},t-\tau_0)\int_{-\infty}^{\infty}\int_V(\tau-\tau_0)^2(\xi_l-\xi_l^0)\dot{m}_{jk}(\boldsymbol{\xi},\tau)dVd\tau \\
& -\frac{1}{2}\dot{G}_{ij,klm}(\boldsymbol{\xi_0},\mathbf{x},t-\tau_0)\int_{-\infty}^{\infty}\int_V(\tau-\tau_0)(\xi_l-\xi_l^0)\dot{m}_{jk,m}(\boldsymbol{\xi},\tau)dVd\tau \\
& +\frac{1}{4}\ddot{G}_{ij,klm}(\boldsymbol{\xi_0},\mathbf{x},t-\tau_0)\int_{-\infty}^{\infty}\int_V(\tau-\tau_0)^2(\xi_l-\xi_l^0)\dot{m}_{jk,m}(\boldsymbol{\xi},\tau)dVd\tau
\end{aligned}
\tag{2.9}
$$

When we use terms up to degree 2 only, we obtain the following formula:

$$
\begin{aligned}
u_i(\mathbf{x},t) = {} & G_{ij,k}(\boldsymbol{\xi_0},\mathbf{x},t-\tau_0)\int_{-\infty}^{\infty}\dot{M}_{jk}(\tau)d\tau - \\
& -\dot{G}_{ij,k}(\boldsymbol{\xi_0},\mathbf{x},t-\tau_0)\int_{-\infty}^{\infty}(\tau-\tau_0)\dot{M}_{jk}(\tau)d\tau + \\
& +\frac{1}{2}\ddot{G}_{ij,k}(\boldsymbol{\xi_0},\mathbf{x},t-\tau_0)\int_{-\infty}^{\infty}(\tau-\tau_0)^2\dot{M}_{jk}(\tau)d\tau + \\
& +G_{ij,kl}(\boldsymbol{\xi_0},\mathbf{x},t-\tau_0)M_{jk,l}(\boldsymbol{\xi_0}) - \\
& -\dot{G}_{ij,kl}(\boldsymbol{\xi_0},\mathbf{x},t-\tau_0)\int_{-\infty}^{\infty}\int_V(\tau-\tau_0)(\xi_l-\xi_l^0)\dot{m}_{jk}(\boldsymbol{\xi},\tau)dVd\tau + \\
& +\frac{1}{2}G_{ij,klm}(\boldsymbol{\xi_0},\mathbf{x},t-\tau_0)M_{jk,lm}(\boldsymbol{\xi_0})
\end{aligned}
\tag{2.10}
$$

For brevity we use term 'second degree moments' for all moments of degree 1 and 2, some authors use different terminology: 'first degree moments' for parameters with first GF derivative and 'second degree moments' for parameters with second GF derivative. Here, we introduce the second degree moments (SDM)

$$M_{jk}^{(n)}(\tau_0) = \int_{-\infty}^{\infty} (\tau - \tau_0)^n \dot{M}_{jk}(\tau) d\tau$$

$$M_{jk,l}^{(1)}(\boldsymbol{\xi_0}, \tau_0) = \int_{-\infty}^{\infty} \int_V (\tau - \tau_0)(\xi_l - \xi_l^0) \dot{m}_{jk}(\boldsymbol{\xi}, \tau) dV d\tau$$

Then, the formula for the displacement can be written as

$$u_i(\mathbf{x}, t) = G_{ij,k} M_{jk} - \dot{G}_{ij,k} M_{jk}^{(1)}(\tau_0) + G_{ij,kl} M_{jk,l}(\boldsymbol{\xi_0}) + \frac{1}{2} \ddot{G}_{ij,k} M_{jk}^{(2)}(\tau_0) - \tag{2.11}$$

$$- \dot{G}_{ij,kl} M_{jk,l}^{(1)}(\boldsymbol{\xi_0}, \tau_0) + \frac{1}{2} G_{ij,klm} M_{jk,lm}(\boldsymbol{\xi_0})$$

This formula describes multipole expansion up to degree two of the displacement expression for point source. In general case this formulation contains 90 parameters. To reduce number of parameters we make assumption that all the components of the moment tensor have the same spatial and temporal history. In that case we simplify relations for second degree moments and reduce number of parameters to 20. For instance, for the SDM which corresponds to temporal centroid we can write

$$M_{jk}^{(1)}(\tau_0) = M_{jk} \Delta\tau$$

And analogicaly for the other SDM:

$$M_{jk}^{(2)}(\tau_0) = M_{jk} \Delta(\tau^2)$$

$$M_{jk,l}^{(1)}(\boldsymbol{\xi_0}, \tau_0) = M_{jk} \Delta(\tau \xi_l)$$

$$M_{jk,l}(\boldsymbol{\xi_0}, \tau_0) = M_{jk} \Delta\xi_l$$

$$M_{jk,lm}(\boldsymbol{\xi_0}, \tau_0) = M_{jk} \Delta(\xi_l \xi_m)$$

where

$$\Delta\tau = \int_{-\infty}^{\infty} (\tau - \tau_0)\, f_1(\tau) d\tau$$

$$\Delta\xi_l = \int_V \left(\xi_l - \xi_l^0\right) f_2\left(\boldsymbol{\xi}\right) dV$$

$$\Delta(\tau\xi_l) = \int_{-\infty}^{\infty} \int_V (\tau - \tau_0)(\xi_l - \xi_l^0) f_3(\boldsymbol{\xi}, \tau) dV d\tau$$

$$\Delta(\tau^2) = \int_{-\infty}^{\infty} (\tau - \tau_0)\, f_1(\tau) d\tau$$

$$\Delta(\xi_l \xi_m) = \int_V \left(\xi_l - \xi_l^0\right) \left(\xi_m - \xi_m^0\right) f_2\left(\boldsymbol{\xi}\right) dV \tag{2.12}$$

are SDM. Functions f_i are normalized functions which are defined by the following relations:

$$f_1(\tau) = \frac{\dot{M}_{jk}(\tau)}{M_{jk}}$$

$$f_2(\boldsymbol{\xi}) = \frac{m_{jk}(\boldsymbol{\xi})}{M_{jk}}$$

$$f_3(\boldsymbol{\xi}, \tau) = \frac{\dot{m_{jk}}(\boldsymbol{\xi}, \tau)}{M_{jk}}.$$

Then, the representation in equation (2.11) results in

$$u_i(\mathbf{x}, t) = M_{jk}[G_{ij,k} - \dot{G}_{ij,k}\Delta\tau + G_{ij,kl}\Delta\xi_l + \frac{1}{2}\ddot{G}_{ij,k}\Delta\left(\tau^2\right) - \tag{2.13}$$

$$-\dot{G}_{ij,kl}\Delta\left(\tau\xi_l\right) + \frac{1}{2}G_{ij,klm}\Delta\left(\xi_l\xi_m\right) + \ldots]$$

where x and ξ are respectively the point of observation and point on the fault, $u_i(x,t)$ is the ground displacement, M_{jk} is the zero degree moment (6 parameters) - standard moment tensor describing the mechanism of a "point source", the others are 2nd degree moments: temporal centroid $\Delta\tau$, spatial centroid $\Delta\xi_l$, spatial-temporal moment $\Delta\left(\tau\xi_l\right)$, second temporal moment $\Delta\left(\tau^2\right)$, and second spatial moment $\Delta\left(\xi_l\xi_m\right)$. Second degree moments can be interpreted in terms of the parameters related to the finite extent of the focus: (a) temporal centroid (1 parameter) specifying the origin time of the finite-extent source estimate; (b) spatial centroid (3 parameters) – specifies the position of a point source substituting the finite-extent focus; (c) spatial-temporal moment (3 parameters): after division by second degree temporal moment it estimates the rupture propagation, i.e. both its direction and speed; (d) second temporal moment (1 parameter) – squared estimate of the source process duration; (e) second spatial moment (6 parameters) – geometrical characteristics of the source: it specifies an ellipsoid (hereinafter the source ellipsoid), the orientation of its major axis indicates the direction of the extension of the focus.

Relation between second degree moments and physical parameters

Second degree moments are related to particular physical parameters of the focus. The type of faulting should be known apriori before interpretation of second degree moments as physical parameters. The most common assumption is dislocation source occuring across a planar surface. For instance, for unilateral propagation, Haskell source model, we can write:

$$\frac{\Delta(\tau\xi_l)}{\Delta(\tau^2)} = \mathbf{v}$$

$$2\sqrt{(\Delta\tau^2)} = T$$

2.1.1 Inversion scheme

The seismic displacement expressed in terms of moments up to the degree two (see eq. 2.13) depends on parameters of the source in a nonlinear way, which introduce diffuculties for the inversion. We use advantageously a separation of the standard moment tensor (MT) and the moments up to degree 2. It is possible thanks to the suitable structure of the formula 2.11, which contains two terms: the standard MT (M_{ij}) and linear form corresponding to SDM. The structure of the formula (2.13) offers an advantageous separation of the MT and the SDM. To invert for both the MT and SDM, we can solve two linear problems, which may be combined in an iterative loop. The first one, the determination of the six parameters of the standard moment tensor M_{ij}, follows the standard MT retrieval, similar e.g., to the MT determination from low frequency data which is routinely performed by seismological agencies. The second one concerns the SDM only and can be designed specificaly to optimize its retieval in terms of applying a necessary constraint. The splitting of (2.13) has several advantages. First, we benefit from removing the non-linearity. Second, we benefit from the separation of the standard MT and SDM in the course of their determination. Another advantage of the separation into two terms is that for the inversion of each term, we can use different frequency range. In the first step concerning the retrieval of the standard MT, we can work in low frequencies in order to recover the MT as a point source characteristics. For the second step (SDM retrieval) we work in a range beyond the low frequency plateau to be able to see the effects of the source finiteness. An additional advantage of separation the inversion into two steps isthe scaling: moment tensor components (first six parameters corresponding to MT solution) are of the order, e.g., of 10e17), while the other 14 parameters corresponding to the SDM part reach the order of about 10e4. The first step, determination of the standard MT from low-pass filtered records, we solve in a standard way by singular value decomposition. The second step concerns as many as 14 SDM parameters.

In principle, it could be solved directly similarly to the first step with the MT. It however appeared necessary to limit the space of the SDM parameters in order to avoid non-physical solutions. We introduce the constraint to keep the four-dimensional 'source volume' non-negative. It is an inherent property of earthquakes, and the constraint in this form was designed by McGuire (2001, 2002). The four dimensional volume is defined by temporo-spatial characteristic of the source. For implementing this condition, we use 10 parameters from our 14 SDM parameters: 6 parameters for source ellipsoid (spatial coordinates), 1 parameter describing duration of the source process and finally 3 parameters containing combination of spatial and temporal quantities. To introduce the condition, we consider

the following matrix as positive semidefinite (for more details refer to McGuire et al. (2001, 2002)).

$$\begin{pmatrix} \Delta(\xi_1\xi_1) & \Delta(\xi_1\xi_2) & \Delta(\xi_1\xi_3) & \Delta(\tau\xi_1) \\ \Delta(\xi_1\xi_2) & \Delta(\xi_2\xi_2) & \Delta(\xi_2\xi_3) & \Delta(\tau\xi_2) \\ \Delta(\xi_1\xi_3) & \Delta(\xi_2\xi_3) & \Delta(\xi_3\xi_3) & \Delta(\tau\xi_3) \\ \Delta(\tau\xi_1) & \Delta(\tau\xi_2) & \Delta(\tau\xi_3) & \Delta\tau^2 \end{pmatrix}$$

We determine the 14 SDM parametersfrom the constrained inversion by using the genetic algoritm (Goldberg 1989)SDM describe integral characteristics of the finite source (size, orientation, etc.) which we can be obviously seen only beyond the low-frequency plateau in regional broadband data. We however need to employ also low-pass filtering because seismograms at high frequencies are too complex for the inversion. It is obvious that for a successful retrieval of the SDM in the second step of the procedure, we need a reliable estimate of the MT in the first step. If we have a centroid position from some previous study, we use that position in the retrieving of SDM (i.e., we choose $\boldsymbol{\xi_0}$ in that centroid position). In case we haven't centroid position, we usually use hypocenter as $\boldsymbol{\xi_0}$ (We can use any position, but the hypocenter position is usually good starting point in adequate distance from the centroid position). Other parameters of a crucial importance are Green's functions and their derivatives which we compute numerically (eq. 2.13) for synthetic tests and for large earthquakes where 1-D velocity models are available, and analytically for mining tremors because we use homogeneous model there. The flow-chart of the algorithm is presented in Fig. 2.1. We start with estimating of the mechanism from the low-pass filtered records in the MT approximation. This solution is the standard moment tensor for point source computed at low frequencies similar to solution routinely determined by common seismological agencies (Global CMT catalog, U.S. Geological Survey, National Research Institute for Earth Science and Disaster Prevention, Schweizerischer Erdbebendienst or Mediterranean Network). We however do not apply the adjustement of the hypocenter position/depth and, more importantly, do not constrain the MT to be deviatoric only. Then, we determine the SDM from the original data with the mechanism fixed at the value from the previous step (Fig. 2.1), and evaluate their synthetic contribution to the data.

Last step of the procedure is to subtract contribution of the SDM from the observed records that is to correct the finite-extent source data for the estimated source finiteness to reconstruct the point-source data. At the end of this loop we go back to the first step (standard point source MT), but with the data corrected for the SDM effect. In principle, the loop can be repeated several times until negligible adjustments of the mechanism are observed, but from the applications performed it seems that one loop is usually enough.

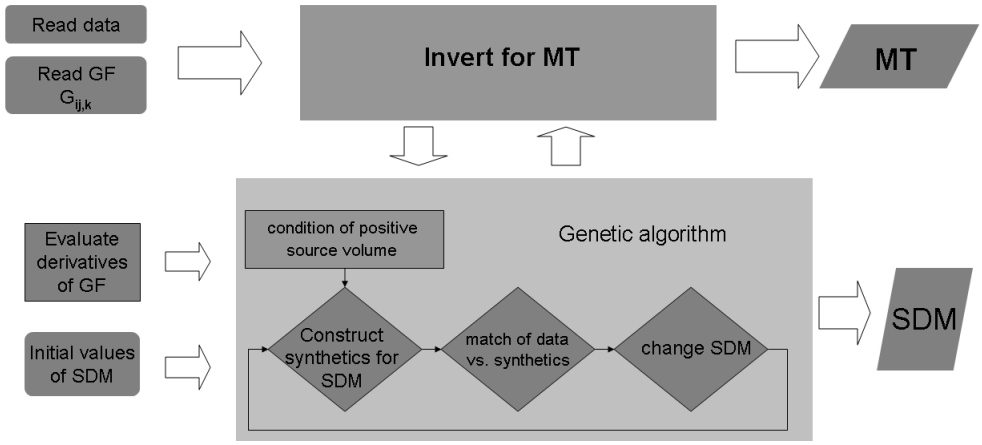

Figure 2.1: Flow chart of the retrieval of the mechanism in the MT representation together with the second degree moments (SDM). MT inversion, top; SDM inversion, bottom. Inputs into the procedure, left; outputs, right. The arrows between the MT and SDM blocks symbolize the iterative loop.

2.2 Synthetic tests

The presented method has a high computational complexity, and for that reason it is necessary to test it on synthetic data first. As a rule, a reliable retrieval of an earthquake mechanism generally requires good station coverage. Similarly to the MT retrieval, it is reasonable to test the resolution and stability of the SDM determination by using such station geometry that is similar to the real configuration of the stations that will be investigated later. Another reason for a thorough testing is the fact that the SDM retrieval hasn't been applied massively yet and, thus, experiments exploring its resolution are scarce (e.g. Doornbos, 1982; Dahm, 1999). The inversion consists of two steps at different frequency ranges. We test each step separately and finally we focus on the second step with SDM, which are even more sensitive to the noise in the data and various types of inconsistency in the inverse procedure because we take into account higher frequencies, which we have to use to observe the source finiteness. Our synthetic experiments simulate actual station configuration from the North Anatolian fault area (Fig. 2.2). These stations were installed by GFZ Potsdam after the large Izmit 1999 earthquake - the network consists from about 50 (mainly short-period) stations. We selected only some of them following two criteria. First, we wanted to have configuration with a good azimuthal coverage and, second, we would like to use stations with records of majority of the aftershocks. Despite the high seismicity and a fairly dense observation, only a relatively simple 1-D velocity model with

flat layers of constant velocities is available for the area, which was provided by Bulut et al. (2007).

Green's functions were computed using dicrete wave number (DWN) method in the independent program package AXITRA (Bouchon and Coutant, 1994). The temporal and spatial derivatives were computed numerically (see eq. 2.11) for all synthetic tests. Numerical differentiation replacing analytical derivatives requires to set a differential step. In its choice we took into account the following facts. We employ frequencies up to 0.2 Hz (for the choice of this limit see later). It means that we work with wavelength around 10 or 20 kilometers (average velocity of S-wave 2 to 4 km/s). Roughly a quarter of wavelength, i.e. about from 2.5 to 5 kilometers, constitutes the upper limit for the differential step. The lower limit is related to the precision of evaluation of seismograms by the DWN method. We evaluated derivatives for a set of trial values of the differential step ranging from 100 meters to 5 kilometers. We observed that roughly within the interval from 300 to 1000 meters, the derivative was stable so we fixed the differential step at the value of 500 meters. As a source model we used unilateral rupture propagation (velocity of rupture propagation was 2.8 km/s), see Fig. 2.3 and geometry of the main shock of Izmit earthquake (strike 90°, dip 72°, rake 180°), buried at a depth of 13 km. Rectangular fault 20 km x 10 km was assumed with the hypocenter in the center; such a size corresponds approximately to magnitude 6 after empirical formulation. For the sake of the artificial data synthesis, the fault was approximated with 120 to 120 subfaults and the contributions of each subfault were summed together with the proper time delay. The physical model of the slip along the finite-extent source implies (eq. 2.13) theoretical values of the SDM summarized in Tab. 2.2: these values were computed using spatial/temporal integration of slip function on the fault (we employed equations 2.12). In addition to the synthetic data described above, we constructed another set of records (second degree approximation data from now on) corresponding just to theoretical values of the MT and SDM parameters (i.e. our synthetic seismograms contain only terms up to degree 2).

Testing the inversion method with the second degree approximation data prior to the data corresponding to the complete slip is reasonable, as the former records are simpler, consisting of the MT and SDM terms only. In other words, here we invert for the same parameters which were used to produce the data. This is not the case in reality, where the measured data correspond to the nature, not to our models. This case will be simulated (in a limited extent, of course) by inverting the data constructed by assuming the complete slip distribution on the fault. The differences between the second degree approximation data and the data describing the complete slip on the fault are shown on Fig. 2.4. While the purpose of the experiment with inverting the second degree approximation data is to test the convergence of the inversion algorithm to the true values of the MT and SDM, i.e. the ability to reach a complete fit of the data, inversion of the slip data estimates the resolution of the average values implied by the slip on the fault, reconstruction of the

integral characteristics of the slip along whole the fault.

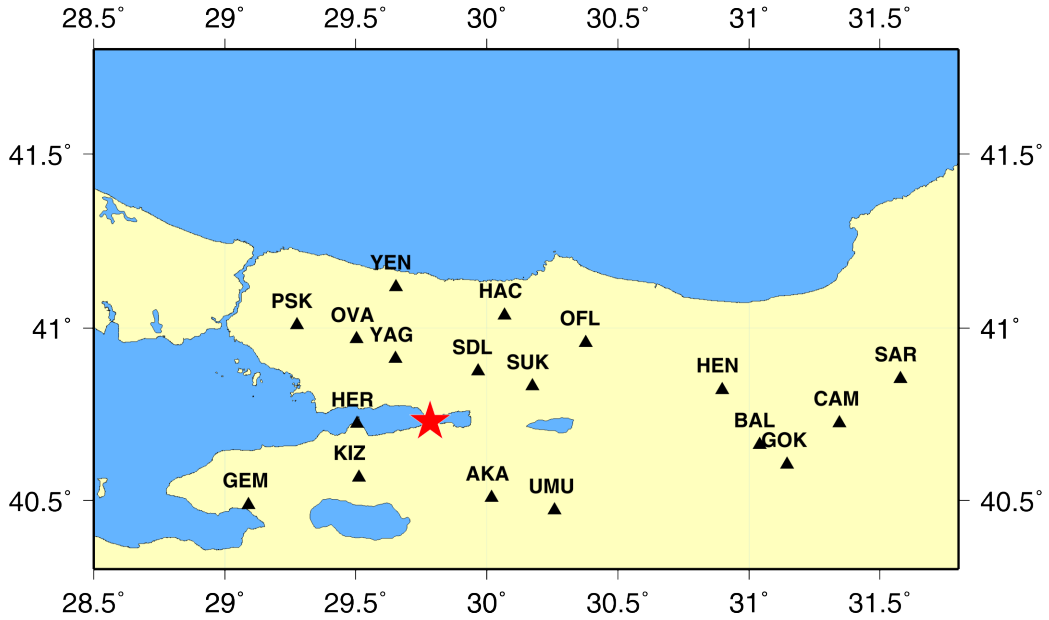

Figure 2.2: Configuration of stations in the following synthetic tests: it simulates a part of the seismic network deployed along the North Anatolian fault around the epicenter of the Izmit earthquake (August 17, 1999) by GFZ Potsdam (Ozalaybey, 2002). Red star - epicenter of the earthquake used in the synthetic test. Black triangles - stations used in the inversion.

2.2.1 Second degree approximation data

We follow the inversion scheme described above. In the first step we estimated standard MT (6 parameters). It is inherent to a point source solution, therefore, taking into account the corner frequency of the records is around 0.1 Hz, we filtered the data within 0.02–0.08 Hz by a Butterworth second order low-pass filter. Fault plane orientation was retrieved in good agreement with initial source model but we obtained a false non-DC component - around 20 %, see Table 2.1, we call this mechanism $\mathbf{M^0}$. The retrieved non-DC component can be caused by approximation of the finite source by point source (for more details see Adamová and Šílený, 2010). The Green's functions and their derivatives were computed in the hypocenter position (i.e. $\boldsymbol{\xi_0}$ coincides with the hypocenter). Using this standard MT solution as an input for second part of inversion, we estimated the 14 SDM parameters in the frequency range 0.02–0.2 Hz. The filter window was tuned to contain frequencies above the corner frequency just to be able to reconstruct the finite-source characteristics described by the SDM parameters, and stay at low frequencies at the same time, in order

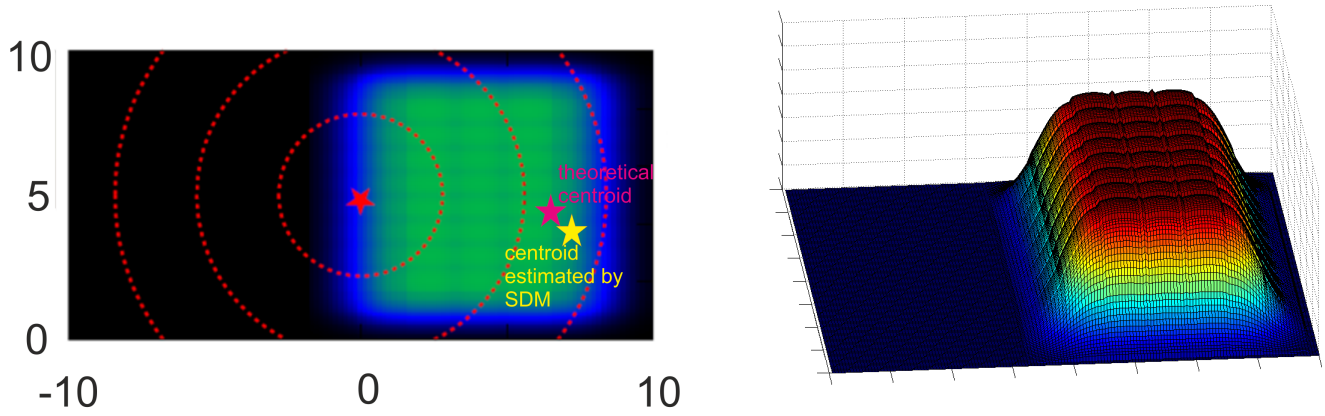

Figure 2.3: Source model for the synthetic test. Moment density distribution along a rectangular 20 km × 10 km steeply dipping fault striking east: initiation point of the unilaterally propagating rupture - red asterisk; dashed circles, isochrones corresponding to 1, 2, and 3 sec. Theoretical and estimated centroid position is plotted by pink and yellow stars, respectively.

to keep the waveform simple (for details about choosing frequency range see Adamová and Šílený, 2010). We obtained a very good agreement with the synthetic data (see Table 2.2). Variance reduction between the synthetic data and synthetics was 95 %. After subtraction of the SDM contribution from the original data we acquire new MT estimate which is better than $\mathbf{M^0}$ (see Table 2.1). We mark this MT $\mathbf{M^1}$ and use it as an input for the next iteration. The Green's function and their derivatives are evaluated in the centroid position estimated in the previous step. After second iteration with the corrected data as the input data ($\mathbf{M^1}$as an input moment tensor and GF computed in the centroid position) we obtain a new MT ($\mathbf{M^2}$) for which the variance reduction increase to 99 %. In the second iteration we had MT ($\mathbf{M^1}$) computed in the previous iteration as the input for the SDM which is very close to the true theoretical mechanism (see Tab. 2.1). For this reason, we were able to obtain an excellent agreement between synthetic data and observed data in this case. The final moment tensor is nearly the same as that one of the true source. In this synthetic test we apply 2 iterations of the inversion method because we worked with synthetic data and we wanted to show the ability of the method to reconstruct synthetic data exactly. We showed that after 2 iterations we can completely reconstruct input data and in the first iteration we obtained a pretty good approximation of the theoretical source (variance reduction 95 %). In the next chapter we will discuss applications to real data where we are in different situations. The improvement of 4 % is comparable with uncertainty in data caused e.g. by improper Green's function or noise, so we accepted first iteration as the final solution.

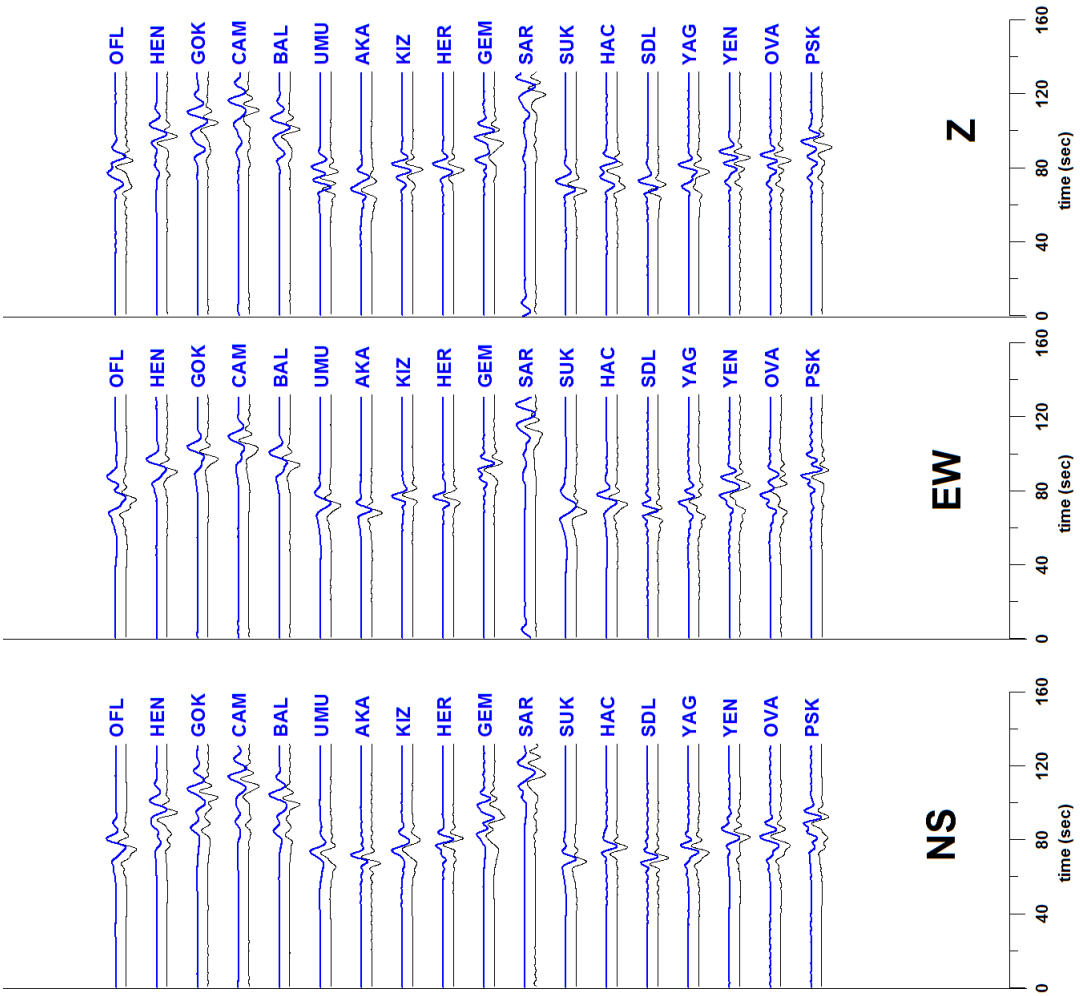

Figure 2.4: Comparison of complete slip distribution data (blue) and second degree approximation data (black) in frequency range 0.02–0.2 Hz.

	theoretical	estimated in the first step ($\mathbf{M^0}$)	estimated after removing SDM ($\mathbf{M^1}$)	estimated after 2nd removing SDM ($\mathbf{M^2}$)
strike [deg]	90	91	91	90
dip [deg]	72	77	77	73
rake [deg]	180	-178	-178	-179
DC [%]	100	78.5	96.7	98.0
CLVD [%]	0	14.0	3.3	2.0
ISO [%]	0	7.5	0	0

Table 2.1: Standard MT for second degree approximation data. First column are theoretical data, second one mechanism estimated from the original data, third and fourth column are mechanism after removing effects of SDM.

	theoretical	estimated SDM	SDM - 2nd iteration
$\Delta\tau[s]$	1.33	1.5	1.33
$\Delta\tau^2[\mathrm{s}^2]$	1.62	1.5	1.62
$\Delta\xi_1[\mathrm{km}]$	4.1	3.9	3.8
$\Delta\xi_2$	6.9	7.2	6.5
$\Delta\xi_3$	0	0.1	0
$\Delta\tau\xi_1[\mathrm{s.km}]$	0	0.2	-0.1
$\Delta\tau\xi_2$	7.4	7.5	7.4
$\Delta\tau\xi_3$	0	0	0
$\Delta(\xi_1\xi_1)[\mathrm{km}^2]$	0.003	0.1	0.047
$\Delta(\xi_1\xi_2)$	0.005	0.15	0.095
$\Delta(\xi_1\xi_3)$	0	0	0
$\Delta(\xi_2\xi_2)$	33	32.5	32.2
$\Delta(\xi_2\xi_3)$	0	0.1	0
$\Delta(\xi_3\xi_3)$	0	0.2	0

Table 2.2: Theoretical SDM computed from the second degree approximation data and as the result of the inversion. Duration of the source process ($\Delta\tau^2$) is computed for centroid position. The other SDM are for $\boldsymbol{\xi_0}$ in hypocenter.

	theoretical	estimated in the first step	estimated after removing SDM
strike [deg]	90	93	93
dip [deg]	72	73	73
rake [deg]	180	-178	-178
DC [%]	100	78	94
CLVD [%]	0	12	4
ISO [%]	0	10	2

Table 2.3: Standard MT for the complete slip distribution data. First column contains theoretical MT value, second column: MT estimated in the first step, i.e. computed from the original data, third column: MT computed from corrected data after removing SDM.

2.2.2 Slip data inversion

Slip data with DC mechanism

The previous section was about inversion of the second degree approximation data, i.e. data originated only by the MT and SDM parameters. It was rather an artificial study, as the data corresponded exactly to the source parametrization. A more realistic, though also synthetic study, is the experiment with inversion of the complete slip distribution data into the MT and SDM, i.e. using a simplified parametrization of the source. These data are computed for the model described in the previous section (see Fig. 2.3). Similarly as in previous test, the first step MT solution contains more than 20 % of non-DC components (see Tab. 2.3 and Fig. 2.5). In the second step we obtained pretty good fit of the main features of the source model (centroid position, unilateral propagation, duration of the source process). Real and estimated centroid position is shown at Fig. 2.3. We work with data corresponding to a source model with more parameters than second degree approximation data so we can expect a worse fit because the parametrization doesn't agree with the data. The complete match is not possible at all, as within the SDM we only estimate integral slip parameters over the whole fault, while the data corresponds to a spatially varying slip. Nevertheless, the variance reduction of data and synthetic seismograms obtained was as high as 0.65. Described data set is more realistic than second degree approximation data but it still does not include common inconsistencies like noise or inconsistencies in Green's functions. In the case of real data we cannot expect a better fit than in the synthetic experiment with exact data. Synthetic tests with some inconsistencies are described in the included paper **P1** (Adamová and Šílený, 2010).

	theoretical	estimated by SDM
$\Delta\tau$[s]	1.33	1
$\Delta\tau^2[s^2]$	1.62	2
$\Delta\xi_1$[km]	4.1	3.4
$\Delta\xi_2$	6.9	7.2
$\Delta\xi_3$	0	1
$\Delta\tau\xi_1$[s.km]	0	0.8
$\Delta\tau\xi_2$	7.4	9.6
$\Delta\tau\xi_3$	0	1.6
$\Delta(\xi_1\xi_1)$[km^2]	0.003	3.4
$\Delta(\xi_1\xi_2)$	0.005	0.2
$\Delta(\xi_1\xi_3)$	0	0.1
$\Delta(\xi_2\xi_2)$	33	27.9
$\Delta(\xi_2\xi_3)$	0	0.1
$\Delta(\xi_3\xi_3)$	0	2.3

Table 2.4: Theoretical SDM evaluated for the slip distribution, and SDM estimated by inverting the seismograms corresponding to the slip distribution. Duration of the source process ($\Delta\tau^2$) is computed for centroid position. The other SDM are for $\boldsymbol{\xi_0}$ in the hypocenter.

Slip data with non-DC mechanism

In the previous experiment, we studied the effect of false non-DC component caused by source finiteness. We used MT with zero non-DC component there. But there can be a real, i.e. a source-generated non-DC component in the data. With the aim to check whether we obtain a good estimate of the source-generated non-DC after the removal of the finiteness effect, we made another synthetic test with non-DC source. As the true source model we adopted shear-tensile fault, a combination of shear slip and tensile crack, see Fig. 2.6 (see Dufumier & Rivera,1997; Vavryčuk, 2001) with slope angle 5 degrees: The slope is the angle of deviation of the slip vector from the fault plane; it is 0^0 for a shear slip and 90^0 for the tensile crack. This source has approximately 20 % of non-DC component (CLVD = 10 % and isotropic component is 12 %, see Tab. 2.5). We want to test if we are able to estimate this non-DC in the source. We work in the same iteration scheme as in synthetic tests with the DC source. In the first step we determine standard MT (6 parameters) where the non-DC components were very similar to the theoretical MT (CLVD = 13 % and isotropic component is 9 %, see Tab. 2.5). It means, almost no

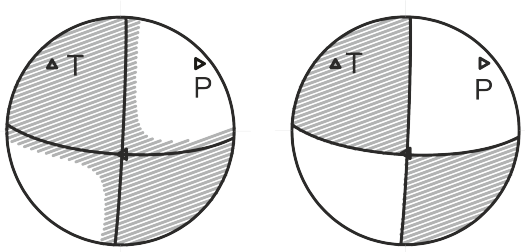

Figure 2.5: Left part: Mechanism reconstructed in the experiment inverting exact synthetic slip data filtered outside 0.02–0.08 Hz, Right part: mechanism from data corrected for the contribution of the second degree moments. In the lower- hemisphere plots of the fault plane solution (FPS), compressions are shown in gray.

spurious non-DC component was detected in this set-up. In the second step of inversion we compute the SDM (14 parameters, see Tab. 2.6). The crucial point is that after computing and subtracting the SDM from the data we obtain the proper value of non-DC component, i.e. it remains nearly the same as before computing the SDM.

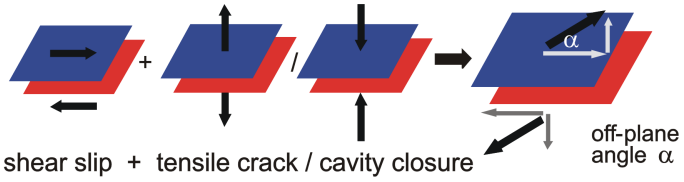

Figure 2.6: Scheme of a shear-tensile fault - composition of a shear fault and a tensile crack (opening or closure of tensile crack).

	theoretical	estimated in the first step	estimated after removing SDM
strike [deg]	87	84	85
dip [deg]	72	74	72
rake [deg]	179	167	170
DC [%]	78	78	75
CLVD [%]	10	13	15
ISO [%]	12	9	10

Table 2.5: Standard MT for non-DC synthetic test.

	theoretical	estimated by SDM
$\Delta\tau$[s]	1.33	1.
$\Delta\tau^2$[s^2]	1.62	2.
$\Delta\xi_1$[km]	4.1	4.2
$\Delta\xi_2$	6.9	7.4
$\Delta\xi_3$	0	0.5
$\Delta\tau\xi_1$[s.km]	0	0.6
$\Delta\tau\xi_2$	7.4	8.2
$\Delta\tau\xi_3$	0	1.2
$\Delta(\xi_1\xi_1)$[s.km]	0.003	2.5
$\Delta(\xi_1\xi_2)$	0.005	0.2
$\Delta(\xi_1\xi_3)$	0	0.1
$\Delta(\xi_2\xi_2)$	33	31
$\Delta(\xi_2\xi_3)$	0	0.2
$\Delta(\xi_3\xi_3)$	0	1.8

Table 2.6: Theoretical SDM computed from the complete slip distribution on the fault. Duration of the source process ($\Delta\tau^2$) is computed for the centroid position. The other SDM are for $\boldsymbol{\xi_0}$ in the hypocenter.

Chapter 3

Application to strong earthquakes

We selected five strong tectonic events with large non-DC components in the Global CMT solution: Kobe earthquake (16/01/1995 at 20:46:59.4,M_w 6.9), Izmit earthquake (17/08/1999 at 0:1:50.1,M_w 7.6), Solomon earthquake (12/06/2003 at 8:59:23.9, M_w 6.2), Tohoku aftershock (07/04/2011 at 14:32:51.4, M_w 7.1), Bolivia earthquake (17/11/2005 at 19:27:0.0, M_w 6.8). Global CMTs are retrieved from long-period waves ranging about 125 - 350 s, while our MT are determined from low-pass filtered regional records in the range 20 - 50 s. Therefore, the MT solution and its non-DC content in particular, need not be necessarily the same. Nomination of eligible candidates was not completely straightforward due to several criteria which we demanded to be fulfilled with the aim of a prospective retrieval of the SDM. First, we need events from the last roughly 15 years because earlier the station distribution was frequently sparse, excluding retrieval of "second-order" source characteristics. Second, we search among large events with magnitude above approximately 6.5 capable to be seen in regional distances, which is the range of available data. Moreover, we prefer to treat events associated clearly to a distinct geological fault, just to be able to verify resulting source parameters. And finally we concentrate on events with large non-DC components expressed in Global CMT and USGS solutions.

- Data quality of the selected earthquakes

We used data from the IRIS (http://www.iris.edu/data) and ORFEUS (http://www.orfeus-eu.org) data center. It should be noted that they can be of rather low quality and must be checked before the processing. There can be problem with polarity, confusion about components, wrong transfer functions, etc. Example of data is shown on Fig. 3.1.

In the following text, we briefly discuss results for the following earthquakes:

- Kobe 1995 earthquake

The Kobe earthquake (M_w= 6.9) occurred on 16th January 1995 in western Japan at a depth of 14 km. The mechanism is a strike slip with a small thrust component (Ide et al,

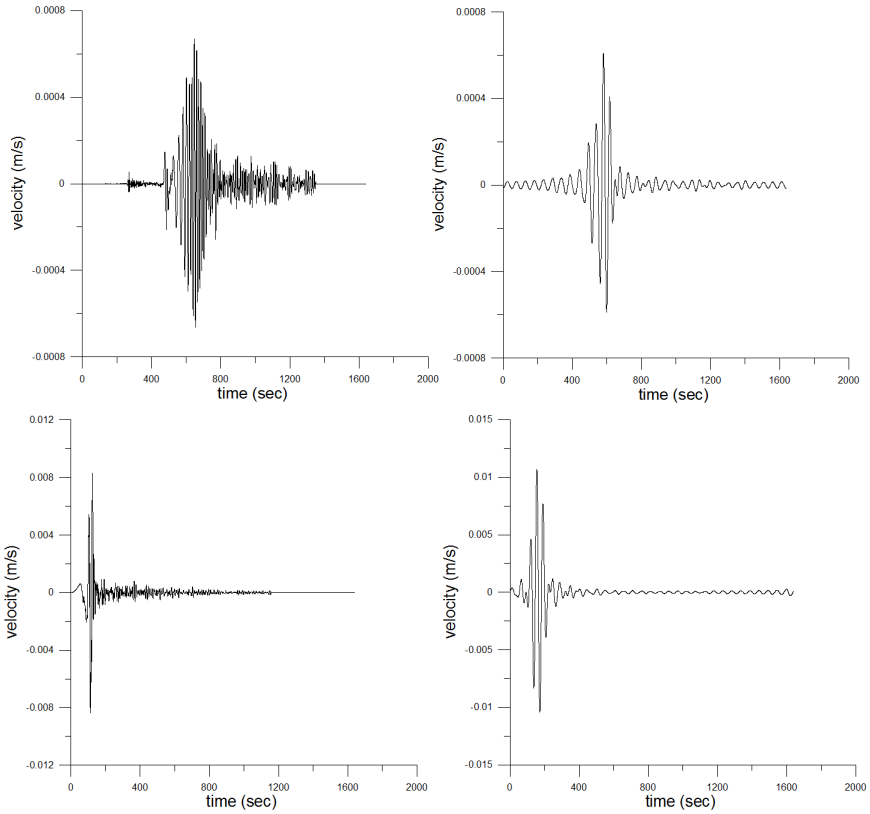

Figure 3.1: Example of two stations recording the Kobe earthquake: left column - raw unfiltered data, right column - data filtered for the MT inversion.

1996). We obtained a very good agreement between the orientation of the source ellipsoid and its shape on one hand, and the aftershock distribution by Ide et al. (1996), on the other: aftershocks are sharply concentrated along a steeply dipping plane striking NE, the source ellipsoid in map view is narrow and stretched in the nearly same azimuth. Rupture velocity vector, if drawn from the Global CMT centroid, points towards the high-slip area, the estimated velocity is 2.8 km/s, see Fig. 3.2. Second degree moments are computed in 2 iterations. We started with Green's function and their derivatives computed in the Global CMT epicenter. It can serve as a test of our solution because in this step we should obtain zero for spatial and temporal centroid.

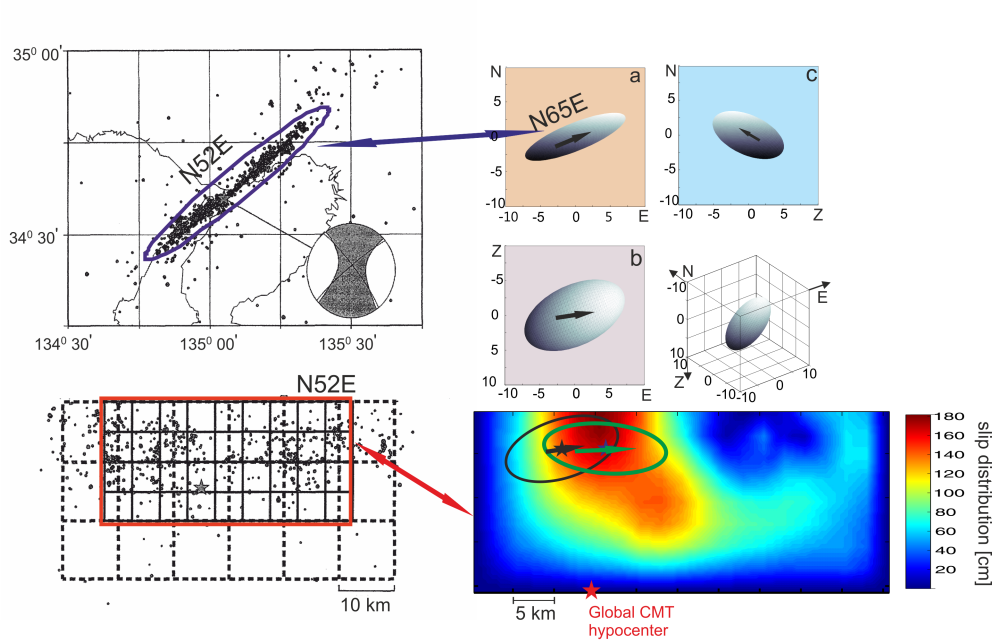

Figure 3.2: Second degree moments for the Kobe earthquake. Left: aftershock distribution by Ide et al. (1996), in the plan view framed in blue for comparison to the source ellipsoid on the right. In the depth view, it is framed in red to compare with the slip distribution in the bottom right. The azimuth of the plane is oriented N52°E. Top right: source ellipsoid in 3D view and its projections (a - map view, b – depth view looking N, c – depth view looking W), axonometric projection; coordinate center in the spatial centroid (geographical coordinates: latitude 34.760, longitude 134.970, depth 15 km), axes in kilometers. The azimuth of the ellipsoid in map view is oriented approximately N62°E. Bottom right: spatial slip distribution derived by Ide et al. (1996) (retrieved from the SRCMOD website) and its integral characteristics plotted on the assumed fault plane: the spatial centroid (green asterisk), projection of the source ellipsoid on the fault plane (green ellipse), and the rupture velocity vector (green arrow). Black symbols: centroid, source ellipsoid projection onto the fault plane, and rupture velocity vector obtained in this study. The velocity vector is multiplied by the source duration, thus in scale to the source ellipsoid.

- Izmit 1999 earthquake

A very strong earthquake (M_w= 7.6) occurred in 1999 on the Northern Anatolian fault in Turkey near the town Izmit. The centroid moment tensor (CMT) reported by agencies contains large amount of the CLVD. Slip distribution of this event was studied by several authors from high frequency data recorded near the fault. Clévédé et al. (2004) analyzed teleseismic surface waves in the periods 50-100 s and were the first who determined second

degree moments of this earthquake. In detail they compared their integral parameters with those derived from slip distributions obtained by several authors from high frequency data recorded near the fault on one hand, and from GPS, SAR and tectonic observations on the other. They showed that although these slip distributions differ a lot, some of the integral characteristics are similar and can be compared with their long-period solution. Then, by evaluating parameters of 'equivalent models', i.e. constrained simplified models of slip distribution on the assumed fault plane, they arrived with conclusions which parameters rule the integral characteristics they decided to compare. We obtained the source ellipsoid well similar in both the shape and size with their study regardless rather different frequencies involved in the data being processed in the two approaches: we inverted low-pass filtered records, while Clevede et al. (2004) evaluated the source ellipsoid from the slip distributions obtained from high frequency data. The average velocity of rupturing was estimated as 2.6 km/s.

- Error estimate for Izmit 1999 earthquake

To test the stability of the SDM retrieval on the data quality, we simulate a noise contamination. We generated random noise of a uniform distribution reaching, in turn, the level 20% and 30% of the maximum amplitude and superimposed it onto the data of Izmit earthquake, then we performed the inversion for 5 samples of noisy records in both the noise levels. In the level 30% the retrieved second degree moments are scattered a lot – standard deviations are rather high, mainly for average rupture velocity and source ellipsoid (Table 4 in P2). In the noise level 20 % we observe much more stability (Table 4 in P2) with acceptably small standard deviations. Second degree moments determined from noisy data are summarized in Table 3 (in P2)for noise levels 30% and 20%, respectively. The results suggest that the level of about 20% is an extreme noise contamination, which still need not destroy the reconstruction of the second degree moments, while 30% is possibly already beyond the limit.

- Solomon 2003 earthquake

The Solomon earthquake (M_w= 6.2) occurred on 12th June 2003 in the Pacific area near Solomon's islands at a depth of 185 km. Source ellipsoid is very slim and elongated in a single direction. This indicates a nearly linear source, where the rupture propagates either unilaterally or bilaterally. The reasonable value of the average rupture velocity derived from the retrieved SDM suggests that the former option is probable.

- Aftershock of Tohoku-oki earthquake

The aftershock of the large Tohoku-oki earthquake (11 March 2011, M_w= 9.1) occurred on 7 April 2011 at a depth of 53 km about 60 km to the west from the main shock. We compare our MT solution with Global CMT and obtained very similar solution, the

only difference is in the non-DC part. In the second step we inverted for the SDM. The parameters obtained are summarized in Table 2 and Fig. 8 in P2.

- Bolivia earthquake

A magnitude 6.8 earthquake occurred on the Bolivia and northern Chile border on 17 November 2005 at a depth of 155 km. The earthquake was centered 110 kilometers east of Calama, Chile, in the Potosi region of Bolivia. In comparison of our MT with Global CMT solution, a good similarity of the fault plane solution can be seen, but there is a small difference in non-DC part of the MT solution. As to the SDM, the results seem to be fairly realistic taken into account the scheme of the subduction process, but we cannot compare it in detail with any previous study. The parameters obtained are summarized in Table 2 and in Fig. 9. in P2.

More detailed results for all events (mainly figures for MT and SDM and comparison with the previous studies) are summarized in paper **P2**.

Chapter 4

Application to mining tremors

Finite sources in mines are rarely investigated by seismologists. Foci of mining tremors are usually treated in the point source approximation and inverted for the moment tensor solution (usually an amplitude MT inversion) which yield basic information about the seismic source. In this chapter, we apply second degree moments method, recently tested on synthetic data (Adamová and Šílený, 2010) and on large tectonic events (Adamová and Šílený, 2013), to mining induced data.

Monitoring of mining induced events underground frequently has an additional advantage compared to recording seismograms of natural earthquakes: stations are not constrained to a single level - the Earth surface, so they are situated both above and below the focus of the event. Also the azimuthal distribution is often better in mines than for events in global seismology. Additionally, identification of phases is significantly simplified, as often only the direct P and S body wave arrivals need to be considered-due to the simplicity of the velocity model.

For this purpose, we tested the method on local records from the deep-level gold mine Ridgeway in East Australia. Ridgeway Mine, situated in the Cadia Valley province in New South Wales, Australia, is a block-cave mine operated by Newcrest Mining. It is one of the largest underground operations in Australia but it will be surpassed by the nearby Cadia East (also Newcrest Mining). The ore body has the shape of an inverted teardrop and is situated 500 m below surface.

A significant advantage of the data set from Ridgeway mine is that it has been processed on a routine basis by the Institute of Mine Seismology (IMS). The Institute provides seismic service for this mine; they manually picked thousands of events and located them. Only part of these events can then be used for the source inversion: they process data with magnitude larger than zero using spectral amplitude inversion method (reference - regular monthly report of the IMS by D. Malovichko). Their results provide basic information about the source while our solution yields more detailed information of seismic source including its size and shape.

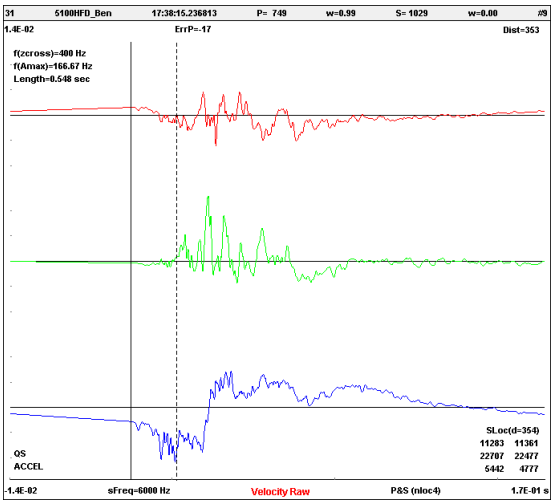

Figure 4.1: Example of poor data quality. Ground motion velocity on the z-component is corrupted by a long period disturbance. Colors represents component: north - south component (red), east-west component (green), vertical component (blue). Vertical lines are P and S wave automatic picking.

Data

The microseismic monitoring system at Ridgeway mine had (apart from later expansion of the system) 21 sensors. This consisted of 14 triaxial and 2 uniaxial accelerometers, as well as 5 triaxial geophones (with natural frequencies of 4.5 Hz, 14 Hz and 30 Hz). The sensors are mounted in boreholes, with orientations validated by observing the P-wave polarisations from large number of events. The main body of sensors is distributed in a 700m×700m×500m volume.

Data quality

There can be several problems with the mining data. The data set from Ridgeway mine was processed by IMS and they removed data with poor orientation, unknown polarity or stations with high noise level. We focused on that in more detail and removed several other stations with some instrumental problems. Such an example is plotted in Fig. 4.1. In principle we have two options what to do with corrupted data: we can remove that station or we can remove long-term disturbance (see e.g. Zahradník and Plešinger, 2005 or Adamová, 2006). In this study we simply remove those stations. Generally, the number of usable stations (see Tab. 4.1) and their coverage is sufficient for our study (see Fig. 4.3). Examples of data used in the inversion for near (epicentral distance 228 m) and distant (epicentral distance 363 m) station are plotted in Fig. 4.2.

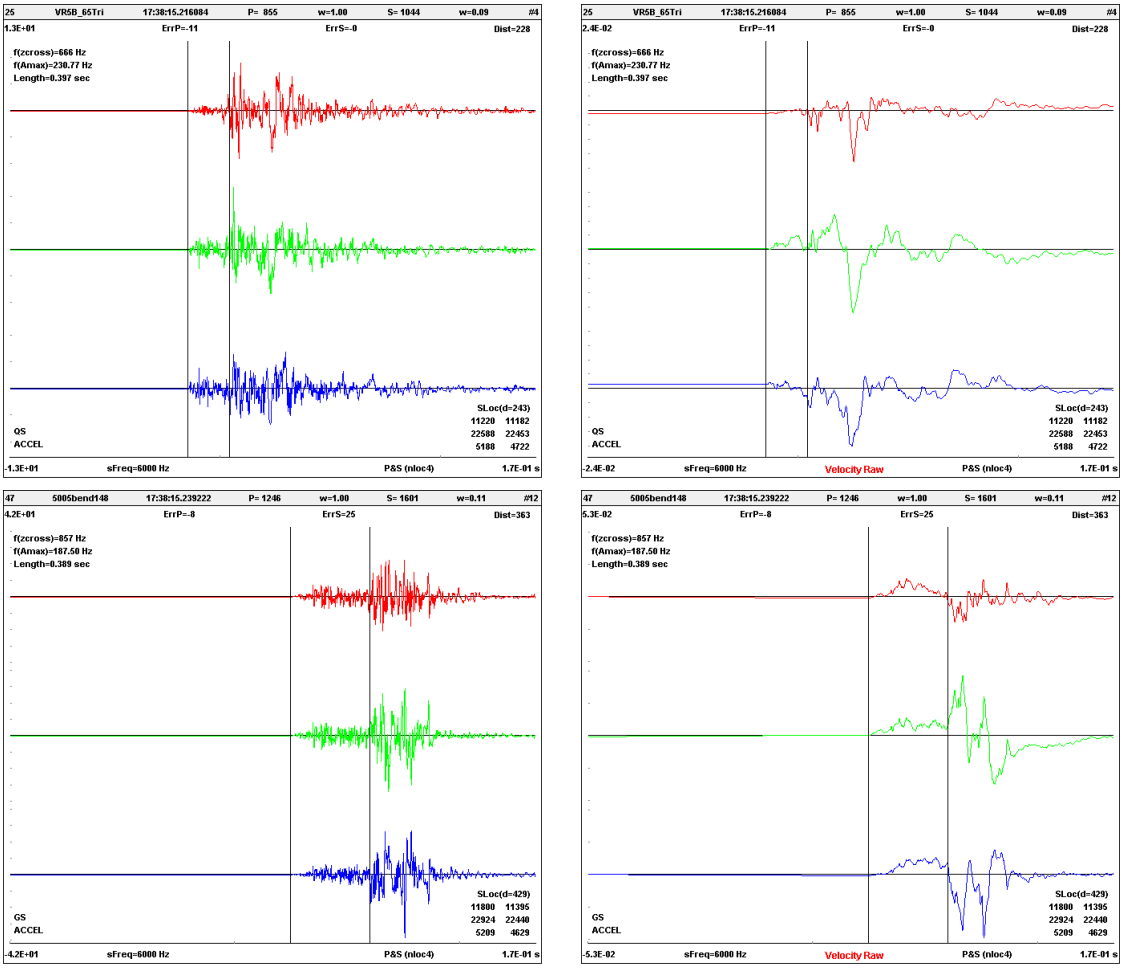

Figure 4.2: Example of waveforms for event 4. Top - near station (epicentral distance 228 m), bottom - distant station (363 m). Colors represents component: north - south component (red), east-west component (green), vertical component (blue). Time window for both station is nearly the same (0.397 s and 0.389 s). Left-hand column figures illustrate raw accelerometer records while on right-hand column are plotted ground motion velocities. Vertical lines are the P and S wave automatic picks.

event	origin time	north [m]	east [m]	up[m]	local magnitude	number of stations
1	4/12/2009 3:19:07	22462.0	11355.1	4783.9	1.3	12
2	4/12/2009 7:35:06	22693.7	11119.1	4967.4	2.1	13
3	7/12/2009 10:57:17	22636.2	11212.8	4876.6	1.4	14
4	8/12/2009 17:38:15	22478.0	11334.3	4775.1	2.1	13
5	26/12/2009 17:31:52	22647.8	11245.9	4908.7	1.4	13

Table 4.1: Location of events in local Ridgeway coordinates.

Standard MT

We start with standard MTs which we can compare with solutions obtained from routine analysis by the IMS. They employed inversion of spectral amplitudes of P and S waves from approximately 10 to 20 stations (mostly accelerographs, a few 14 Hz geophones in addition). We apply different method: full waveform inversion in the time domain. The chosen frequency range for all events is from 5 to approximately 20 or 30 Hz. The upper limit is selected slightly below corner frequency (see Table 4.2) because we need to see the source as a point. Corner frequency is derived from displacement spectra. For all events we used from 12 to 14 three-component stations. We approximate the medium by the homogeneous model with P wave velocity $v_p = 5.6$ km/s and S wave velocity $v_s = 3.2$ km/s. These stations are selected from the set of IMS stations installed at Ridgeway mine. We excluded all uni- and bi-axial sites from the source mechanism estimation. From the rest of the stations (18 sites) we chose stations with proper orientation, correct response function and sufficient data quality.

Resulting standard MTs are plotted in Figure 4.4 (middle line) and summarized in Table 4.2. For events 1-3 they are in a fairly good agreement with the IMS solutions from spectral amplitude inversion. There are some differences for events 4 and 5. We think that it can be caused by worse station coverage on the focal sphere, mainly for event 4 the azimuthal gap is nearly 180 degrees. The fit of data and synthetics for events 1 and 2 is plotted at Figure 4.5.

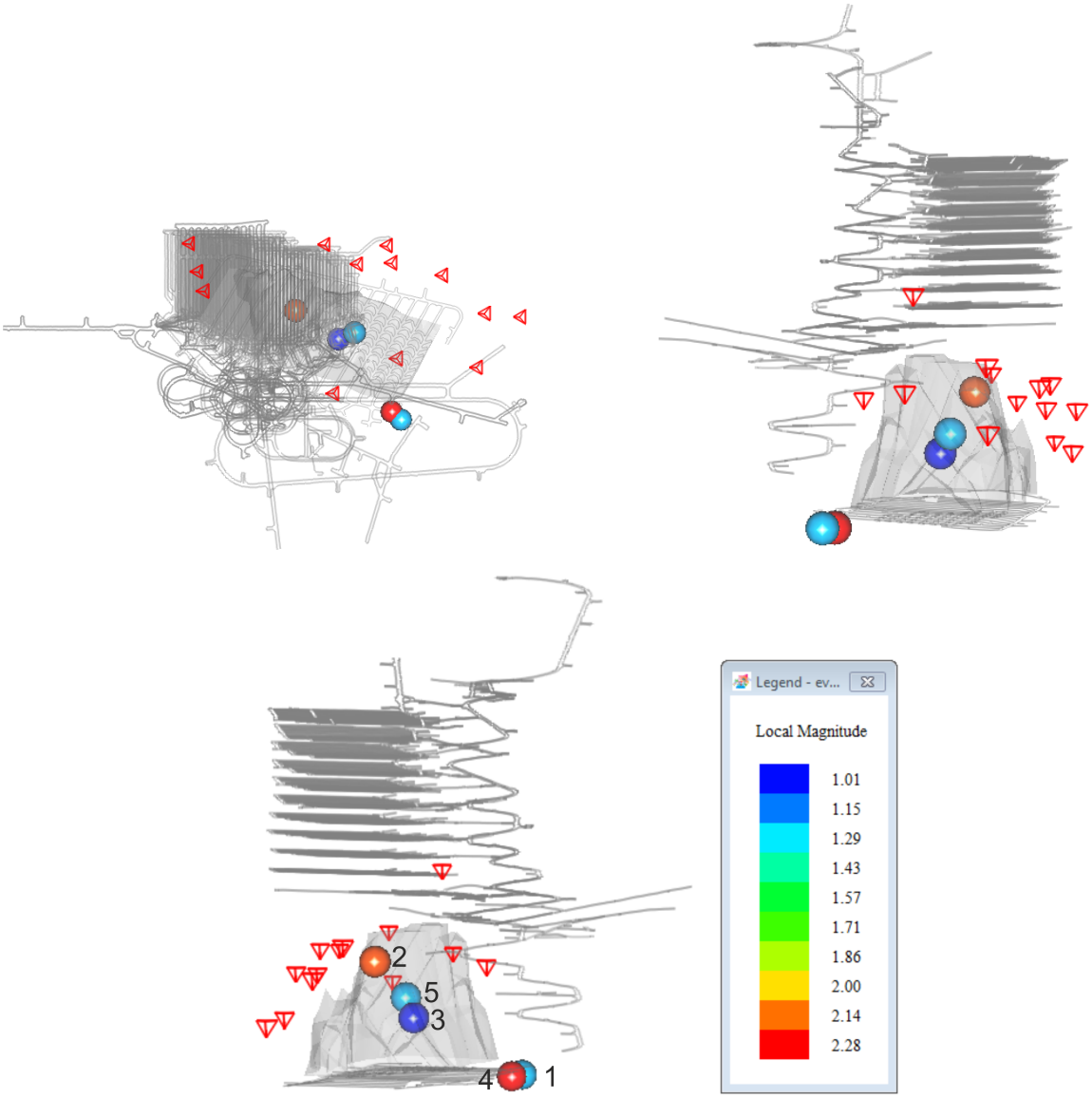

Figure 4.3: Location of the selected events (spheres colored according to magnitude), numbers correspond to Tab. 4.1. Triangles - stations providing the data. Top left - plan view, top right - section view looking east, bottom left - section view looking north. Grey lines and areas - mine tunnels and mined out areas, respectively.

event no.	corner frequency [Hz]	filtration [Hz]	strike [deg]	dip [deg]	rake [deg]	DC [%]	CLVD [%]	ISO [%]	variance reduction
1	30	5 - 30	120/316	47/44	78/102	38	25	37	40
2	21	5 - 20	136/321	44/46	87/93	51	30	19	51
3	37	5 - 30	167/284	54/58	140/43	32	68	0	41
4	17	5 - 16	178/295	22/80	151/71	68	4	28	38
5	36	5 - 28	137/329	45/46	81/98	29	29	42	37

event no.	strike [deg]	dip [deg]	rake [deg]	DC [%]	CLVD [%]	ISO [%]
1	120/316	47/44	78/102	40	23	37
2	170/287	52/55	142/45	58	28	14
3	168/282	55/60	142/41	28	69	3
4	182/295	21/80	154/69	84	0	16
5	135/328	44/45	80/96	35	27	38

Table 4.2: Parameters of data filtration, moment tensors, their decomposition and synthetics vs. data fit in the inversion for the MT (top). Moment tensors and their decomposition after removing the contribution of the SDM from the data (bottom).

Second degree moments

Benefits of evaluation of the second degree moments are twofold. Mining tremors frequently exhibit significant non-DC mechanisms, which reflects the complex mining environment (caves, tunnels, etc.) and ambient stress field. The SDM method allows for making the estimate of the non-DC contents more precise than for the large non-DC components described in the previous section. In the case of the five mining tremors investigated, the change of the non-DC components was very small, see Table 4.2. This implies that the non-DC component was not caused by source finiteness, but rather has a different origin including a real non-DC source. The other advantage provided by the SDM technique is the hint about the fault plane, which is particularly beneficial in the mining environment, where knowledge about small scale tectonics is frequently scarce. Large faults within the mine are regularly mapped by mine geologists by in situ observation.

We apply the same methodology as for large earthquakes. We choose frequencies slightly above corner frequency for estimation of SDM. A careful trade-off needs to be made here, as on the one hand the effects of a finite source need to be preserved in the seismograms, whilst simultaneously the seismograms should be simple enough to allow for successful inversion.

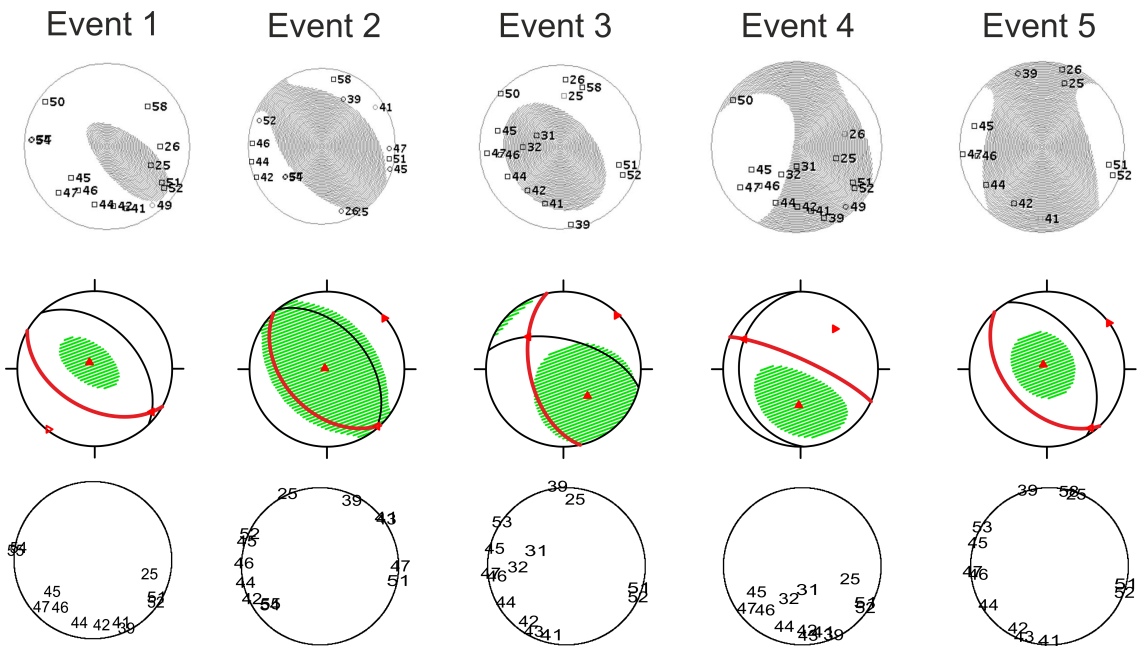

Figure 4.4: Standard MTs for the 5 mining events investigated. Top: IMS fault-plane solutions from spectral amplitudes together with projections of the stations providing the data; compressions - grey. Middle: fault-plane solutions obtained in this study. Compressions - green; T, P and N axes - triangle up, right and left, in turn. Solid lines - nodal lines. The plane determined as the fault from the SDM solution (see later) is marked in red. Bottom: projections of stations used in this study. In 3-D view, station distribution is displayed in Fig. 4.3.

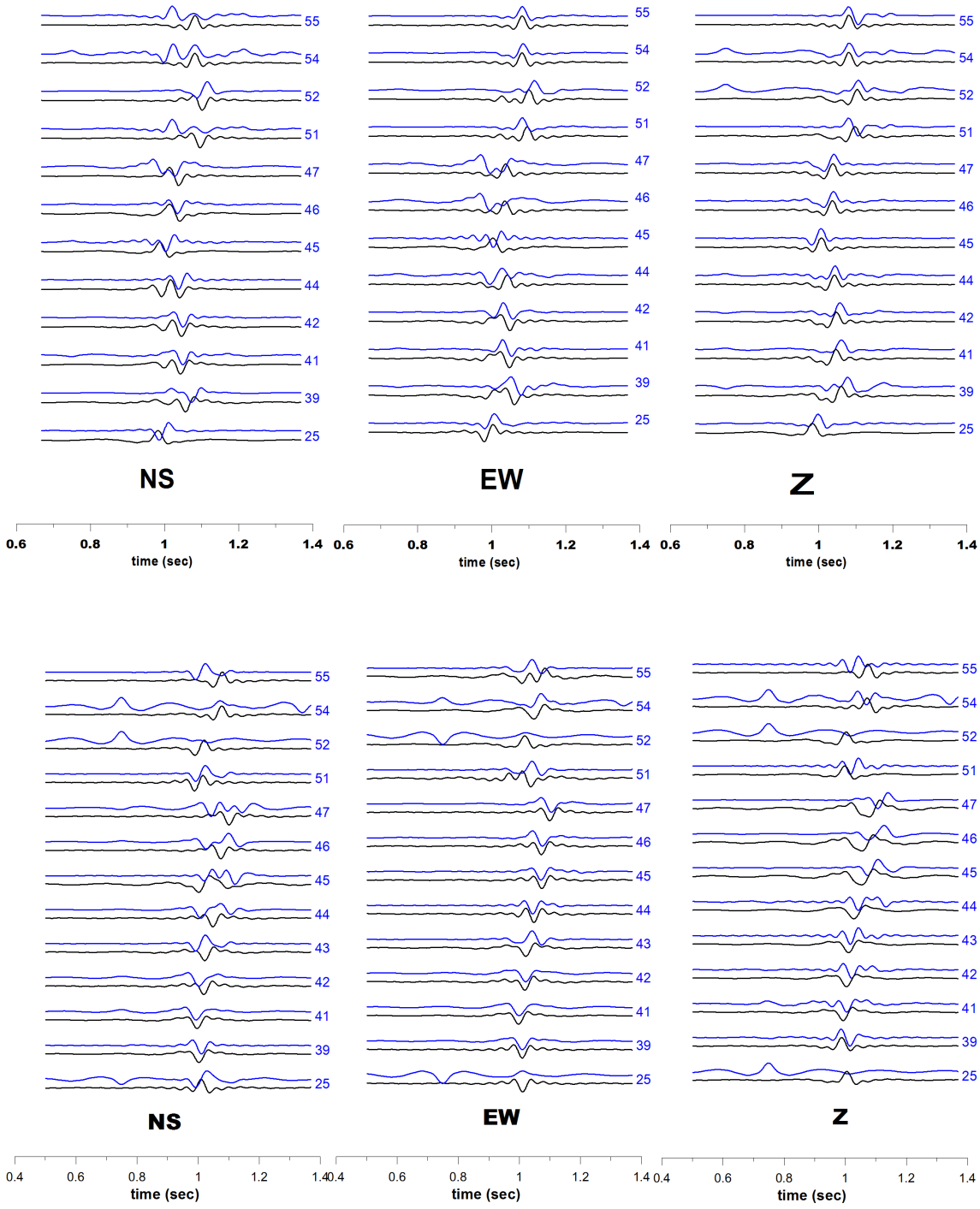

Figure 4.5: Data (blue) vs. synthetic seismograms (black) for events 1 (top) and 2 (bottom). The synthetics constructed from the MTs retrieved in the first step of the procedure. Records filtered in the range 5-30 Hz (event 1) and 5-20 Hz (event 2).

A simple indication of the finiteness of the source is the observation of directivity effects in the records, namely distinct pulse widths at different azimuths. We found that the SDM parameters involving time are much more stable than those containing spatial information - temporal parameters converge to their final value faster than the spatial ones. The less stable parameter is the source ellipsoid because it contains the second order spatial derivative. Moreover, the temporal and spatial centroid are determined more easily (i.e. parameters connected with the Green's function's first derivative) than the other second order moments - it needs much less iterations during the numerical procedure. This is not surprising, as the centroids are related to the Green's function derivatives of lower order than for the other SDM parameters. A very important description of a finite-size focus is the average velocity of rupture propagation. It can be determined as a ratio of two parameters from the SDM set (for unilateral rupture it is defined as the ratio of the term containing combination of spatial and temporal derivative and term with second temporal derivative - for details see the Theory section). For all events we obtain a rupture velocity of around 2 km/s. Detailed values for each of the 5 events are summarised in Table 4.3. This value is quite realistic: it is approximately 0.6 of shear wave velocity.

Removing ambiguity of the fault plane

The source ellipsoid is a characteristics of the focus which is of extreme importance, as it can help to eliminate the ambiguity involved in the fault-plane solution, thus to identify the correct fault plane from the couple of nodal planes that are indistinguishable from the radiation pattern in the classical DC solution. The source ellipsoid (as symmetric 3×3 matrix) is defined by the six SDM parameters. By evaluating its eigenvalues and eigenvectors we can determine the directions and lengths of its principal axes. For all the events considered, the source ellipsoids display a large eccentricity, i.e. they are stretched in a single particular direction. This is an important feature, as they can be used as a hint to discern the fault from the two nodal planes determined by the DC part of the MT solution: the fault should be identified with that plane which contains the major axis of the source ellipsoid. In this way, for Events 1, 3, 4 and 5 the fault was determined clearly (see Table 4.3), while for Event 2 the ellipsoid lies very near to intersection of fault and auxiliary plane, see the scheme in Figure 4.8. However, it seems that the plane plotted by the red curve in Figure 4.4 is the more likely fault plane for the event 2.

Comparing our fault plane solutions with the known geological faults at Ridgeway Mine, we find generally a good agreement. Our solutions (in the form of the source ellipsoids) as well as the 3D representation of the faults are shown at Figure 4.10 for comparison.

Resolution test for two events

We tested resolution of the SDM parameters by jack-knife test for events 3 and 5. In each test we removed one station from the data set and computed standard MT and then SDM

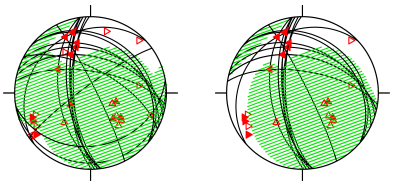

Figure 4.6: Mechanisms from the jack-knife test for event 3. Left: all jack-knife trials, right: jack- knife trials except of removal of stations 25 and 39.

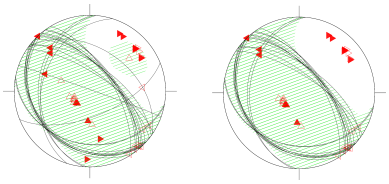

Figure 4.7: Mechanisms from the jack-knife test for event 5. Left: all jack-knife trials right: jack- knife trials except of removal of stations 41 and 42.

solution. The MT solutions are plotted in Figure 4.6.

Event 3

The left plot summarised all jack-knife trials, in the right plot there are all jack-knife trials except removal of stations 25 and 39. The solutions without these two stations are different from the others, therefore it indicates that stations 25 and 39 are particulary important during inversion. Thus, we didn't exclude them during inversions for second degree parameters. In this way, we obtained 13 MT solutions and 11 SDM solutions. The SDM parameters were very stable except for the source ellipsoid.

Event 5

For the source ellipsoid the differences were larger (maximum difference was 10 %), see Figure 4.11. The correlation with the known geological fault is still acceptable.

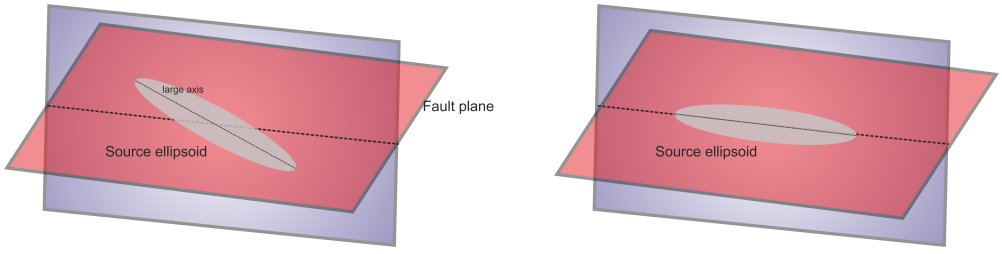

Figure 4.8: Sketch of a convenient (left) and an inconvenient (right) orientation of the source ellipsoid with respect to the nodal planes of the fault-plane solution derived from the MT: In the latter case, the major axis is oriented close to the intersection of nodal planes and the fault plane cannot be distinguished.

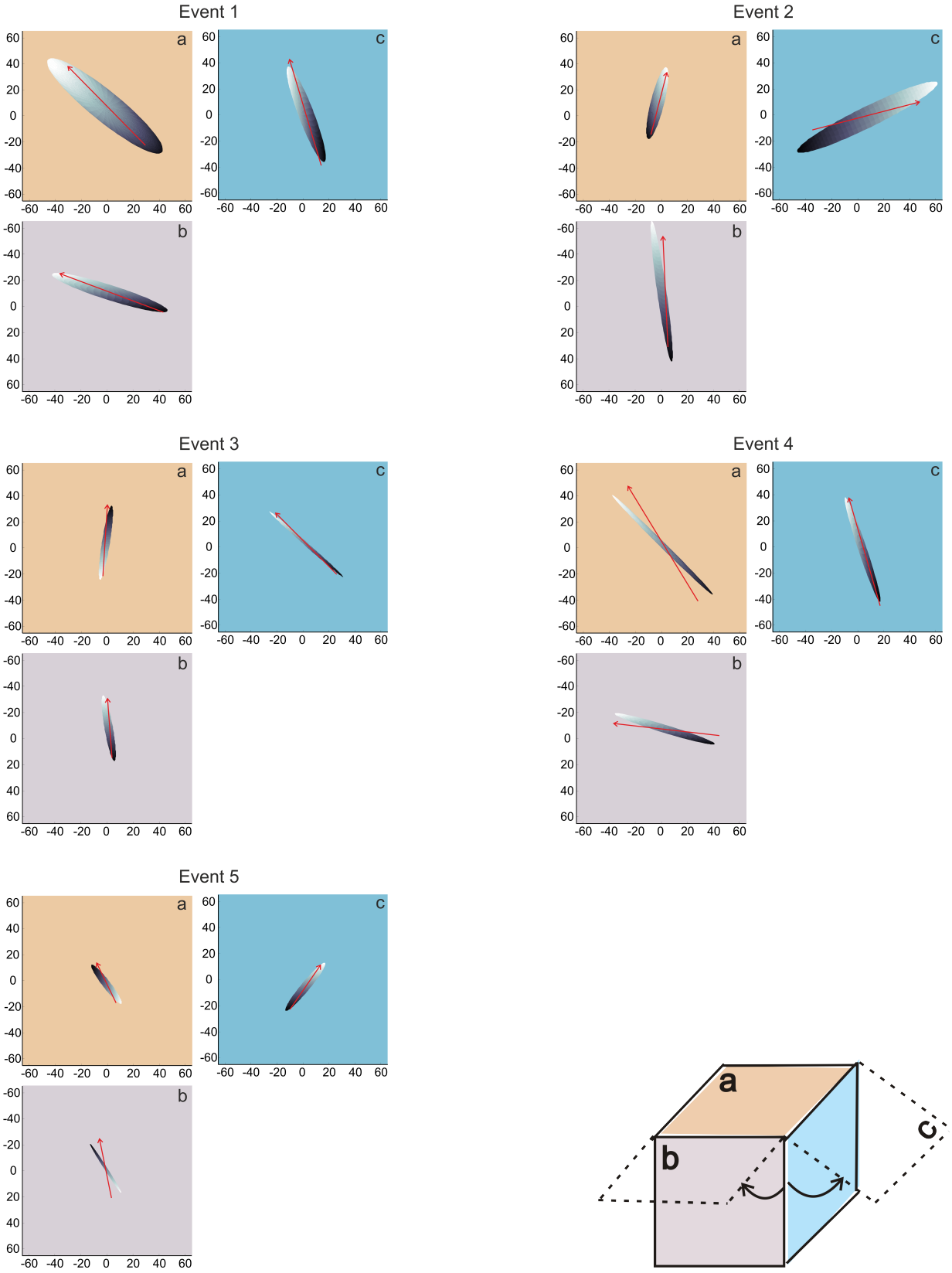

Figure 4.9: Source ellipsoid and rupture velocity vector (red arrow) for all the Ridgeway events investigated. For each event the three sections are plotted: plan view (top left), depth section view looking west (top right), depth section view looking north (bottom left). Bottom right: schematic sketch of the three projections.

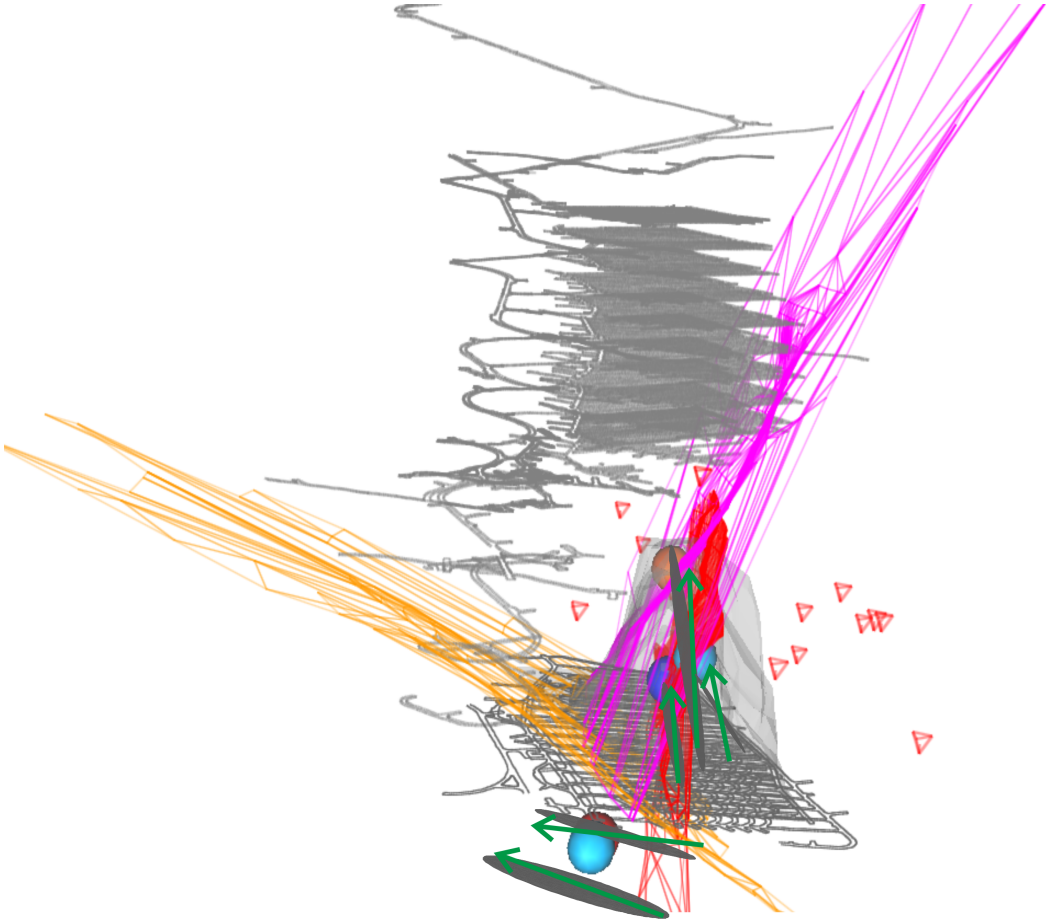

Figure 4.10: Location of all events with source ellipsoids in view looking east. Geological faults in Ridgeway mine are plotted in the same figure: orange, red and purple planes. Source ellipsoids are slightly shifted from their right positions to see them clearly.

event	variance reduction	rupture velocity [km/s]			spatial centroid [m]			temp. centroid [s]	source duration [s]
		NS	EW	Z	NS	EW	Z		
1	0.44	0.7	1.9	0.1	5	7	10	0.01	0.1
2	0.61	1.9	0.1	0.5	2	4	0	0.025	0.15
3	0.45	0.1	-0.1	2.1	1	1	-10	0.01	0.18
4	0.42	0.8	2.1	0.2	4	6	7	0.03	0.21
5	0.42	0.5	0.1	2.0	2	3	-8	0.01	0.15

event	source ellipsoid						
	λ_1	λ_2	λ_3	$\Delta_1[^0]$	$\Delta_2[^0]$	$\Delta_3[^0]$	$\alpha[^0]$
1	10.2	50.4	4.52	50	10	10	15
2	8.4	2.8	60.3	15	26	8	3
3	1.1	3.2	38.1	8	48	10	10
4	2.4	65.2	3.5	45	7	12	23
5	4.2	1.2	30.7	5	35	32	18

Table 4.3: Second degree moments for the 5 mining tremors investigated. For the source ellipsoid, the lengths λ_j of the axes are presented, which illustrate the amount of the eccentricity. To display the orientation, the angles, the angles Δ_j indicate the deviation of the major axis of the ellipsoid, in turn, from the east–west, north-south and up-down directions. The angle α indicates deviation of major axis of the ellipsoid from the line of intersection of the two nodal planes of the DC part of the MT solution.

Assessment of the mine application

Up to now, SDM were used exlusively for crustal earthquakes, we show here that this can also yield useful information about finie extent sources in mines.

Similarly to the standard moment tensor retrieval and even in a higher frequency, the importance of having a good azimuthal distribution of good quality recordings is obvious. The reason is that the directivity of the source, which is one of the manifestations of source finiteness, can only be detected by careful comparison of recordings at different azimuths. In the domain of induced seismicity (as for events recorded in mines) we generally benefit from good station coverage as sensors can be available around the source, and not only limited to the Earth's surface.

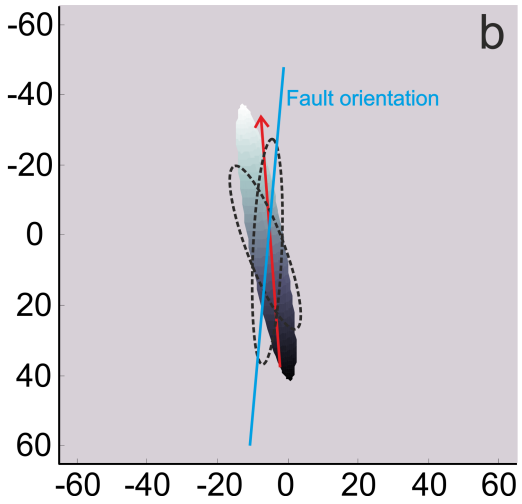

Figure 4.11: Jack-knife test for the Event 3. Side view looking to the north. Blue line: Fault plane from the geological model. Gray ellipsoid: ellipsoid computed using all stations. Dashed ellipsoids - jack-knife trials with the maximum deviation.

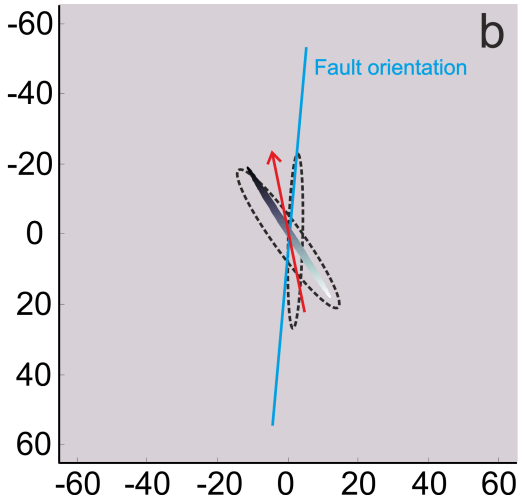

Figure 4.12: Jack-knife test for the Event 5. Side view looking to the north. Blue line: Fault plane from the geological model. Gray ellipsoid: ellipsoid computed using all stations. Dashed ellipsoids - jack-knife trials with the maximum deviation.

The approach was applied to five large events from Ridgeway mine, Australia. Assessment of these case studies indicates the possibility of partly automating the procedure in the future.

We have showed that the information provided by the SDM allows for fault plane detection, in particular by comparing the source ellipsoid and its principal axes to the candidate fault planes.

The resolution and stability of the solution was tested using two of our events. Jackknife testing was applied, which showed good stability for all the parameters. The most robust parameters were temporal parameters, and the least robust parameters were spatial parameters (in particular, the shape and orientation of the source ellipsoid). Nevertheless, even with these variations, derived rupture velocity vector for the event is still very stable.

Chapter 5

Discussion and conclusion

The second degree moment approach beneficially provides additional information to standard MT: geometry of the source, duration of the source process, spatial and temporal centroid and rupture velocity vector. In addition to the usefulness of them for gaining more insight about the source, the SDM can help to obtain a more accurate estimate of the mechanism, especially concerning its DC vs. non-DC contents. To do that, we proceed in an iterative loop, where we determine the zero degree MT from the data filtered below the corner frequency, use it to estimate the second degree moments from the data keeping the information from the frequency range reaching beyond the corner frequency, subtract their effects from the records, and invert them subsequently for the zero degree MT. In this way we have demonstrated the following:

• Neglect of source finiteness, the effects of which remain in the data even after excessive low-pass filtering, yields spurious non-DC components in the reconstructed MT;

• The orientation of the mechanism, that is, the position of the fault plane solution is, however, almost unbiased;

• Correcting the data for source finiteness by subtracting the contribution of the second degree moments reduces spurious non-DC components substantially.

With the skill to reduce spurious non-DC component of the mechanism, we have a good chance to reconstruct the genuine non-DC originated by the source process itself, in particular, to decide between DC and non-DC events.

With this aim we studied five events with large non-DC component using SDM approach (Kobe 1995, Izmit 1999, Solomon 2003, Bolivia 2005 and aftershock of Tohoku-oki 2011). For all 5 events we determined standard MT and estimated the SDM. For Kobe and Izmit earthquake we performed the jack-knife test which demonstrated the robustness of the results. We compared the SDM obtained for Kobe and Izmit earthquakes with previous studies and found our results largely in agreement with them. Then, we removed the SDM contribution from the data and recomputed the standard MT by using the data without the SDM effects. We demonstrated that the large non-DC component was probably the

effect of the source finiteness, which remained in the data even after the low-pass filtering.

The second application was to mining tremors, where we studied five events from the large Ridgeway data set. The MT solutions are similar to that obtained by IMS from the spectral amplitude inversion.

Unfortunately, the Ridgeway SDM cannot be compared with any previous study because our evaluation is the first application of the methodology to mining tremor data. The major benefit for the practice is foreseen in the capability of the approach to remove the ambiguity of the two nodal planes within the traditional MT solution, i.e. to identify the genuine fault plane. We demonstrated this advantage clearly on the sample events. As a completely novel approach, the IMS company is interested to implement it into their processing package as an advanced extension of the existing routine procedures.

Chapter 6

Included papers

P1: P. Adamová, J. Šílený (2010). Non-double-couple earthquake mechanism as an artifact of the point source approach applied to a finite-extent focus, *Bull. Seis. Soc. Am.*, **100**(2), 447-457.

P2: P. Adamová, J. Šílený (2013). Disputable non-double-couple mechanisms of some strong earthquakes – second degree moment approach, *Bull. Seis. Soc. Am.,* in press

Chapter 7

References

Adamová P. (2006). Earthquake source process and its complexity. Master thesis, Charles University, Prague.

Adamová P., Šílený J. (2010). Non-double-couple earthquake mechanism as an artifact of the point source approach applied to a finite-extent focus, *Bull. Seis. Soc. Am.*, **100**(2), 447-457

Backus, G.(1977a). Interpreting the seismic glut moments of total degree two or less, *Geophys. J. R. astr. Soc.*, **51**, 1-25.

Backus, G., 1977b. Seismic sources with observable glut moments of spatial degree two, *Geophys. J. R. astr. Soc.*, **51**, 27-45.

Bouchon, M., Coutant O. (1994). Calculation of synthetic seismograms in a laterally varying medium by the boundary-element discrete wavenumber method, *Bull. Seismol. Soc. Am.* **84**, no. 6, 1869–1881.

Bukchin, B.G., Levshin, A.L., Ratnikova, L.I., Dost, B., Nolet, G. (1992). Estimation of spatio-temporal source parameters from the 1988 Spitak, Armenia, earthquake from broadband surface wave records, *Comp. Seismol. Geodyn.*, **2**, 156-161.

Bulut, F., Bohnhoff M., Aktar M., Dresen G. (2007). Characterization of aftershock-fault plane orientations of the 1999 Izmit (Turkey) earthquake using high-resolution aftershock locations, *Geophys. Res. Lett.* **34**, L20306.

Clevede, E., Bouin M.-P., Bukchin B., Mostinskiy M., Patau G. (2004). New constraints on the rupture process of the 1999 August 17 Izmit earthquake deduced from estimates of stress glut rate moments, *Geophys. J. Int.* **159**, 931-942.

Dahm, T., Krüger, F.(1999). Higher-degree moment tensor inversion using far-field broad-band recordings: theory and evaluation of the method with application to the 1994 Bolivia deep earthquake, *Geophys. J. Int.*, **137**, 35-50.

Das, S., Kostrov, B.V. (1997). Determination of the polynomial moments of the seismic moment rate density distribution with positivity constraints, *Geophys. J. Int.*, **131**, 115-126.

Doornbos, D. J. (1981). Seismic moment tensors, *Identification of Seismic sources*, 207-232, Dordrecht, Holland.

Doornbos, D. J. (1982). Seismic moment tensors and kinematic source parameters, *Geophys. J. R. Astr. Soc.* **69**, 235–251.

Dufumier H., Rivera L. (1997). On the resolution of the isotropic component in moment tensor inversion, *Geophys. J. Int.* 131(3), 595-606.

Goldberg D. E. (1989). Genetic Algorithms in Search, Optimization, and Machine Learning, Addison-Wesley, Reading, Massachusetts, 412 pp.

Gusev A.A., Pavlov V.M. (1986). Detailed study of the focus of a deep earthquake (Fiji, Feb. 15, 1971) as a radiator of elastic waves, II. Calculation of the first- and second-order power moments, *Volc. Seism.*, **8**, 929-954.

Gusev A.A., Pavlov V.M. (1988). Determination of space-time structure of a deep earthquake source by means of power moments, *Tectonophysics*, **152**, 319-334.

Haskell N. A. (1964). Total energy and energy spectral density of elastic wave radiation from propagating faults, *Bull. Seismol. Soc. Am.*, **54**, 1811-1841.

Ide S., Takeo M., Yoshida Y. (1996). Source process of the 1995 Kobe earthquake: determination of spatio-temporal distribution by bayesian modeling, *Bull. Seismol. Soc. Am.* **86**(3), 547-566.

Julian, B.R, Miller A. M., Foulgar G.R. (1998). Non-double-couple earthquakes 1. Theory, *Reviews of Geophysics* 36(4), 525-549.

McGuire J. J., Zhao L., Jordan T.H. (2001). Teleseismic inversion for the second-degree moments of earthquake space-time distribution, *Geophys. J. Int.* **145**, 661–678.

McGuire, J. J., Zhao L., Jordan T.H. (2002). Predominance of unilateral rupture for a global catalog of large earthquakes, *Bull. Seismol. Soc. Am.* **92**, no. 8, 3308–3317.

Miller A.M., Foulgar G.R., Julian B.R. (1998). Non-double-couple earthquakes 2. Observations, *Reviews of Geophysics* **36**(4), 551-568.

Ortlepp W.D. (1984). Rockbursts in SA gold mines: a phenomenological view. 1st Int. Rockbursts and Seismicity in Mines. SAIMM Symposium Series 56 Johannesburg.

Ozalaybey S., Ergin M., Aktar M., Tapırdamaz C., Bicmen F., Yoruk A. (2002). The 1999 Izmit Earthquake Sequence in Turkey: Seismological and Tectonic Aspects. *Bull. Seis. Soc. Am.* , **92**(1), 376-386.

Savage J. C. (1966). Radiation from a realistic model of faulting, *Bull. Seism. Soc. Am.*, **56**, 577-592.

Silver P., Jordan T.H. (1983). Total moment spectra of fourteen large earthquakes, *J. Geophys. Res.*, **88**, 3273-3293.

Silver P., Masuda T. (1985). A source extent analysis of the Imperial Valley earthquake of October 15, 1979 and the Victoria earthquake of June 9, 1980, *J. Geophys. Res.*, **90**, 7639-7651.

Stump B.W., Johnson L.R. (1982). Higher-degree moment tensors – the importance of source finiteness and rupture propagation on seismograms, *Geophys. J. R. astr. Soc.*, **69**, 721-743.

Vavryčuk V. (2001). Inversion for parameters of tensile earthquakes, *J. Geophys. Res.*, 106(B8), 16339-16355.

Zahradník, J., Plešinger A. (2005). Long-period pulses in broadband records of near earthquake, Bull. Seis. Soc. Am. 95, 1928-1939.

List of Tables

List of abbreviations

MT	moment tensor
SDM	second degree moments
non-DC	non double couple
DC	double couple
CLVD	compensated linear vector dipole
ISO	isotropic part
CMT	centroid moment tensor
DWN	discrete wave number

Bulletin of the Seismological Society of America, Vol. 100, No. 2, pp. 447–457, April 2010, doi: 10.1785/0120090097

Non-Double-Couple Earthquake Mechanism as an Artifact of the Point-Source Approach Applied to a Finite-Extent Focus

by Petra Adamová and Jan Šílený

Abstract A sizable amount of moderate and strong earthquakes exhibit a considerable percentage of non-double-couple (non-DC) components in the mechanism, as reported by agencies determining moment tensors on a routine basis from long-period seismograms. As most of them are tectonic events where a simple shear slip is anticipated along a roughly planar fault (at least in the optics of the long periods used), suspicion arises about their source origin. Leaving aside anisotropy in the source region, we assign them to be side effects of the application of the first degree moment tensor approximation to data still containing (after low-pass filtering) information about the source finiteness. We verify the hypothesis in a synthetic experiment simulating a finite-extent source—a unilaterally propagating shear slip—and invert the synthetic data into moments up to degree 2. The first degree moment—traditional moment tensor—exhibits more that 20% of non-DC components. If we restitute the data by subtracting the contribution of the second degree moments, these spurious components are suppressed and the mechanism becomes almost pure double couple. The orientation of the mechanism is, however, not affected discernibly. Spurious non-DC components can be generated also by noise contamination of the observed seismic records and by using an improper Green's function when inverting the data, which happens in cases of mislocation of the hypocenter and/or mismodeling the velocity/attenuation in the area. In additional synthetic experiments, we demonstrate that reasonably estimated effects just listed do not mask the phenomenon of appearance of the non-DC originated by neglecting the source finiteness and correcting for the second degree moments reveals the proper mechanism.

Introduction

During recent years, the moment tensor (MT) approach in retrieving the earthquake mechanism has become a standard, replacing the formerly universal description of the source by a double couple (DC). In many cases this more general approach is well substantiated physically, as for volcanic earthquakes, various types of induced seismicity like the activity in mines, and seismicity related to injection experiments in wells in the oil, gas, and geothermal industry (for a review, see, for example, Miller *et al.*, 1998). Tectonic earthquakes, especially the strong and moderate events, are, however, supposed to be simple shear slips along approximately planar faults in the view of the long-periods processed, and the MT approach is used merely as an advantageous tool in the waveform inversion because of its linearity. This is the case of all the standard routines of determining the mechanism from teleseismic and regional records, like the Global Centroid Moment Tensor Catalog (e.g., Ekstrom *et al.*, 2005), U.S. Geological Survey (e.g., Sipkin and Zirbes, 2004), National Research Institute for Earth Science and Disaster Prevention (Kubo *et al.*, 2002), Schweizerischer Erdbebendienst (SED) (e.g., Bernardi *et al.*, 2004), the Mediterranean Network (e.g., Pondrelli *et al.*, 2002), and Instituto Andaluz de Geofisica (Stich *et al.*, 2003). In these catalogs, many events—even strong earthquakes—are reported as possessing a noticeable percentage of the non-double-couple (non-DC) component in the mechanism, which is obviously spurious in most cases. We suspect that it may be due to applying the first degree MT approach (which, in common understanding, is regarded as a point-source mechanism) to data from events that are rather large to be treated using this approach. A clear indication of this discrepancy is the directivity.

An advantageous framework in which to consider finite-source effects, while keeping the point-source approach, is implementing higher degree moments into the source description. The concept was originated by Backus

(1977a,b). Subsequently, considerable effort was invested to determine the finite-extent source parameters described by higher degree moments by inverting seismic data. Doornbos (1982) designed the source model based on second degree moments and related its parameters to the Haskell model. Kagan (1988) used the expansion of seismic radiation of a finite source in higher degree MTs and suggested discerning the complexity or nonplanarity of the source from the presence of particular higher degree moments. Das and Kostrov (1997) formulated the inverse problem of determining the temporal and spatial power moments of the seismic source moment rate density distribution, in which its positivity (i.e., the absence of back-slip on the fault) is enforced through a set of linear equations. They suggested proceeding from low-degree moments retrieved from long periods to higher-degree moments estimated from high frequencies. The necessity to subdivide the source region to achieve a low approximation error of Green's functions (GFs) was stressed by Dahm and Krueger (1999). Inversion schemes to determine higher degree moments were also designed by Gusev and Pavlov (1988) and Bukchin (1995). McGuire *et al.* (2001) developed a method for retrieving second degree moments by inverting the shifts in the travel time and amplitude of various seismic phases at global stations and stressed the importance of imposing the physical constraint of keeping the volume of the source region positive. McGuire *et al.* (2002) evaluated the mixed spatiotemporal moment estimating the propagation of the rupture for a number of $M_w > 7$ earthquakes in different tectonic regions. Using this tool to distinguish between unilateral and bilateral rupture propagation, they found that about 80% of large shallow ruptures are predominantly unilateral.

We follow the method by Doornbos (1982), whose source model up to the second degree consists of 20 parameters. The general representation of the displacement due to forces distributed in the source volume can be replaced by the point source after expanding the GF around a reference source point. The Taylor expansion up to degree two of the response function (RF) (spatial derivative of GF) in the representation theorem yields the expression for seismic displacement that contains 90 parameters; the smoothing assumption of a common space and time history of the components of the MT density reduces the number to 20 and the expression becomes

$$u_i = M_{jk}[G^i_{j,k} - \dot{G}^i_{j,k}\Delta\tau + G^i_{j,kl}\Delta\xi_l + \frac{1}{2}\ddot{G}^i_{j,k}\Delta(\tau^2) - \dot{G}^i_{j,kl}\Delta(\tau\xi_l) + \frac{1}{2}G^i_{j,klm}\Delta(\xi_l\xi_m) + \ldots], \quad (1)$$

where $u_i(\mathbf{x}, t)$ is the ground displacement; and M_{jk} is the first degree moment (6 parameters), classical MT describing the mechanism of a point source; the other variables are second degree moments: temporal centroid $\Delta\tau$, spatial centroid $\Delta\xi_l$, spatiotemporal moment $\Delta(\tau\xi_l)$, second temporal moment $\Delta(\tau^2)$, and second spatial moment $\Delta(\xi_l\xi_m)$. $G^i_{j,k}(\mathbf{x}, \boldsymbol{\xi}, t, \tau)$ is the RF; $\dot{G}^i_{j,k}(\mathbf{x}, \boldsymbol{\xi}, t, \tau)$ is the time derivative of the RF; $G^i_{j,kl}(\mathbf{x}, \boldsymbol{\xi}, t, \tau)$ is the spatial derivative of the RF; $\ddot{G}^i_{j,k}(\mathbf{x}, \boldsymbol{\xi}, t, \tau)$ is the second time derivative; $\dot{G}^i_{j,kl}(\mathbf{x}, \boldsymbol{\xi}, t, \tau)$ is the combination of the time and spatial derivative; and $G^i_{j,klm}(\mathbf{x}, \boldsymbol{\xi}, t, \tau)$ is the second spatial derivative. $\mathbf{x}$ and $\boldsymbol{\xi}$ are, respectively, the point observation and point on the fault. Second degree moments can be interpreted in terms of the parameters related to the finite extent of the focus:

1. Temporal centroid (1 parameter): specifies the origin time of the finite-extent source estimate;
2. Spatial centroid (3 parameters): specifies the position of a point source substituting the finite-extent focus;
3. Spatiotemporal moment (3 parameters): after division by second degree temporal moment it estimates the rupture propagation, that is, both its direction and speed;
4. Second temporal moment (1 parameter): squared estimate of the source process duration;
5. Second spatial moment (6 parameters): geometrical characteristics of the source; it specifies an ellipsoid (hereinafter the source ellipsoid), the orientation of its major axis indicates the direction of the extension of the focus.

We use the previous description of the second degree moments to express the finiteness of the earthquake focus. In a synthetic test, we check the hypothesis that the mechanism is distorted when the data that originated in a finite-extent source are inverted using the point-source description. For a simple shear slip along a planar fault embedded in an isotropic medium we obtain an MT possessing a considerable percentage of non-DC components. We design a procedure to correct the data for the source finiteness and reconstruct the proper mechanism.

Method

The seismic displacement expressed in terms of moments up to degree two depends on the parameters of the source in a nonlinear way: equation (1) contains a product of the first degree moment M_{ij} describing the source mechanism with the terms corresponding to the second degree moments related to the finiteness of the focus. Therefore, we solve the task of waveform inversion in iterations. First, we estimate the mechanism from the low-pass filtered records in the first degree MT approximation, where we benefit from the linearity of the task and invert the data in a single-step procedure. Then, we determine the second degree moments from the original data with the mechanism fixed at the value from the previous step (Fig. 1). The second degree moments having been determined (see the next paragraph), we evaluate their synthetic contribution to the data and subtract it from the observed records, that is, we correct the finite-extent source data for the estimated source finiteness to reconstruct the point-source data. Subsequently, we invert the corrected data in the first degree MT approach and obtain the estimate of the true mechanism not biased by the effect of the finiteness. This loop, in principle, can be repeated several

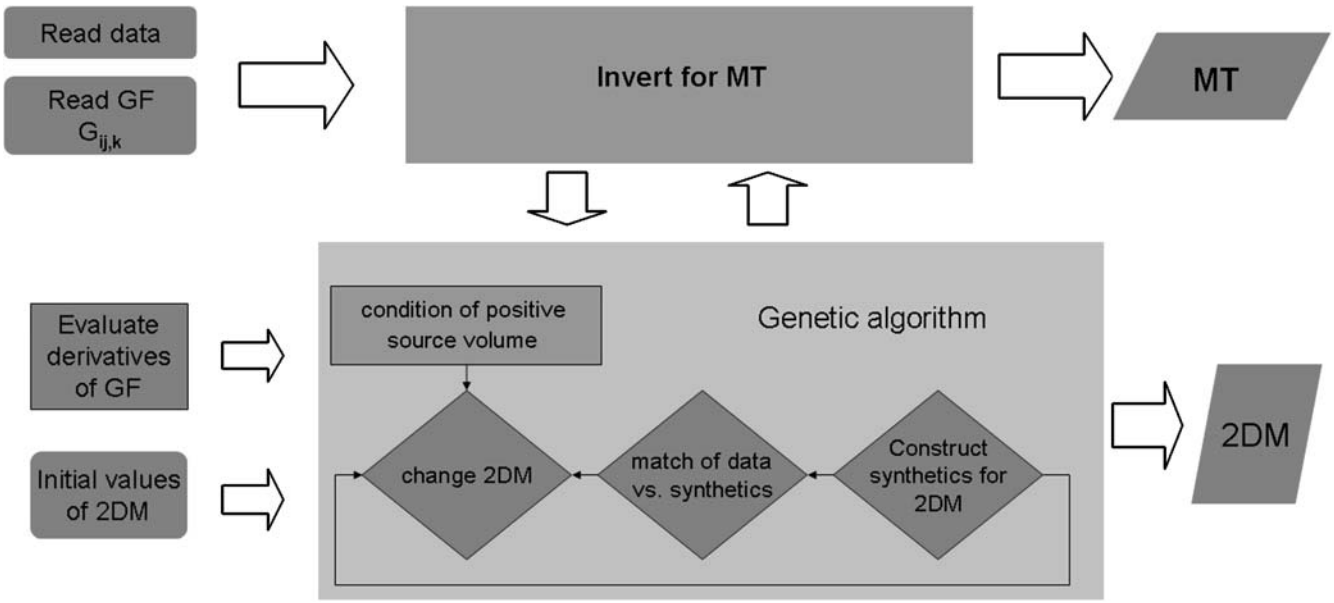

Figure 1. Flow chart of the retrieval of the mechanism in the MT representation together with the second degree moments (2DM). MT inversion, top; second degree moments inversion, bottom. Inputs into the procedure, left; outputs, right.

times until nonnegligible adjustments of the mechanism are observed. In our synthetic experiments, however, a single iteration appeared to be enough.

Splitting the inverse problem with the synthetics expressed by equation (1) into two stages, namely, in turn, by neglecting the second degree moments and keeping the first degree moment constant, provides us, in principle, with two subsequent linear problems. The first stage, determining the M_{ij} from low-pass filtered records, we solve advantageously by single value decomposition. The second stage, evaluating the 14 parameters related to the second degree moments with M_{ij} fixed, though also linear must, however, be solved iteratively as an additional nonlinear constraint is employed, which ensures keeping the volume of the focus nonnegative (McGuire *et al.*, 2001). Therefore, we proceed as with a generally nonlinear functional. We determine the 14 parameters describing the second degree moments by using the genetic algorithm (Goldberg, 1989) with the additional constraint of keeping the four-dimensional source volume nonnegative, which is an inherent property of all earthquakes (McGuire *et al.*, 2002).

Data

We verify the hypothesis of generating spurious non-DC source components in the mechanism of a simple shear slip propagating unilaterally along a fault, when seen by using the standard first degree MT approach. We designed a synthetic experiment simulating a hypothetical earthquake on the North Anatolian fault at the site of the strong Izmit earthquake of 17 August 1999 (00:01:38, M_w 7.5). Four days after the main event, a network of seismic stations was deployed by GeoForschungsZentrum (GFZ) Potsdam (Özalaybey *et al.*, 2002). It consisted of nearly 50 stations; in our synthetic experimentation we consider 18 of them (Fig. 2). Synthetic data were computed for the geometry of the main shock (strike = 90°, dip = 72°, rake = 180° in the Aki and Richards, 2002, convention), at a depth of 13 km a rectangular fault, 20 km long and 10 km wide, was assumed. In accordance with the observation, unilateral rupturing directed eastward was modeled, the velocity of rupture propagation reaching 2.8 km/sec. The synthetic data for the finite-extent source at the stations in Figure 2 were computed by J. Burjánek, ETH Zurich (Fig. 3). The one-dimensional layered model by Bulut *et al.* (2007) was used (Fig. 4). GFs are identical for constructing the synthetic data and their subsequent inversion and are computed by DWN/reflectivity code AXITRA (Bouchon and Coutant, 1994), modified by Sokos and Zahradník (2008)). The GF derivatives requested in equation (1) are evaluated by numerical differentiation.

It is worth pointing out the well-pronounced directivity in the records of stations in various azimuths, which indicates the significant contribution of the terms describing the finiteness of the focus, see, for reference, the records of stations east of the epicenter (in the forward direction) and to the west (reverse direction) of the epicenter (Fig. 5).

Frequency Tests

For the sake of necessary simplification of the inversion process, the data have to be low-pass filtered as much as possible, but they still should keep the second degree effects. To determine the optimum frequency range, we performed a series of tests varying the cutoff frequency and comparing the resulting second degree moments. We filtered the synthetic

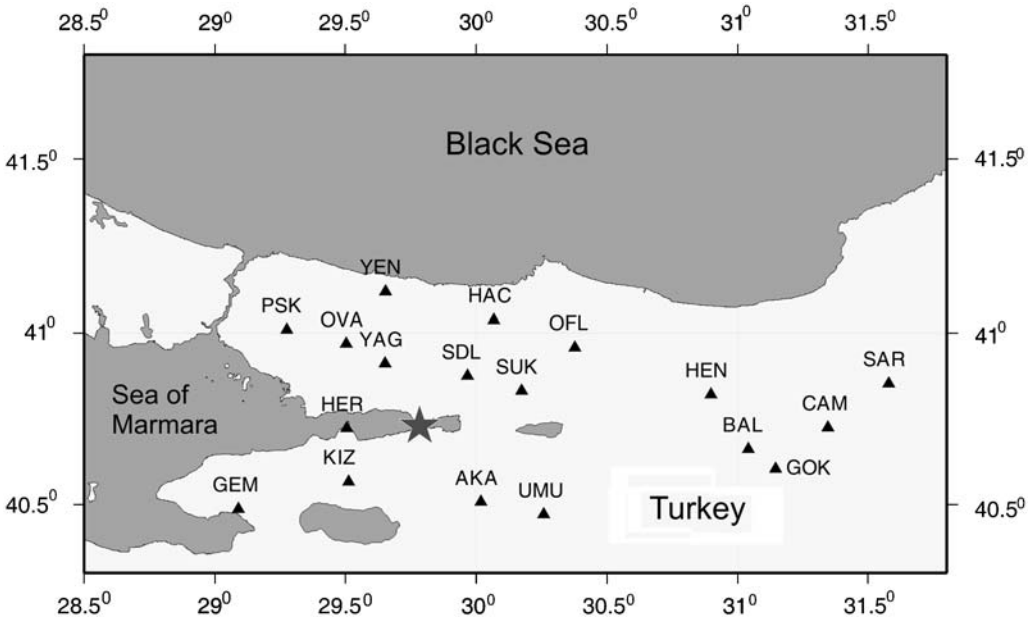

Figure 2. Configuration of stations in synthetic tests: simulates part of the seismic network deployed on the North Anatolia fault around the epicenter of the Izmit earthquake (17 August 1999) by GeoForschungsZentrum (GFZ) Potsdam (Özalaybey *et al.*, 2002). Earthquake's epicenter, star.

records by a band-pass third order Butterworth filter with a low cutoff at 0.02 Hz (for all tests) and a high cutoff at 0.1, 0.2, 0.3, and 0.4 Hz. The first degree moment was determined from the data in the range 0.02–0.08 Hz (see Fig. 6). In the second stage of the inversion, we estimated the second degree moments from the data filtered up to the four values of the frequency mentioned previously. We have obtained similar results for frequencies of 0.2, 0.3, and 0.4 Hz (see Fig. 7, Table 1). The result for the frequency interval 0.02–0.1 Hz is out of the pattern of the higher frequencies, which may indicate that it is difficult to retrieve second degree moments here. Thus, we accepted the frequency range 0.02–0.2 Hz as the optimum.

Synthetic Tests—Exact Data

In the first stage of the procedure—determination of the first degree moment—we invert the band-pass filtered data in the 0.02–0.08 Hz window to enhance the point-source characteristics of the focus and suppress its finite-extent features. It is largely the common MT solution routinely reported by the agencies listed in the Introduction; it should be noted that they search for deviatoric MT. Contrary to the agencies, our solution is unconstrained MT, which also possesses an isotropic component (ISO). We use the widely accepted decomposition of the MT into the DC, ISO, and compensated linear

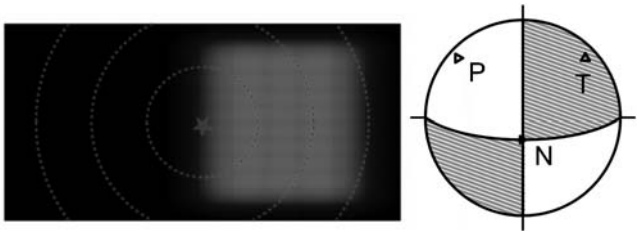

Figure 3. Source model for the synthetic test. Moment density distribution along a rectangular 20 km × 10 km steeply dipping fault striking east (left-hand panel): initiation point of the unilaterally propagating rupture, star; dashed circles, isochrones corresponding to 1, 2, and 3 sec. Lower-hemisphere plot of the FPS (right-hand panel). Compressions are shown in gray.

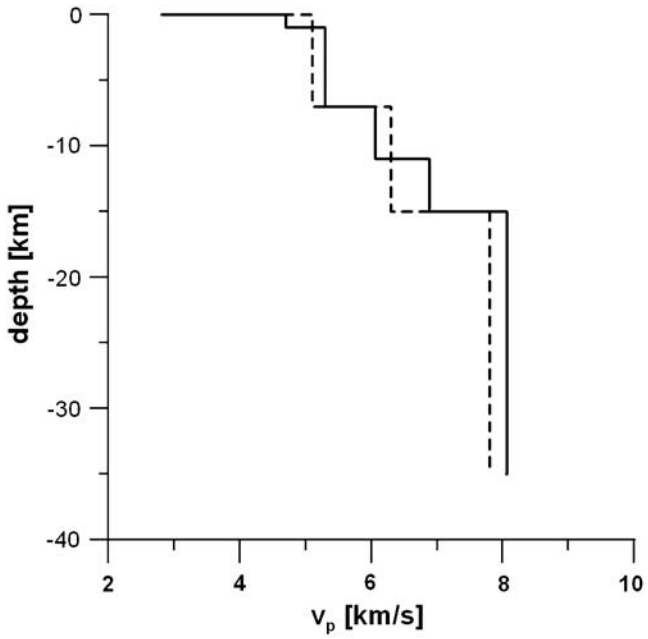

Figure 4. Velocity profile for the North Anatolia area by Bulut *et al.* (2007) (solid line) and the simplified model for simulating the effect of the velocity mismodeling (dashed line).

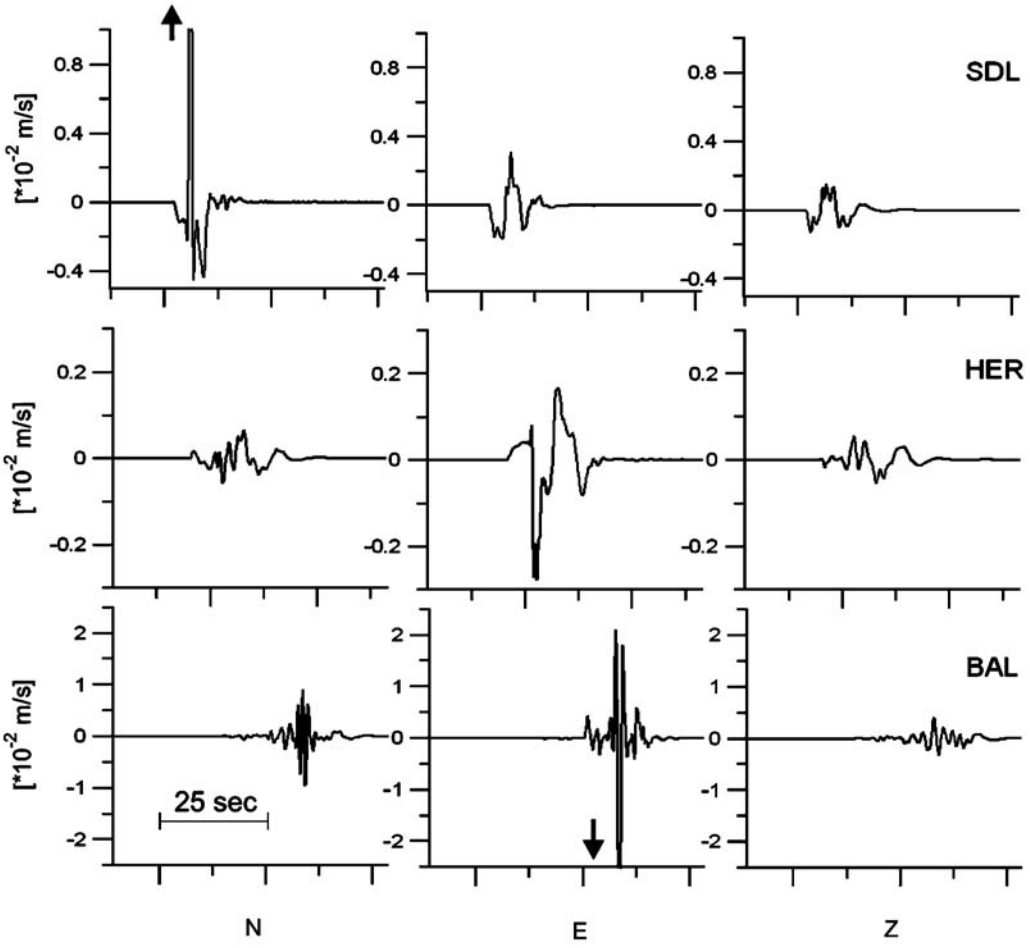

Figure 5. Examples of the unfiltered synthetic data demonstrating the source directivity: station BAL in the forward direction, station HER in the reverse direction, and station SDL in the direction perpendicular to the fault strike.

vector dipole (CLVD) and evaluated the percentages of the individual components according to Vavryčuk (2001). We obtained a mechanism oriented fairly close to the theoretical DC source (strike = 93°, dip = 73°, rake = −178°) but possessing rather large non-DC components: 12% of CLVD and 10% of ISO (Fig. 8, top left). The large non-DC components are the consequence of the existence of the remnants of directivity due to the source finiteness, which remained in the data even after the heavy low-pass filtering. It should be pointed out that this directivity cannot be discerned by visually inspecting the low-frequency records.

The scalar moment of the theoretical source model was 10^{18} N m, while its value provided by the experiment remained at 7.7×10^{17} N m. The underestimation is due to the destructive interference resulting from the source finiteness, which is not accounted for in the source parametrization by the first degree MT in the first stage of our algorithm.

In the second stage, we estimate the second degree moments from data filtered up to 0.2 Hz. We obtained good estimates of the temporal centroid (the output value $\Delta\tau = 1$ sec is low in accordance with the undelayed initiation of the theoretical source), the spatial centroid $\Delta\xi_l$ (with

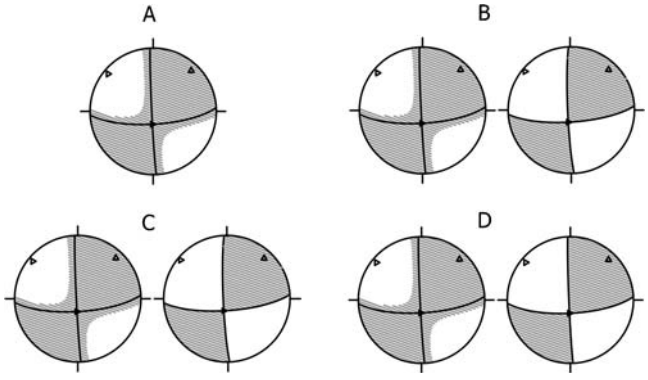

Figure 6. Mechanisms reconstructed in the testing frequency range. For each frequency a couple of mechanisms is displayed: the mechanism obtained by inverting data filtered outside 0.02–0.08 Hz (left) and the mechanism from data corrected for the contribution of the second degree moments (right). In the lower-hemisphere plot of the FPS, compressions are shown in gray. The letters A, B, C, and D are for frequencies used in the inversion of second degree moments: A, 0.02–0.1 Hz; B, 0.02–0.2 Hz; C, 0.02–0.3 Hz; and D, 0.02–0.4 Hz.

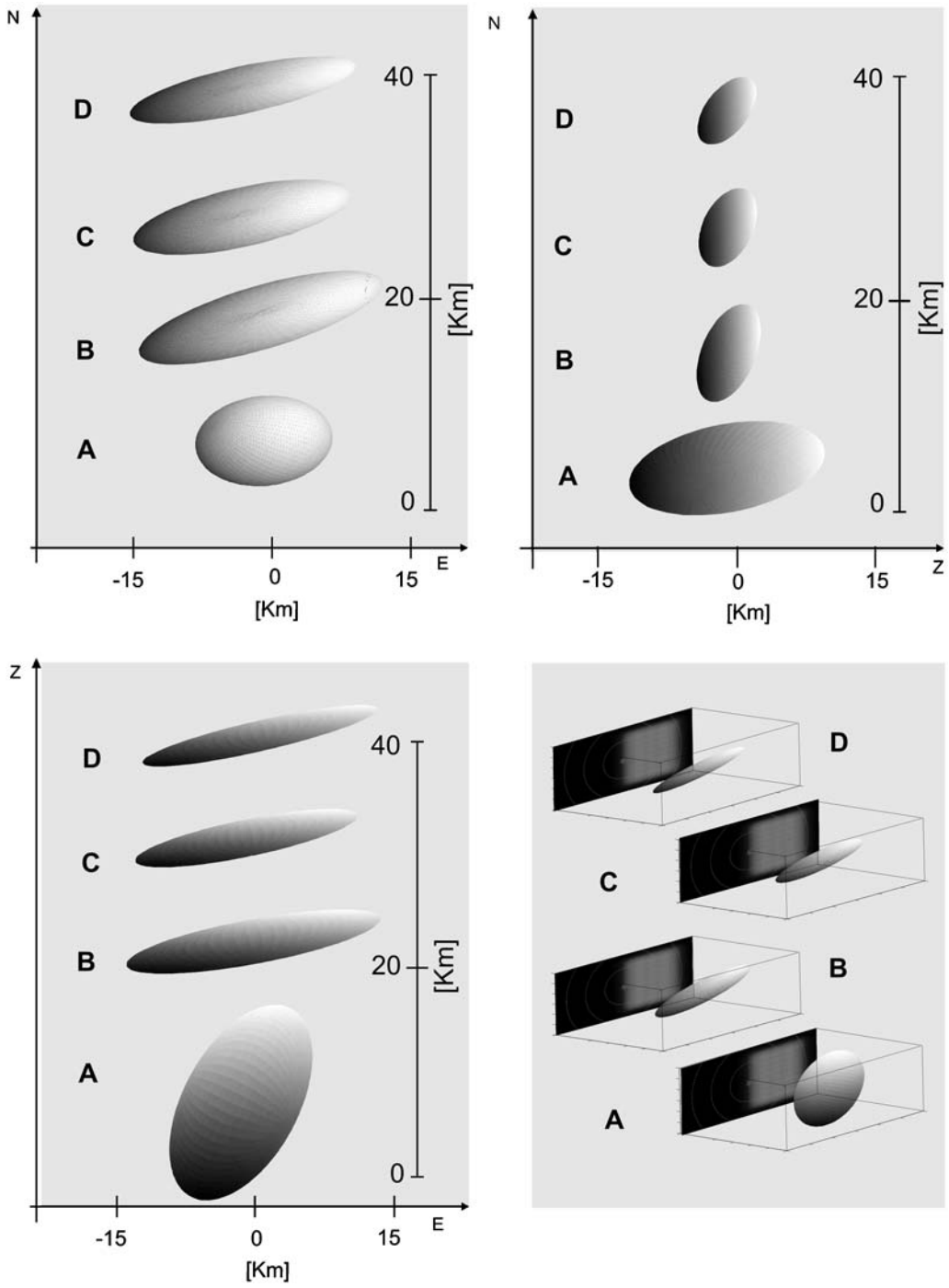

Figure 7. Geometrical characteristics of the source from second degree moments: the source ellipsoid, the major axis of which indicates the direction of the extension of the focus. Frequency intervals: A, 0.02–0.1; B, 0.02–0.2; C, 0.02–0.3; and D, 0.02–0.4 Hz. Shown are the map view (top left); depth section, view from east (top right); depth section, view from south (bottom left), three-dimensional view together with the source model in the background (bottom right).

the final position [3.4, 7.2, 1] in the coordinate system originated in the hypocenter with axes pointing north, east, and vertically downwards, while the theoretical position is [0, 5, 0], see Fig. 3), and the time duration (2 sec), which is a reasonable estimate because the theoretical source is a unilateral rupture propagating along the 10 km length of the fault at a speed of 2.8 km/sec. The geometrical characteristics of the focus, expressed by the double spatial moment $\Delta(\xi_l \xi_m)$, are stretched roughly in the east–west direction as expected because of the east–west orientation of the rectangular fault, Figure 9. The spatiotemporal moment, the three parameters which—after having been divided by the squared time duration—specify the vector of velocity of the rupture propagation. In accordance with the theoretical model we

Table 1

Experiments Exploring the Influence of the Frequency Content Considered in Determining the Second Degree Moments

Experiment	Variance Reduction	Spatial Centroid (km)			Temporal Centroid (sec)	Propagation Velocity Vector (km/sec)			Source Duration (sec)	Geometrical Characteristics					
										λ_2/λ_1	λ_3/λ_2	λ_1	λ_2	λ_3	Δ (°)
A	0.45	4.2	3.1	3	2	1.5	1.8	1.4	4	1.36	1.83	3.6	4.9	9	23
B	0.65	3.4	7.2	1	1	0.2	2.4	0.4	2	1.55	4	1.8	2.8	11.2	14
C	0.62	2.8	6.8	1.4	1	0.1	2.7	0.2	2	1.73	3.73	1.5	2.6	9.7	11
D	0.63	2.6	7	0.6	1	0.4	2.4	0.5	2	1.75	4.9	1.2	2.1	10.3	9

Synthetic records filtered by the band-pass third order Butterworth filter with the low cutoff at 0.02 Hz and high cutoff at 0.1 (A), 0.2 (B), 0.3 (C), and 0.4 Hz (D).

obtain prevailingly eastward propagation $\Delta(\tau\xi_l)/\Delta(\tau^2) = (0.2, 2.4, 0.4)$ (Fig. 10); the rupture rate was estimated at 2.4 km/sec, while the true velocity was 2.8 km/sec. Having determined the second degree moments, we evaluate their contribution in the synthetic seismograms and subtract it from the data. These records, corrected for the source finiteness, are just the data that should be matched by the first degree MT retrieved in the first stage if the procedure of elimination of source finiteness was successful. Figure 11 displays comparisons of our synthetic data and the seismograms predicted by the model at stations HER (in the reverse direction with respect to the rupture propagation) and BAL (in the forward direction); we can see that the fit is very good.

Synthetic Tests—Experiments Simulating Inconsistencies during the Data Inversion

In the experiment inverting exact data, we obtained the mechanism and parameters of the source finiteness fairly close to the true model values. In practice, however, GFs are inexact due to inaccurate hypocenter location and/or improper velocity/attenuation model of the medium, and seismic records are contaminated by noise. As a result, spurious non-DC components, which hamper the resolution of the true mechanism, can be generated. With the aim of checking if these spurious non-DC components do not mask the non-DC due to neglecting the source finiteness (which would prevent us from their proper identification and elimination), we perform additional synthetic tests simulating (1) hypocenter mislocation, (2) velocity profile mismodeling, and (3) noisy data. In the setups (1–3) we have chosen realistic values, namely,

1. Mislocation of the hypocenter when evaluating the GF: 1 km to the east, 1 km to the south, 2 km deeper than the true hypocenter. The larger error in depth than in the horizontal coordinates simulates a smaller location precision due to stations on the surface only;
2. Mismodeling of the velocity profile: for the sake of constructing the GF, the true one-dimensional model used to synthesize the data was simplified, Figure 4 (three layers only and velocities changed randomly by 10%);
3. Noise in data (ranging randomly within 15–30% of the maximum amplitude at each station). The low-pass filtering decreases the noise level by about 10%.

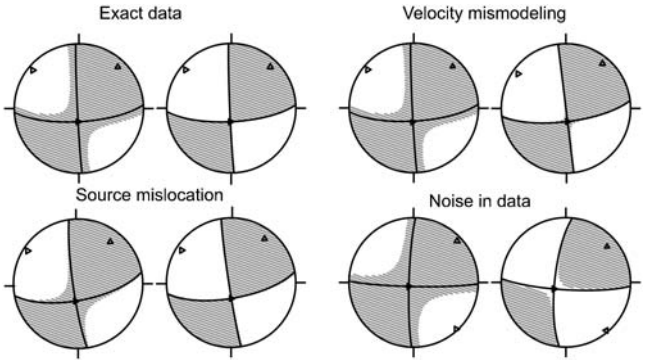

Figure 8. Mechanisms reconstructed in the experiment inverting exact synthetic data (top left), in the experiment simulating the hypocenter mislocation (bottom left), in the seismic velocity profile mismodeling (top right), and in the experiment with noisy data (bottom right). A couple of mechanisms are displayed for each experiment: the mechanism obtained by inverting data filtered outside 0.02–0.08 Hz (left), and the mechanism from data corrected for the contribution of the second degree moments (right). In the lower-hemisphere plots of the FPS, compressions are shown in gray.

Hypocenter Mislocation

The magnitude of the hypocenter mislocation chosen previously is realistic, taking into account the usual uncertainties involved in the localization process. It can be expected *a priori* that its effect on the resolution of the mechanism determined in the frequency band applied will be small because a mislocation of several kilometers is not very significant where wavelengths of tens of kilometers are concerned. In accordance with this, we have confirmed that the influence on both the first and second degree moments was very small: the centroids, source duration, rupture propagation vector, and the ellipsoid acquire very similar values (Table 2, Figs. 9 and 10). The only discernible effect is in the MT orientation: the strike angle of the fault-plane solution (FPS) of the mislocated solution is increased by about 10°.

Velocity Profile Mismodeling

An inaccurate estimate of the velocity profile in the crust is a common shortcoming occurring during source studies. How much it affects the result depends primarily on the frequencies applied in the data inversion: if the scale of the

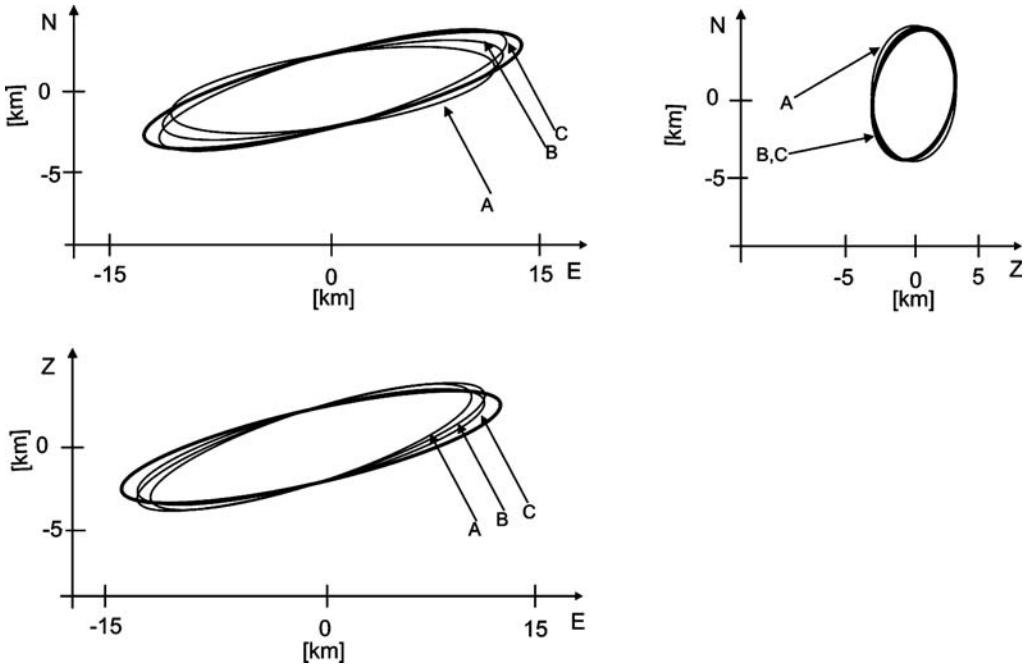

Figure 9. Source ellipsoids from the experiments simulating inconsistencies during the data inversion: A, mislocation of the hypocenter when evaluating GF; B, mismodeling of the velocity profile, the true one-dimensional model used to synthesize data, simplified when evaluating GF; C, noisy data. For comparison, the source ellipsoid obtained from noise-free data and exact GF is shown with the bold line.

velocity model change remains within the prevailing wavelength, a significant bias of the reconstructed source need not be expected. To assess the influence of a realistic mismodeling of the crust, we simplified the model available for the North Anatolia zone by merging some layers and modifying their velocity by as much as 10% of the original values. Thus, the mismodeling can be regarded as very slight when seen by 10+ sec waves used in the first inversion stage retrieving the point-source mechanism in the traditional way. In accordance with this, the MT obtained from the biased GF differs very little from that determined with the exact GF: the orientation is practically the same and the non-DC contents differ by 3% only (Table 3, Fig. 8). In the second stage (second degree moments retrieval) we use less-filtered data, and for 5+ sec waves the velocity profile modification is already more significant. This is reflected in a larger error of the second degree moments parameters, in particular of the vector of rupture propagation (Fig. 10) and the source ellipsoid (Fig. 9), which deviate from the expected east–west orientation. The new estimate of the first degree MT from the data corrected for the second degree moments parameters differs from hypocenter mislocation case just due to a larger error in second degree moments, but the difference is not essential and remains only in the strike angle (Table 3, Fig. 8).

Noisy Data

Real seismograms nearly always contain some noise. To simulate rather extreme contamination, we chose random white noise uniformly distributed between 15% and 30% of the maximum amplitude at each station to model moderate to strong noise. The low-pass filtering decreases the noise level by about 10%. The noise adds preferentially some ISO into the MT, which may be due to the fact that noise has no directivity, but also affects the orientation of the FPS (Table 3, Fig. 8). The second degree moments parameters are biased similarly to the velocity profile mismodeling case but the

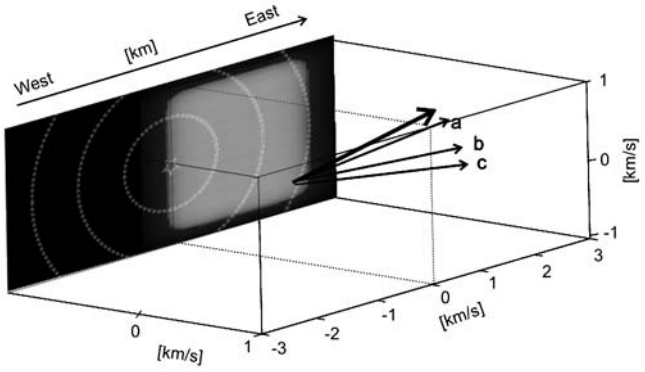

Figure 10. Vectors of the rupture propagation velocity obtained as the ratio of second degree moments $\Delta(\tau\xi_i)/\Delta(\tau^2)$ determined, in turn, in the synthetic experiment with exact data (thick black arrow), in the experiment simulating the hypocenter mislocation (arrow a), in the seismic velocity profile mismodeling (arrow b), and in the experiment with noisy data (arrow c). The background shows the vertical projection of the source model: the moment density distribution of the unilaterally propagating rupture (gray area) together with the 1, 2, and 3 sec isochrones.

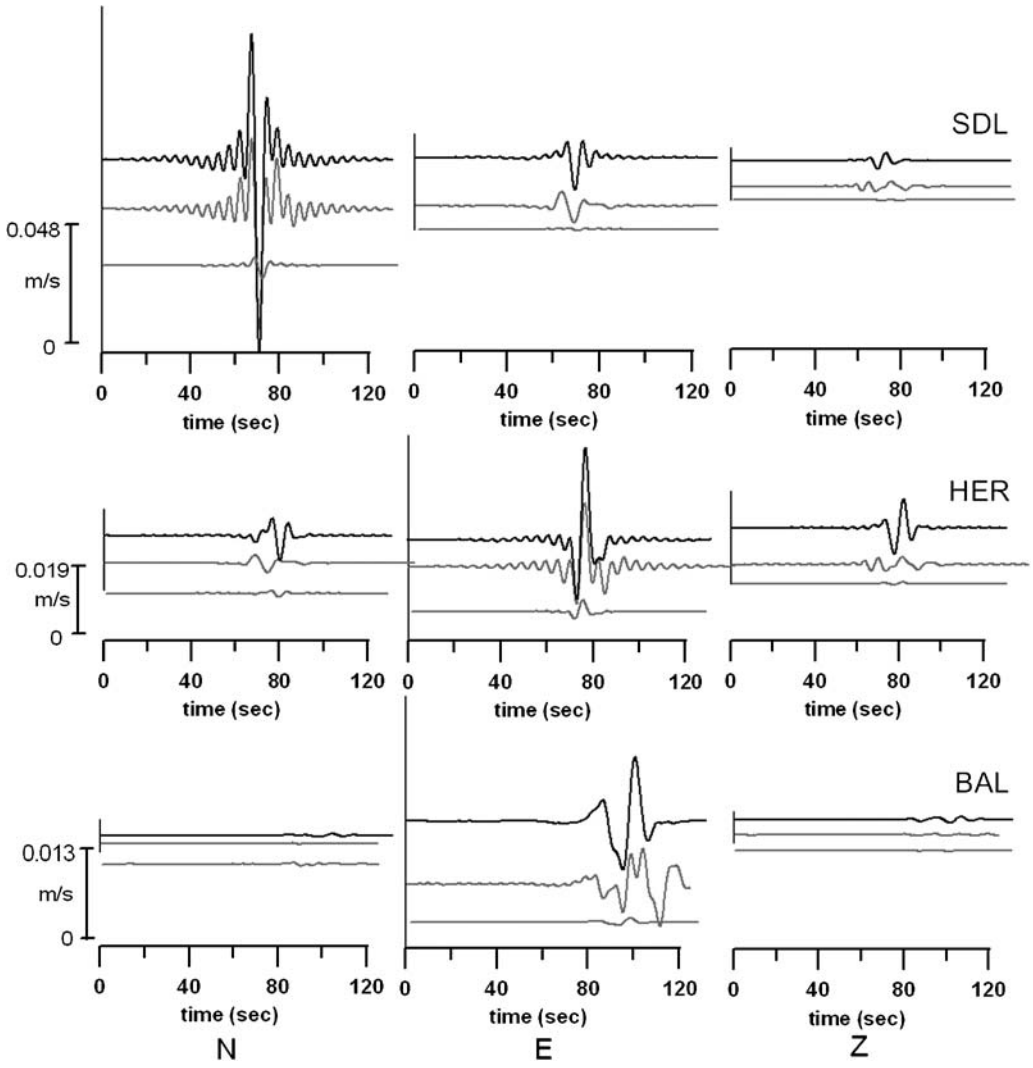

Figure 11. Synthetic data (black curve) versus synthetic seismograms predicted by the model (middle gray curve), together with the separate contribution of the second degree moments (bottom gray curve). Station BAL in the forward direction, station HER in the reverse direction, and station SDL in the direction perpendicular to the fault strike. The frequency range is 0.02–0.2 Hz.

vector of rupture propagation and the source ellipsoid deviate to opposite directions (Figs. 9 and 10). The reconstruction of the point-source mechanism, after subtracting the second degree moments effects, yields a satisfactory result comparable to the experiments (hypocenter mislocation, velocity profile mismodeling). This is encouraging as a rather high amount of noise was included and real data may be less contaminated.

Table 2

Second Degree Moments Retrieved in Synthetic Experiments with Exact Data, Mislocated Hypocenter, Inaccurate Modeling of the Velocity Profile, and Noisy Data

Experiment	Variance Reduction	Spatial Centroid (km)			Temporal Centroid (sec)	Propagation Velocity Vector (km/sec)			Source Duration (sec)	Geometrical Characteristics					
										λ_2/λ_1	λ_3/λ_2	λ_1	λ_2	λ_3	Δ (°)
Exact data	0.65	3.4	7.2	1	1	0.2	2.4	0.4	2	1.55	4.0	1.8	2.8	11.2	14
Mislocation	0.66	2.5	6.8	2	1	0.1	2.3	0.5	2	1.60	3.74	1.8	2.9	10.8	8
Inaccurate model	0.62	4.3	7.5	0.8	1	0.3	2.2	0.6	2	1.50	3.82	1.9	2.9	11.0	12
Noisy data	0.60	3.8	7.1	1.3	0	0.4	2.3	0.3	2	1.52	3.91	1.8	2.8	10.9	16

Spatial centroid and propagation velocity vector in (north, east, z) coordinate system. For the geometrical characteristics, the lengths λ_j of the axes are determined and the ratios presented, which illustrate the amount of the eccentricity. Angle Δ indicates the deviation of the major axis of the ellipsoid from the east–west direction.

Table 3

MT (First Degree Moment) Retrieved in Synthetic Experiments with Exact Data, Mislocated Hypocenter, Inaccurate Modeling of the Velocity Profile, and Noisy Data

Experiment	Strike (°)	Dip (°)	Rake (°)	DC (%)	CLVD (%)	ISO (%)	M (10^{17} N m)
Exact data	93/93	73/73	−178/−178	78/94	12/4	10/2	7.7
Mislocation	100/100	70/70	−177/−173	80/95	10/5	10/5	7.5
Inaccurate model	93/97	73/73	−179/−180	81/98	12/2	7/0	7.9
Noisy data	88/87	80/81	−174/−172	78/96	2/0	19/4	7.2

Decomposition into the DC, CLVD, and ISO according to Vavryčuk (2001); the orientation of the DC part is expressed in terms of strike, dip, and rake angles. The couple of values a/b in each cell indicates retrieval from data filtered by the 0.02–0.08 Hz passband filter (a) and from data corrected for the contribution of the second degree moments (b).

Discussion and Conclusions

Obviously it is reasonable to doubt the reality of the non-DC components in the unconstrained or deviatoric MTs of strong and moderate earthquakes, which are sometimes reported in the solutions issued by seismological agencies. Physically, these events, dominantly of a tectonic nature, are believed to be mostly shear slips. The non-DC components sometimes obtained are usually attributed to the complicated geometry of the portion of the fault participating in the slippage or to the anisotropy in the focal zone of the earthquake. We suggest an additional reason for the appearance of spurious non-DC components in MTs of strong and moderate earthquakes, namely, the directivity of the radiation caused by a rupture propagating along a finite length of the active fault, which is misinterpreted during inversion of the data by an algorithm applying the point-source approximation. Such approach does not take into account the directivity present in the data and converts it spuriously into the complexity of the reconstructed MT—appearance of non-DC components. In the standard approach, the influence of the source finiteness is believed to be suppressed by inverting low frequencies only; the appearance of spurious non-DC components, however, indicates that there are remnants of the directivity in the records even after the heavy low-pass filtering has been applied.

We suggest a procedure for reducing the effects of the source finiteness in the data before inverting them for the mechanism and for obtaining the MT unbiased by the directivity still present in the long-period records. We demonstrate its effectiveness in the synthetic experiment simulating the situation on the North Anatolia fault and the seismic network existing there. In particular, we simulate a unilaterally propagating rupture represented by a nearly vertical strike slip. To consider a finite-extent focus and remain in the point-source representation, second degree moments are used to an advantage. In the iterative loop, we determine the first degree MT from filtered data, use it to estimate the second degree moments from unfiltered data, subtract their effects from the records, and invert them subsequently for the first degree MT. In this way we have demonstrated the following:

- Neglect of source finiteness, which remains in the data even after excessive low-pass filtering, underestimates the scalar moment by almost 30%;
- At the same time, it yields spurious non-DC components in the reconstructed MT;
- The orientation of the mechanism, that is, the position of the FPS, is, however, almost unbiased;
- Correcting the data for source finiteness by subtracting the contribution of the second degree moments reduces spurious non-DC components substantially. Thus, we should be able to reconstruct the genuine non-DC originated by the source process itself, in particular, to decide between DC and non-DC events.
- Noise in the data, hypocenter mislocation, and velocity profile mismodeling may also originate spurious non-DC components in the mechanism. We, however, demonstrate that with realistic values of these effects, which can be encountered in practice, the spurious non-DC components remain small in comparison with the non-DC caused by the source finiteness.

Data and Resources

No data were used in this article. Station configuration simulates the surface seismic network monitoring the seismicity at the North Anatolian fault in Turkey, deployed by GFZ Potsdam (Özalaybey *et al.*, 2002). The velocity model of the Anatolian area was provided by Bulut *et al.* (2007). GFs were made using the program AXITRA (Bouchon and Coutant, 1994), modified by Sokos and Zahradnik (2008).

Acknowledgments

The Czech Republic Grant Agency supported the project under Grant Number 205/09/0724. We are indebted greatly to J. Burjánek for synthesizing the data used in our synthetic experiments.

References

Aki, K., and P. G. Richards (2002). *Quantitative Seismology*, Second Ed., University Science Books, Sausalito, California.

Backus, G. (1977a). Interpreting the seismic glut moments of total degree two or less, *Geophys. J. R. Astr. Soc.* **51,** 1–25.

Backus, G. (1977b). Seismic source with observable glut moments of spatial degree two, *Geophys. J. R. Astr. Soc.* **51,** 27–45.

Bernardi, F., J. Braunmiller, U. Kradolfer, and D. Giardini (2004). Automatic regional moment tensor inversion in the European–Mediterranean region, *Geophys. J. Int.* **157,** 703–716.

Bouchon, M., and O. Coutant (1994). Calculation of synthetic seismograms in a laterally varying medium by the boundary-element discrete wavenumber method, *Bull. Seismol. Soc. Am.* **84,** no. 6, 1869–1881.

Bukchin, B. G. (1995). Determination of stress glut moments of total degree 2 from teleseismic surface wave amplitude spectra, *Tectonophysics* **248,** 185–191.

Bulut, F., M. Bohnhoff, M. Aktar, and G. Dresen (2007). Characterization of aftershock-fault plane orientations of the 1999 Izmit (Turkey) earthquake using high-resolution aftershock locations, *Geophys. Res. Lett.* **34,** L20306.

Dahm, T., and F. Krueger (1999). Higher-degree moment tensor inversion using far field broad-band recordings: Theory and evaluation of the method with application to the 1994 Bolivia deep earthquake, *Geophys. J. Int.* **137,** 35–50.

Das, S., and B. V. Kostrov (1997). Determination of the polynomial moments of the seismic moment rate density distribution with positivity constraints, *Geophys. J. Int.* **131,** 115–126.

Doornbos, D. J. (1982). Seismic moment tensors and kinematic source parameters, *Geophys. J. R. Astr. Soc.* **69,** 235–251.

Ekstrom, G., A. M. Dziewonski, N. N. Maternovskaya, and M. Nettles (2005). Global seismicity of 2003: Centroid-moment-tensor solutions for 1087 earthquakes, *Phys. Earth Planet. Int.* **148,** 327–351.

Goldberg, D. E. (1989). Genetic Algorithms in Search, Optimization, and Machine Learning, Addison-Wesley, Reading, Massachusetts, 412 pp.

Gusev, A. A., and V. M. Pavlov (1988). Determination of space-time structure of a deep earthquake source by means of power moments, *Tectonophysics* **152,** 319–334.

Kagan, Y. Y. (1988). Multipole expansions of extended sources of elastic deformation, *Geophys. J.* **93,** 101–114.

Kubo, A., E. Fukuyama, H. Kawai, and K. Nonomura (2002). NIED seismic moment tensor catalog for regional earthquakes around Japan: Quality test and application, *Tectonophysics* **356,** 23–48.

McGuire, J. J., L. Zhao, and T. H. Jordan (2001). Teleseismic inversion for the second-degree moments of earthquake space-time distribution, *Geophys. J. Int.* **145,** 661–678.

McGuire, J. J., L. Zhao, and T. H. Jordan (2002). Predominance of unilateral rupture for a global catalog of large earthquakes, *Bull. Seismol. Soc. Am.* **92,** no. 8, 3308–3317.

Miller, A. D., G. R. Foulger, and B. R. Julian (1998). Non-double-couple earthquakes. 2. Observations, *Rev. Geophys.* **36,** 551–568.

Özalaybey, S., M. Ergin, M. Aktar, C. Tapırdamaz, F. Biçmen, and A. Yörük (2002). The 1999 Izmit earthquake sequence in Turkey: Seismological and tectonic aspects, *Bull. Seismol. Soc. Am.* **92,** no. 1, 376–386.

Pondrelli, S., A. Morelli, G. Ekström, S. Mazza, E. Boschi, and A. M. Dziewonski (2002). European–Mediterranean regional centroid-moment tensors: 1997–2000, *Phys. Earth Planet. Int.* **130,** 71–101.

Sipkin, S. A., and M. D. Zirbes (2004). Moment-tensor solutions estimated using optimal filter theory: Global seismicity, 2002, *Phys. Earth Planet. Int.* **145,** 203–217.

Stich, D., C. J. Ammon, and J. Morales (2003). Moment tensor solutions for small and moderate earthquakes in the Ibero-Maghreb region, *J. Geophys. Res.* **108,** 2148.

Sokos, E., and J. Zahradnik (2008). ISOLA a Fortran code and a Matlab GUI to perform multiple-point source inversion of seismic data, *Comput. Geosci.* **34,** 967–977.

Vavryčuk, V. (2001). Inversion for parameters of tensile earthquakes, *J. Geophys. Res.* **106,** no. B8, 16,339–16,355.

Institute of Geophysics
Academy of Sciences of the Czech Republic
Boční II 1401
14131 Praha 4
Prague, Czech Republic

Manuscript received 7 December 2008

Bulletin of the Seismological Society of America, Vol. 103, No. 5, pp. –, October 2013, doi: 10.1785/0120130014

Disputable Non-Double-Couple Mechanisms of Several Strong Earthquakes: Second-Degree Moment Approach

by Petra Adamová and Jan Šílený

Abstract The earthquake source mechanism (description of the geometry of the source and its strength in terms of forces equivalent to rupturing of the rock mass) is routinely modeled as a moment tensor (MT) describing the earthquake focus as a point. However, sometimes this approximation is not satisfied, and seismic radiation keeps the directivity due to the finite extent of the source. Inversion into the MT then may yield a biased mechanism. Synthetic study in the Adamová and Šílený (2010) demonstrated the appearance of spurious non-double-couple components in the mechanism even for a pure double-couple (DC) source. Their method was designed to reduce the spurious source components by using the second-degree moments to evaluate their contribution into the records and subtract it from the data. Here we applied the procedure to five moderate to large regional events with large nonshear components. They are mostly located on large tectonic faults where predominantly pure shear slip is expected. We studied one event on the prominent North Anatolian fault, three events in the Pacific area, and one event in Bolivia. In most cases, the non-DC components essentially were reduced, and the geometry of the mechanism remained largely unchanged. This confirms the hypothesis that part of the non-DC components in regional MT solutions may be spurious due to the neglect of the source finiteness in the routine procedure of the MT retrieval. In addition, the geometrical and kinematical characteristics of the foci provided by the second-degree moments (the source ellipsoid and rupture velocity vector) are mostly consistent with the fault geometry, aftershock distribution, and estimates of rupture speed from available previous studies.

Introduction

The mechanism is an important characteristic of an earthquake, providing the first insight into the physics of the source in terms of a description of the geometry of forces in the rock mass continuum, which generates the same wavefield as the rupture. Since the 1970s, several agencies have been determining moment tensors (MT) of earthquakes from moderate to strong events ($M_w > 5$). Applying the concept of the MT expands the earthquake focus description from the fault-plane solution corresponding to a shear slip along the fault plane to more general types of dislocation. The force equivalent of a pure shear slip is a double couple (DC, for a planar fault within an isotropic medium), while general types of dislocation imply appearance of non-DC components. The MT approach in the retrieval of an earthquake mechanism has become a standard, replacing the formerly universal description of the source by a DC. Using the full MT, we can study some of the physical features of the source in addition to the geometrical characteristics described by the traditional fault-plane solution. Major seismological agencies, such as Global Centroid Moment Tensor (Global CMT; Ekström *et al.*, 2005), U.S. Geological Survey (USGS; Sipkin and Zirbes, 2004), and Schweizerischer Erdbebendienst (SED; Bernardi *et al.*, 2004), routinely evaluate MT, though they are usually constrained to be purely deviatoric in order to obtain stable solutions. Until recently, the seismological and geological community has been requesting mostly the DC component for the purpose of tectonic studies; however, the retrieved non-DC is receiving increasing attention now. Nevertheless, the main reason for a description of the earthquake source by the MT is the linearity of the inversion, while constraining to the DC yields a nonlinear problem. The deviatoric constraint (zero MT trace, or zero isotropic component, then the remaining non-DC component is only the compensated linear vector dipole [CLVD]), routinely applied in the agency solutions, keeps the linearity of the task and at least partially expands the description of the dislocations in the focus. It can, however, distort the retrieved "best DC," so that it does not represent the optimum estimate of the genuine DC in the focus (Henry *et al.*, 2002). It is well known that retrieval of non-DC components is vulnerable to several factors violating

the setup of the inverse task: mislocation of the hypocenter, mismodeling of the velocity profile, noise contamination of the data, and quality of the station distribution (Henry *et al.*, 2002; Šílený, 2009). In such cases, the non-DC components determined can simply be artifacts of an ill-posed inversion. It is very important to properly estimate which part is spurious and which is related to the source. The assessment of the latter is highly significant from the viewpoint of fracture mechanics. From the non-DC components, we can distinguish between a tensile crack or the collapse of a void space on one side and the shear along a pre-existing fault on the other.

Non-DC components have been widely studied during recent years. They can be originated by several effects (Julian *et al.*, 1998; Miller *et al.*, 1998): (1) processes involving net forces such as landslides, volcanic eruptions, and unsteady fluid flow; (2) complex shear faulting, such as multiple shear events, volcanic ring faults, and Ortlepp shear fault (Ortlepp, 1984); and (3) tensile faulting, such as opening of tensile cracks as the effect of migration of pressurized fluids, combined tensile and shear faulting (Dufumier and Rivera, 1997; Vavryčuk, 2001; Šílený and Milev, 2008), and shear faulting in an anisotropic medium (Kawasaki and Tanimoto, 1981). In terms of fracture mechanics, tensile faulting may be expected for events induced by industrial activities involving fluid injection to fracture the rock mass in the vicinity of boreholes (e.g., during hydrofracturing in oil and gas wells; Šílený *et al.*, 2009), during geothermal energy exploitation (Jost *et al.*, 1998; Julian *et al.*, 2010), or during hydrofracturing of deep research boreholes (Vavryčuk *et al.*, 2008). Tensile faulting also may be important in foci of natural seismic events, mainly for some small intraplate earthquakes (Horálek *et al.*, 2002; Vavryčuk, 2011). On the other hand, strong events representing a slip along a large fault are mostly shear, and tensile faulting is probably less relevant here. If some non-DC components occur in these cases, they may be suspected to be spurious.

In the catalogs of MTs collected by seismological agencies, many events—even strong earthquakes—are reported as possessing a noticeable percentage of the CLVD, which is assumed to have originated mostly by unmodeled 3D Earth structure (Henry *et al.*, 2002; Ferreira and Woodhouse, 2006). We studied the generation of the false non-DC components in frequencies corresponding to regional data, hypothesizing that they are due to inverting records from a finite-extent source by the standard MT approach. In the synthetic example, we demonstrated that even after substantial low-pass filtering, a directivity remains in the radiation that is converted into spurious non-DC components in the standard MT approach (Adamová and Šílený, 2010).

In this paper, we aim to demonstrate this effect on real data. We apply the method of second-degree moments (SDM) to several moderate to strong earthquakes that exhibit a considerable percentage of non-DC components in the mechanism: three events from the Pacific, one event on the North Anatolian fault, and one event from Bolivia. The SDM approach is a convenient alternative to a detailed modeling of slip distribution, for which the data are not available in many cases; at least the rough information on the source finiteness provided by the SDM is valuable. In terms of the SDM, we can estimate several finite source parameters from the point-source approximation: geometry of the source, duration of the source process, temporal–spatial centroid, and rupture velocity vector. One of the greatest benefits of the SDM is obviously its capacity to distinguish the fault plane from the couple of nodal planes just by comparing the retrieved source ellipsoid to the fault-plane solution. It has been demonstrated in particular case studies (including those by Gusev and Pavlov (1988), who demonstrated the approach on a moderate deep earthquake, and by McGuire (2004) and Chen *et al.* (2010), who were dealing with resolving the fault-plane ambiguity for small earthquakes) and is implicit in the study by McGuire *et al.* (2002) in their determination of the unilateral versus bilateral rupture propagation for a set of $M_w > 7$ earthquakes. With the aim of assessing the effect of the source finiteness on the mechanism, we evaluate both the standard MT and the SDM and compare them with the agency catalogs and available evidences from geology. We also draw comparisons between SDM parameters and the aftershock distribution published in available literature. We show that after removing the SDM effects from the data, the amount of the non-DC part of the mechanism is reduced, which indicates that it may be an artifact of the source directivity that is neglected in the standard MT approach. It is important to note that this effect is supposed to take place in regional source inversions, where waveforms with periods ranging across tens of seconds are inverted. The Global CMT solutions are retrieved using data with periods typically up to the first hundreds of seconds: they use periods of 35–40 s for body waves, periods around 50 s for surface waves, and periods of 150–200 s for mantle surface waves. At these periods, the source finiteness is expected to have much smaller effect than in inversion from regional data. Spurious non-DC components in a Global CMT solution are likely due to unmodeled 3D inhomogeneities (Henry *et al.*, 2002; Ferreira and Woodhouse, 2006). Importance of the proper modeling of the medium in periods relevant to regional distances was demonstrated by Covellone and Savage (2012); they compared unconstrained MT inversions by 1D versus 3D velocity models and showed that in the periods of 25–125 s there is a notable deficit of 1D mechanisms, with high DC percentage compared to the 3D solutions. This means that in the former there was a statistically higher content of non-DC components.

Method

The first papers about higher-degree moments were published by Backus (1977a,b). After this pioneering work, the concept of higher-degree moments was developed by several authors in the early 1980s (Doornbos, 1982; Stump and Johnson, 1982). We follow the approach of Doornbos

(1982). We describe seismic displacement using representation theorem. When we express it in second-degree terms (i.e., we apply the Taylor expansion up to degree 2), we obtain a description of seismic source parameters in a nonlinear way. Applying Doornbos's notation, we can separate the standard MT solution (M_{ij}) and second-degree terms:

$$u_i(x,t) = M_{jk}[G^i_{j,k} - \dot{G}^i_{j,k}\Delta\tau + G^i_{j,kl}\Delta\xi_l + \frac{1}{2}\ddot{G}^i_{j,k}\Delta(\tau^2) - \dot{G}^i_{j,kl}\Delta(\tau\xi_l) + \frac{1}{2}G^i_{j,klm}\Delta(\xi_l\xi_m) + \cdots], \quad (1)$$

in which M_{ij} is the zero-degree moment (six parameters) standard MT describing the mechanism of an instantaneous source. The others are second-degree moments: temporal centroid $\Delta\tau$, spatial centroid $\Delta\xi_l$, temporal–spatial moment $\Delta(\tau\xi_l)$, double temporal moment $\Delta(\tau^2)$, and double spatial moment $\Delta(\xi_l\xi_m)$. $G^i_{j,k}(\mathbf{x},\xi,\mathbf{t},\tau)$ is the response function (RF), $\dot{G}^i_{j,k}(\mathbf{x},\xi,\mathbf{t},\tau)$ the time derivative of RF, $G^i_{j,kl}(\mathbf{x},\hat{\mathbf{l}},\mathbf{t},\tau)$ the spatial derivative of RF, $\ddot{G}^i_{j,k}(\mathbf{x},\xi,\mathbf{t},\tau)$ the second time derivative, $\dot{G}^i_{j,kl}(\mathbf{x},\xi,\mathbf{t},\tau)$ the combination of the time and spatial derivative, and $G^i_{j,klm}(\mathbf{x},\xi,\mathbf{t},\tau)$ the second spatial derivative. Second-degree moments have the following physical interpretation: temporal centroid, spatial centroid, rupture propagation vector, source process duration, and geometrical characteristic of the source (for details see Adamová and Šílený, 2010).

Throughout the computation, we work in the time domain and use complete waveforms in the inversion. In the first step, we compute zero-degree (standard) MT in the low frequency range. In the second step, we estimate second-degree terms at a frequency range beyond the low frequency plateau. We use a genetic algorithm with an additional constraint to keep the 4D (temporal–spatial) volume of the focus nonnegative (McGuire *et al.*, 2002). In other words, we keep the following matrix positive semidefinite:

$$\begin{bmatrix} \Delta(\xi\xi) & \Delta(\tau\xi)^T \\ \Delta(\tau\xi) & \Delta(\tau^2) \end{bmatrix}. \quad (2)$$

This matrix contains three terms from Doornbos's notation:

- $\Delta(\xi\xi)$ is a term related to the source ellipsoid.
- $\Delta(\tau\xi)$ is a temporal–spatial term related to the average velocity on the fault.
- $\Delta(\tau^2)$ is a term related to the source duration.

Green's functions (GF) are computed using the discrete wavenumber (DWN)/reflectivity code AXITRA (Bouchon and Coutant, 1994), modified by Sokos and Zahradník (2008). The GF derivatives in equation (1) are evaluated by numerical differentiations that replace the analytical derivatives. Numerical derivatives require setting a differential step. In order to choose this, we took into account the following facts. We employ frequencies up to 0.2 Hz (we use a different frequency range for each event, but for all of them we are slightly below 0.2 Hz; i.e., we work with wavelengths around 20 or 30 km). Roughly a quarter of a wavelength (approximately 5–7 km) constitutes the upper limit for the differential step. The lower limit is related to the precision of evaluation of seismograms by the DWN method. We evaluated derivatives for the set of trial values of the differential step ranging from 100 to 5 km. Within the approximate interval of 300–1000 m, we observed that the derivative was stable, so we fixed the differential step at the value of 500 m. We applied the same methodology as Adamová and Šílený (2010) for our SDM approach.

Applications: Standard MT

We selected five strong earthquakes with a large non-DC component in the Global CMT solution (Fig. 1): Izmit (17 August 1999 at 00:01:50.1, M_w 7.6, CLVD = 16%), Solomon (12 June 2003 at 08:59:23.9, M_w 6.2, CLVD = 79%), Kobe (16 January 1995 at 20:46:59.4, M_w 6.9, CLVD = 29%), the Tohoku aftershock (7 April 2011 at 14:32:51.4, M_w 7.1, CLVD = 19%), and Bolivia (17 November 2005 at 19:27:0.0, M_w 6.8, CLVD = 25%). Global CMTs are retrieved from long-period waves ranging from periods of about 50 s for body waves to 125–350 s for mantle surface waves, while our MTs are determined from low-pass filtered regional records in the 20–50 s range. Therefore, the MT solution (including its non-DC content) need not be necessarily the same. In addition, we determine a complete MT, while the Global CMT is constrained to be deviatoric (i.e., its non-DC component is represented only by a CLVD).

For the construction of the GFs, we used 1D velocity models with an earth-flattening approximation. Because regional models for individual localities mostly were not available, we applied the Iasp91 model (Kennett and Engdahl, 1991) for the Kobe and Solomon earthquakes, the Tohoku aftershock, and the Bolivia earthquake. The only exception within our set is the Izmit earthquake, for which the regional model derived by Bulut *et al.* (2007) is available (Fig. 2).

As is usual in the task of mechanism retrieval, the key issue is the pattern of distribution of the stations with respect to the epicenter. Apart from the effort to invert data from stations with similar epicenter distances, this was the principal criterion in selecting suitable events for the study. Of course, there is not enough data to achieve a regular and dense coverage of the focal sphere by the station projections; nevertheless, the configurations for the events selected represent still reasonable setups. For individual events, from five to eight stations are available with gaps in azimuth. In the cases of the Bolivia and Izmit earthquakes, we have a gap of approximately 180°; for the other events this gap doesn't exceed 90°.

To retrieve the MT analogous to the Global CMT solution (hereafter referred to as the standard MT), we invert the regional records in the low-frequency domain to enhance the point-source characteristics. The MT obtained is compared to

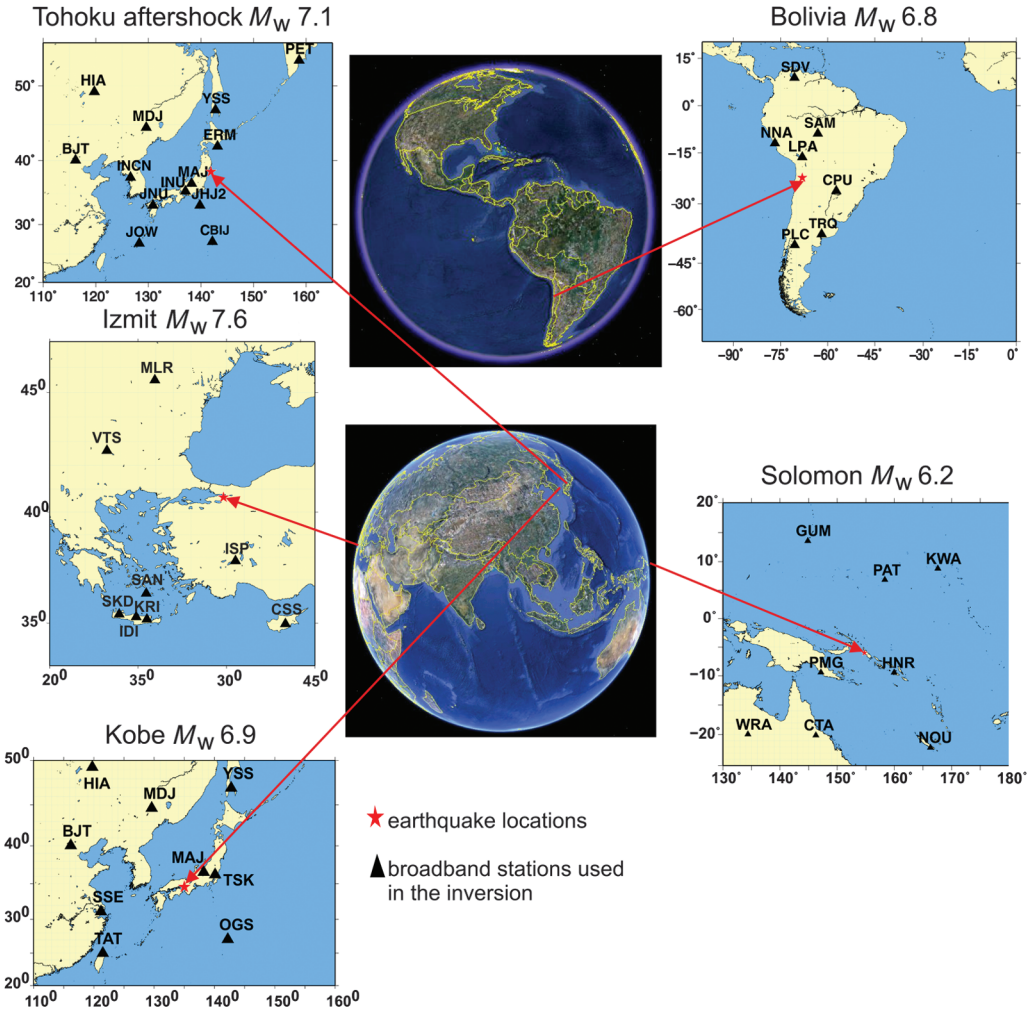

Figure 1. Locations of the earthquakes investigated: 17 August 1999 M_w 7.6 Izmit earthquake; 6 December 2003 M_w 6.2 Solomon earthquake; 16 January 1995 M_w 6.9 Kobe earthquake; 4 July 2011 M_w 7.1 Tohoku aftershock; 17 November 2005 M_w 6.8 Bolivia earthquake.

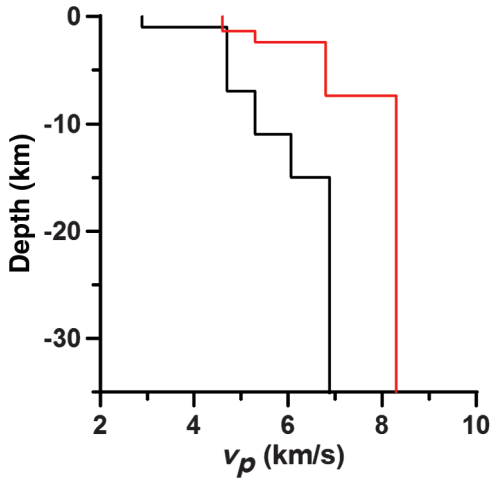

Figure 2. Crustal models applied in the inversion. (Red line, model by Bulut (2007) for the Izmit earthquake; black line, Iasp91 model.)

the Global CMT solution. For each event, we use a different frequency range during the band-pass filtering of the records according to their frequency contents corresponding to the magnitude of the event (Table 1). We invert the complete seismograms (both the body and surface waves together), assuming the hypocenter is in the position of the Global CMT centroid.

Regardless of the difference in the data processed, for four events (Kobe, Izmit, Tohoku aftershock, and Bolivia) we obtained solutions similar to the Global CMT. For the Solomon earthquake, however, our mechanism is almost a DC with only 9% of non-DC components. This difference is probably due to the large difference in the input data sets: the CMT of the Solomon event is the result of inverting 79 worldwide stations (in the frequency range 125–350 s), while our MT is determined from records of 8 stations only (filtered as specified in Table 1). We nevertheless process this event as well, just to verify that the non-DC content in the solution corrected for the effect of the source finiteness remains low.

Table 1
Frequency Ranges Used for Standard MT Inversion and for Second Degree Moment (SDM) Inversion

Event	Frequency Range [Hz] Standard MT	Frequency Range [Hz] SDM
Kobe	0.02–0.04	0.02–0.12
Izmit	0.02–0.04	0.02–0.08
Solomon	0.02–0.04	0.02–0.15
Tohoku	0.02–0.04	0.02–0.08
Bolivia	0.02–0.04	0.02–0.12

Fault-plane solutions corresponding to the Global CMT and the standard MT are similar for most events (Fig. 3). Deviation in the directions of the nodal lines remains below about 20°. Such dissimilarity is acceptable, taking into account the difference in the input data mentioned above. Also, the match of the synthetics, as constructed with the final MT, to the data is fairly good (see the variance reduction in Table 2).

16 To assess the credibility of our solutions, we checked their robustness using a jackknife test. In turn, we exclude a single station from the set of stations and recompute the standard MT from the remaining stations. We applied the jackknife test for the Izmit and Kobe earthquakes, for which we have sufficient number of stations; in the case of the other earthquakes, the jackknife trials unfortunately would not reasonably represent overdetermined inversions. For Kobe, excluding the nearest station (MAJ) yields a different solution from that derived from all the stations. In contrast, excluding any of the more distant stations results in nearly the same solution as when using all stations. This indicates the crucial importance of the nearest station in the inversion. For the Izmit earthquake, we observed a similar feature (the nearest station is SAN; Fig. 4). Moreover, for this event we obtained a dual solution yielded by the data set lacking the CSS station: the variance reduction differs by less than 1%. In addition, for the Kobe earthquake, we performed an additional jackknife trial: we inverted the data from just the two nearest stations. The results indicate their importance for the retrieval of the mechanism, as both the resulting MT and the quality of the match of the synthetics to the data are very similar to the solution obtained from the complete data set. Thus, to obtain a good estimate of the standard MT for the Kobe earthquake, it is sufficient to consider only the two closest stations. This is, however, not the case with the second-degree moments, for the retrieval of which we need more stations in different azimuths.

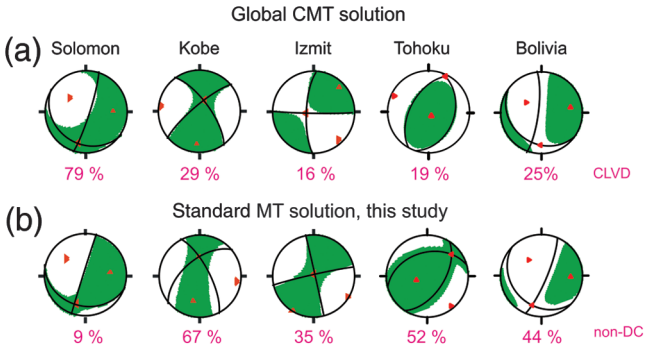

15 **Figure 3.** Focal mechanisms of selected earthquakes. Top: Global CMT solution with the percentage of the non-DC component. Bottom: standard MT solution of this study (frequency range 0.02–0.04 Hz). The decomposition of the standard complete MTs in this study was done according to Vavryčuk (2001), which for deviatoric MTs yields the same percentage as the decomposition applied in the Global CMT solutions.

Second Degree Moments

Second-degree moments are the terms in expansion (1) 17 that carry information on finite-extent source properties. Therefore, contrary to the standard MT describing the mechanism of the point source and thus determined from the low-frequency part of the spectrum in the low-frequency plateau, second-degree moments must be retrieved from higher frequencies beyond the plateau. However, we cannot go far beyond the plateau because we are only able to invert relatively simple waveforms due to availability of simple models of the structure. In this tradeoff, we extend the frequency interval for the inversion of the second-degree moments only slightly beyond the plateau by just involving the initial piece of the slope of the spectrum. The frequency range has to be tuned empirically, depending on the magnitude of the event processed (Adamová and Šílený, 2010). With this criterion, for the earthquakes studied, we arrived at the choice of frequency ranges shown in Table 1. Within these frequency ranges for individual events, we invert the 18 data for 14 parameters (spatial centroid, temporal centroid, duration of the source process, average rupture velocity, and source ellipsoid). We successfully followed the two-step procedure of evaluating the standard MT and the SDM for all five events in Table 1.

Kobe Earthquake

The Kobe earthquake (M_w 6.9) occurred on 16 January 1995 in western Japan at a depth of 14 km. Strong ground motions were recorded at a number of seismic stations well around the epicenter and inverted into the slip function distribution along the fault. According to Ide *et al.* (1996), most of the rupture was located southwest of the hypocenter, implying a unilateral propagation of the rupture. There are, however, other estimates favoring bilateral rupture propagation (Yoshida *et al.*, 1996; McGuire *et al.*, 2002). The mechanism is a strike slip with a small thrust component (Ide *et al.*, 1996). We obtained a fairly good agreement between the orientation and shape of the source ellipsoid and the aftershock distribution by Ide *et al.* (1996). The aftershocks are sharply concentrated along a steeply dipping plane striking N52°E; the source ellipsoid in the map view is narrow and stretched in the azimuth of 62° (Fig. 5, Table 2). In the depth view, it is 19

Table 2
53 Second Degree Moments

Event	Variance Reduction*	Temporal Centroid (s)	Source Duration (s)	Spatial Centroid (km)†			Average Velocity Vector (km/s)†			Source Ellipsoid‡				Directivity Ratio
										λ_2/λ_1	λ_3/λ_2	$\Delta 1$ (°)	$\Delta 2$ (°)	
Kobe	0.51	2.	3.5	15.	−4.5	15.	1.8	1.9	0.2	2.2	1.9	62	50	0.28
Kobe (Ide *et al.*, 1996)	x	x	x	x	x	x	2.1	1.8	0.1	2.0	1.8	52	47	x
Izmit	0.52	6.25	7	2.	−8.5	12.	0.2	2.8	0.3	5.6	5.2	76	75	0.93
Izmit (Clévédé *et al.*, 2004)	x	x	15	x	x	x		3.6–4.2		x	x	x	x	x
Solomon	0.55	1.0	5	−6	9	185.	0.6	0.4	3.1	5.8	4.1	−45	10	0.48
Tohoku	0.57	9.5	5	15	3	50.	3.1	0.8	0.1	5.3	4.8	10	25	0.38
Bolivia	0.51	8.5	10	−12	−10	158.	0.4	0.3	3.5	5.2	4.7	77	−18	0.92

*Variance reduction is computed from the formula $\mathrm{var}_{\mathrm{red}} = 1 - \frac{|d-s|_{L_2}}{|s|_{L_2}}$, in which d represents the data and s the synthetic seismograms. Data and synthetics are in frequency ranges from Table 1, second column.

†Spatial centroid and propagation velocity vector in the (north, east, Z) coordinate system. For the Izmit event, the SDM values obtained by Clévédé *et al.* (2004), which were listed explicitly in their paper, are added for the comparison; similarly for the Kobe earthquake processed by Ide *et al.* (1996), we evaluated the SDM from the slip distribution published at the SRCMOD website (see Data and Resources).

‡Concerning the source ellipsoid, the lengths λ_j of its axes are determined and their ratios presented, which illustrate the amount of the eccentricity. Angles $\Delta 1$ and $\Delta 2$ indicate the deviation of the ellipsoid from the north (measured positive towards the east) and from the Z direction, respectively.

wider, indicating that the focal zone is fairly thin and dipping steeply, which corresponds well to the depth distribution of the aftershock hypocenters. Availability of the slip distribution determined by Ide *et al.* (1996) at the SRCMOD website allows us to evaluate the spatial centroid and projection of the source ellipsoid into the fault plane and compare it with the centroid and source ellipsoid obtained in this study (bottom right, Fig. 5). As expected, the centroid related to Ide *et al.* (1996) slip distribution is situated near the center of the high-slip zone. The centroid of this study is shifted to the southwest by only about 5 km so still resides close to the zone of the maximum slip. The ellipse related to Ide *et al.* (1996) and projection of the source ellipsoid of this study exhibit a similar shape. The former one is nearly horizontal; the latter is inclined by only 20° from the horizontal, and their size is very similar (Table 2). The rupture velocity vector determined in this study roughly coincides with the source ellipsoid orientation (the maximum deviation amounts to only 10°) and the estimated velocity is 2.8 km/s. This is in good agreement with corresponding parameters evaluated from the slip distribution by Ide *et al.* (1996); the rupture velocity differs by 0.4 km/s only.

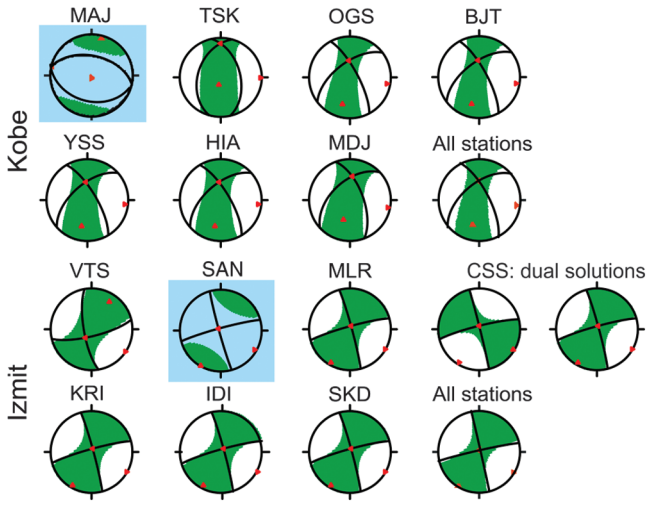

Figure 4. Jackknife test for (top row) the Kobe and (bottom row) Izmit earthquakes. The bottom right part of each panel shows the MT solution derived from all of the stations providing the data (see Fig. 1). The other solutions are MTs from jackknife trials with a single station missing from the data set. In the case of the Izmit earthquake, we obtained the dual solution for the trial with the CSS station missing (difference in the correlation below 1%). Removal of the nearest station is marked by a shaded background.

Izmit Earthquake

A very strong earthquake (M_w 7.6) occurred in 1999 on the North Anatolian fault in Turkey near the town of Izmit. It was the seventh event in the series of earthquakes migrating along the North Anatolian fault (with interevent time intervals ranging from 3 months to 32 years). The earthquake rupturing over a period of 45 s (USGS) was derived from several subsources. The centroid moment tensor (CMT) reported by agencies contains a large amount of the CLVD. In addition to 20
standard CMT retrieval, the event was studied in detail by several authors by using both long-period and high-frequency data.

Clévédé *et al.* (2004) analyzed teleseismic surface waves in the periods 50–100 s and were the first to determine 21
second-degree moments of this earthquake. They performed detailed comparisons of their integral parameters with those derived from slip distributions obtained by several authors from high-frequency data recorded near the fault on one hand and from Global Positioning System (GPS), Synthetic Aper- 22
ture Radar (SAR), and tectonic observations on the other. They showed that, although these slip distributions differ a lot, some of the integral characteristics are similar and can be compared with their long-period solution. Then, by evaluating parameters of equivalent models (i.e., constrained simpli- 23
fied models of slip distribution on the assumed fault plane),

they identified which parameters determine the integral characteristics they decided to compare. Their model, characterized by a relatively short source duration and a high directivity, is between models by Bouchon *et al.* (2002; short duration and small directivity) and Delouis *et al.* (2000; long duration and high directivity). Their smart modeling provides the insight that the long-period data can provide a useful constraint to slip models constructed from detailed high-frequency data.

Our regional records contain higher frequencies: we inverted the range 12.5–50 s (Table 1). To align our integral characteristics into the list considered by Clévédé *et al.* (2004), our SDM model is close to the model by Bouchon *et al.* (2002). We obtained even shorter source duration; however, our directivity of 0.45 is between their value of 0.23 and values of 0.85 (Delouis *et al.*, 2000) and 0.84–0.98 (Clévédé *et al.*, 2004). An important feature of the SDM solution is the orientation of the source ellipsoid. Clévédé *et al.* (2004) determine it in a constrained inversion (major axis constrained within the fault plane) and obtain two equivalent positions inclined ±25° from the horizontal axis of the fault plane. Our ellipsoid is more horizontal but deviates slightly from the east–west direction of the fault (Table 2). The orientation is, in fact, very similar to the ellipses evaluated by Clévédé *et al.* (2004) from various existing slip models derived from high-frequency records and GPS and SAR data (Fig. 6).

Estimate of Error Due to Noise for the Izmit Earthquake. With the aim of estimating the stability of individual SDM parameters retrieved by inversion of the regional waveforms, we simulated an artificial contamination of the records by a noise. We generated random noise from a uniform distribution reaching levels of 20% and 30% of the maximum amplitude and superimposed it onto the records of the Izmit earthquake. We then performed the inversion for five samples of noisy records, assuming both noise levels (Table 3). For the 30% level, the retrieved second-degree moments are scattered widely and imply rather high standard deviations, mainly for the average rupture velocity and source ellipsoid (right-hand column of Table 4). For the 20% noise level, we

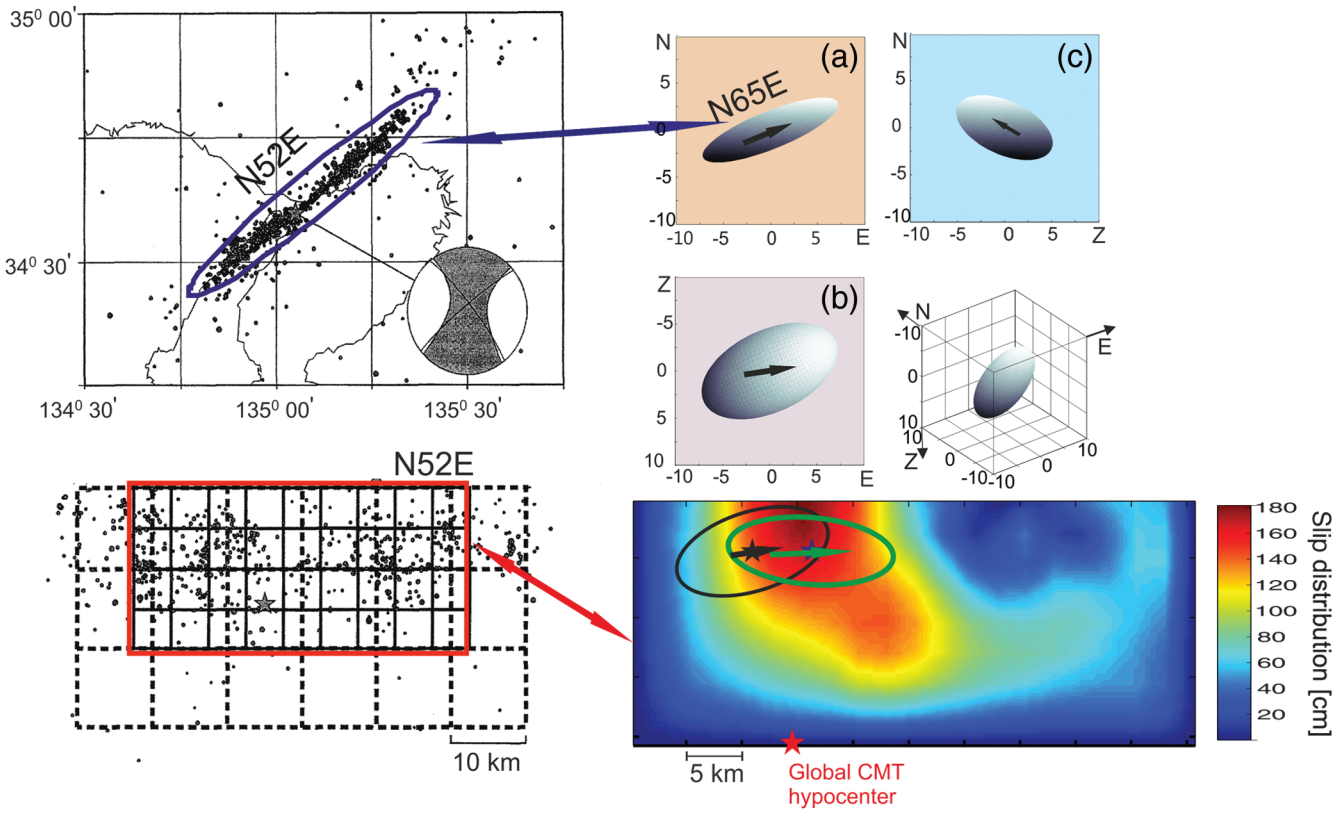

Figure 5. Second-degree moments for the Kobe earthquake. Top left: aftershock distribution by Ide *et al.* (1996), in the plan view framed in blue for comparison to the source ellipsoid on the top right. Bottom left: In this depth view, it is framed in red to compare with the slip distribution in the bottom right. The azimuth of the plane is oriented N52°E. Top right: source ellipsoid in 3D view and its projections (a, map view; b, depth view looking north; c, depth view looking west; and axonometric projection). In the axonometric projection, the coordinate center in the spatial centroid has geographical coordinates of latitude 34.76°, longitude 134.97°, and depth 15 km; the axes are shown in kilometers. The azimuth of the ellipsoid in the map view (a) is oriented approximately N62°E. Bottom right: spatial slip distribution derived by Ide *et al.* (1996; retrieved from the SRCMOD website) and its integral characteristics plotted on the assumed fault plane. The spatial centroid (green star), projection of the source ellipsoid on the fault plane (green ellipse), and the rupture velocity vector (green arrow). Similar black symbols indicate the centroid, source ellipsoid projection onto the fault plane, and rupture velocity vector obtained in this study, respectively. The velocity vector is multiplied by the source duration, thus is in scale to the source ellipsoid.

Table 3
54 SDM from Noisy Records

Noise Sample	Event	Noise Level (%)*	Variance Reduction	Temporal Centroid (s)	Source Duration (s)	Spatial Centroid (km)			Average Velocity Vector (km/s)			Source Ellipsoid†			
												λ_2/λ_1	λ_3/λ_2	$\Delta 1$ (°)	$\Delta 2$ (°)
1	Izmit	30	0.48	6	6.5	2	−7.	11.5	0.5	2.	0.8	4.1	4.7	75	59
		20	0.51	6.1	6.5	2	−8	12	0.3	2.5	0.2	5.3	4.8	77	80
	Tohoku	20	0.40	8.1	7	10	1	55.	2.5	0.4	0.2	4.2	3.1	30	35
2	Izmit	30	0.41	5.7	5.5	1.5	−8.	10.	0.1	3.5	1.1	3.4	7.3	60	79
		20	0.49	6.	7	1	−8.5	11	0.1	2.8	0.1	5.1	4.9	80	72
	Tohoku	20	0.42	7.	4.1	12	−3	52.	2.0	0.1	0.1	3.2	3.5	5	40
3	Izmit	30	0.44	7.	6.3	1	−8.5	13.	0.9	2.2	0.2	7.3	3.5	85	65
		20	0.5	6.4	7	2	−8.	11	0.1	3	0.2	5.8	4.7	73	68
	Tohoku	20	0.38	12.5	10.1	5	8	48	2.5	0.3	0.8	7.1	6.2	30	20
4	Izmit	30	0.45	5.8	8	2.5	−8.	12.	0.1	3	0.8	2.5	4.1	61	53
		20	0.5	6.3	7.5	1.5	−9	13.	0.2	2.7	0.2	5.	5.3	78	69
	Tohoku	20	0.41	8.2	5.8	20	9	45	2.9	0.8	0.2	4.5	4.2	40	50
5	Izmit	30	0.47	6.1	7.5	2	−7.	11.	0.7	2.5	0.5	3.1	4.2	70	45
		20	0.48	6.4	6	2	−7.5	11	0.1	2.5	0.3	5.9	5.1	75	70
	Tohoku	20	0.44	6.1	6.2	16	5	50	3.0	0.5	0.2	5.1	3.5	26	5

*Izmit earthquake with noise contamination amounting to 20% and 30% of the peak data amplitude and Tohoku aftershock with 20% noise.
†Angle $\Delta 1$ is the azimuth of the source ellipsoid orientation measured from the north positive to the east; $\Delta 2$ indicates the deviation of the source ellipsoid from the vertical.

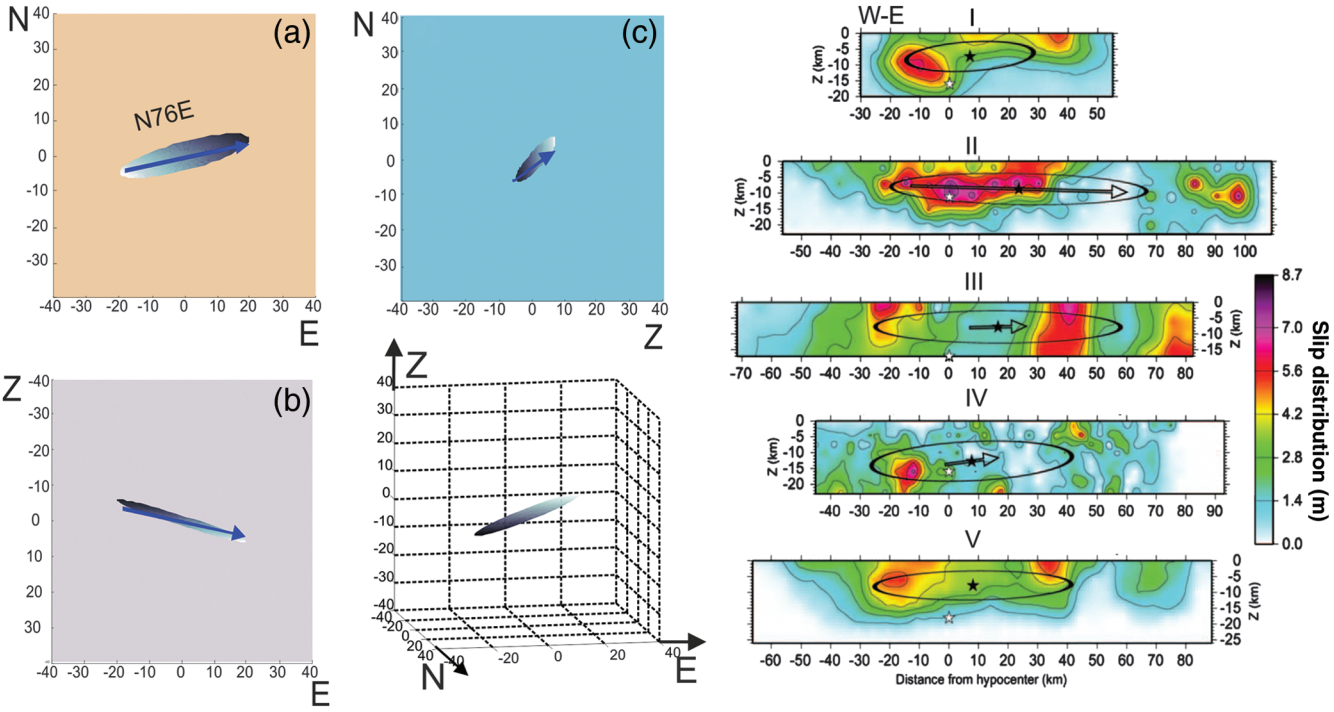

Figure 6. Second-degree moments for the Izmit earthquake. Left: source ellipsoid in 3D view and its projections (a, map view; b, depth view looking north; c, depth view looking west; and axonometric projection), with the coordinate center in the spatial centroid (geographical coordinates: latitude 40.67°, longitude 29.73°, depth 12 km) and axes in kilometers. The azimuth of the ellipsoid in map view is oriented approximately N76°E. The blue arrow indicates the velocity vector in the 3D view; the velocity vector is multiplied by the source duration, thus is in scale to the source ellipsoid. Right: slip distributions from previous papers summarized by Clévédé *et al.* (2004), who complemented them by evaluation of the source ellipse (black) and velocity vector. Panels: I, Yagi and Kikuchi (2000), from body waves + strong motions; II, Delouis *et al.* (2000), from SAR + body waves + strong motions; III, Bouchon *et al.* (2002), from strong motions; IV, Sekiguchi and Iwata (2002), from strong motions; and V, Cakir *et al.* (2003), from GPS, SAR, and tectonic observations. The fault plane in I–V is assumed vertical and oriented east–west (i.e., the direction of the view corresponds to cross section b, bottom left). The coordinate center in the projections on the left corresponds to the black star in maps I–V on the right.

Table 4
55 SDM Deviations Due to Noise Contamination

	Izmit				Tohoku	
Second Degree Moments	20%	30%	Rel. 20%	Rel. 30%	20%	Rel. 20%
Temporal Centroid	0.18	0.52	0.029	0.085	2.46	0.29
Source Duration	0.57	1.	0.08	0.15	2.2	0.33
Spatial Centroid r (km)	1.10	0.96	0.08	0.07	2.78	0.05
Spatial Centroid ϕ (°)	4.38	3.39	0.01	0.01	26.51	1.46
Spatial Centroid Θ (°)	2.36	1.41	0.07	0.04	6.58	0.41
Average Velocity Vector r (km)	0.20	0.59	0.08	0.21	0.43	0.16
Average Velocity Vector ϕ (°)	2.11	9.04	0.02	0.11	3.1	0.35
Average Velocity Vector Θ (°)	1.72	6.3	0.02	0.08	4.45	0.05
Source Ellipsoid: λ_2/λ_1	0.41	1.89	0.075	0.46	1.45	0.30
Source Ellipsoid: λ_3/λ_2	0.24	1.48	0.048	0.31	1.24	0.30
Source Ellipsoid: $\Delta 1$ (°)	2.7	10.2	0.035	0.15	12.9	0.49
Source Ellipsoid: $\Delta 2$ (°)	4.82	12.9	0.067	0.21	17.7	0.59

SDM deviations due to noise contamination of the data of the Izmit earthquake and the Tohoku aftershock: standard deviations of individual SDM parameters evaluated from five samples of noisy records, assuming noise levels 20% and 30% of the peak data amplitude for the Izmit and 20% for the Tohoku events. The spatial centroid and average velocity vector are expressed in spherical coordinates by the absolute value r, azimuth ϕ (clockwise from the north) and inclination Θ (from vertical downward). The "Rel." columns contain the relative values of the standard deviation normalized to the value of the corresponding SDM parameter.

observe a much more stable solution (left-hand column of Table 4) with acceptably small standard deviations. Second-degree moments determined from the noisy data are summarized for both noise levels in Table 3. The results suggest that a level of about 20% is an extreme noise contamination that does not necessarily prevent the reconstruction of the second-degree moments, while 30% is possibly already beyond the limit. Size of the average velocity vector and proportions of the source ellipsoid are biased largely, in relative values above 20% and 30%, respectively.

Solomon Earthquake

The Solomon earthquake (M_w 6.2) occurred on 12 June 2003 in the Pacific area near the Solomon Islands at a depth of 185 km. The geologic and tectonic structure in that area is very complex (Mann and Taira, 2004), and we are not aware of any papers discussing this event in detail. Thus, we cannot compare our results with any previous study. The source ellipsoid we determined is very slim and elongated along a single principal axis, which indicates that the rupture propagated in the single direction. The average rupture velocity is supposed to have a realistic value of 3.2 km/s (Table 2). Moreover, as it is reasonably high above zero, we may thus assume that the propagation was unilateral. The remaining SDM parameters are summarized in Table 2 and in Figure 7.

The event is of an intermediate depth, and from this viewpoint the occurrence of a noticeable non-DC component need not be surprising. Kuge and Kawakatsu (1993) demonstrated several events from this depth range that have consistent non-DC and argued this was unlikely to have been caused by unmodeled propagation effects or an instability of the inversion procedure. In comparison, our solution is mostly DC and remains such even after correcting for the SDM. This suggests that the source finiteness is of a minor influence on the mechanism in this case. The non-DC percentage itself is difficult to discuss anyway. Taking into

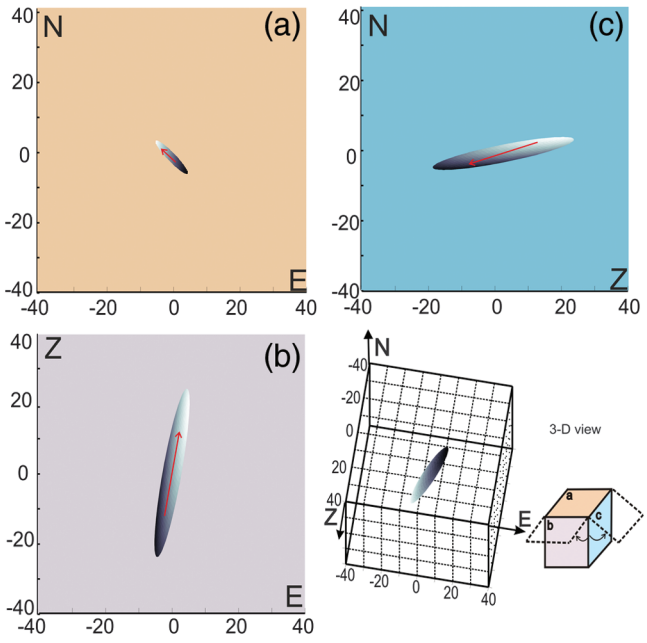

Figure 7. Solomon 2003 earthquake: source ellipsoid in 3D view and its projections (a, map view; b, depth view looking north; c, depth view looking west, and axonometric projection), with the coordinate center in the spatial centroid (geographical coordinates: latitude −6.04°, longitude 154.86°, depth 185 km) and axes in kilometers. The velocity vector (red arrow) is in scale to the source ellipsoid. Box at bottom right: scheme of the projections (a)–(c) of the 3D ellipsoid.

account the depth of the event, the non-DC component may be real; on the other hand, for the same reason, we cannot be sure that, in the frequencies of the regional data, we are able to accurately model the velocity structure up to this depth.

Tohoku Earthquake Aftershock

The aftershock of the large Tohoku earthquake (11 March 2011, M_w 9.1) occurred on 7 April 2011 (M_w 7.1) at a depth of 53 km about 60 km to the west of the mainshock. 27 Standard MT obtained from regional records is very similar to the Global CMT solution, apart from the non-DC part, which in our solution, is significantly larger than in the Global CMT. Similar to the Solomon 2003 earthquake, the SDM yield a very slim source ellipsoid (in this case oriented nearly vertically; Fig. 8) and rupture velocity of 3.1 km/s (Table 2). The value of the directivity ratio $d = 0.38$ (Table 2) indicates a unilateral propagation of the rupture. For the event, the jackknife test with noise contamination amounting to 20% was performed, which indicated rather low stability of the reconstructed SDM (see the Bolivia Earthquake section).

Bolivia Earthquake

An M_w 6.8 earthquake occurred on the border of Bolivia and northern Chile on 17 November 2005 at a depth of 155 km. The earthquake was centered 110 kilometers east of Calama, Chile, in the Potosi region of Bolivia. Standard MT was evaluated by inverting regional records of seven stations around South America (Fig. 1, top right) and displays a good similarity to the Global CMT as concerns the fault-plane solution, while the amount of non-DC components differs somewhat (Fig. 3); both values are, however, large enough. The 28 SDM imply a narrow source ellipsoid steeply dipping northeast (Fig. 9), which seems to be realistic, taking into account the scheme of the subduction in the area. We are not able to check it independently, as no relevant studies of this earthquake are available.

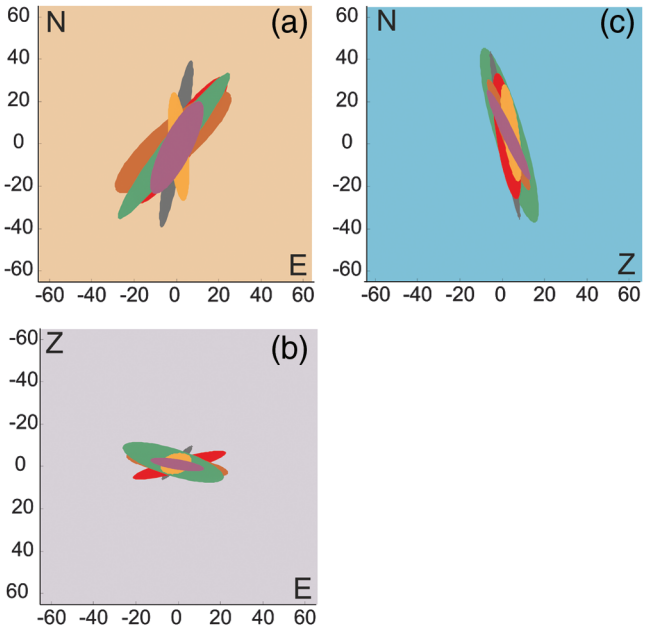

Figure 8. Aftershock of the Tohoku 2011 earthquake: source ellipsoids from noise-free data (gray) and from five realizations of noisy data (colors). Records contaminated by random noise reaching 20% of peak data amplitude. Source ellipsoids in 3D view and its projections (for details, see the caption for Fig. 7); geographical coordinatesare latitude 38.5°, longitude 141.92°, and depth 50 km.

Removing Spurious Non-DC

The aim of this study is to discuss the non-DC content in the mechanism of selected strong earthquakes and check its possible bias due to neglect of the finite-source effects in the seismograms inverted by means of standard MT (i.e., assuming a point source). Thus, we evaluate the contribution of the finite-source effects (which we describe by the second-degree moments) to the seismograms and subsequently subtract it from the data. These records, corrected for the source finiteness in this way, are the data that should be matched by the standard MT retrieval. The approach is described in detail by Adamová and Šílený (2010), whereby the decrease of the spurious non-DC part of the mechanism is demonstrated using the SDM methodology on synthetic data.

For five strong earthquakes selected (Solomon 2003, Kobe 1995, Izmit 1999, Tohoku aftershock 2011, and Bolivia 2005), we reduced the initially mostly large non-DC component. Contrary to the Global CMT solution (possessing 29

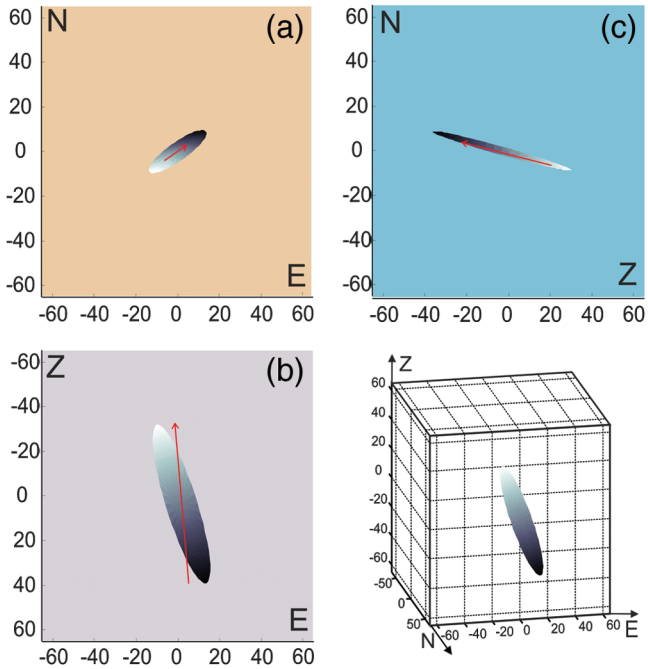

Figure 9. Bolivia 2005 earthquake: source ellipsoid in 3D view and its projections (for details, see the caption for Fig. 7; geographical coordinates are latitude −22.46°, longitude −68.13°, and depth 155 km.

Table 5
MT Parameters

Event	Strike (°)	Dip (°)	Rake (°)	Non-DC (%)	Variance Reduction
Kobe	232/324	73/86	176/17	67	0.46
	229/324	67/78	167/24	8	0.60
Izmit	347/257	89/87	3/180	35	0.43
	164/74	80/88	2/170	8	0.78
Solomon	111/20	29/89	−178/−60	9	0.51
	110/18	30/88	−177/−59	9	0.55
Tohoku	32/254	56/42	64/123	52	0.45
	1/213	82/8	85/122	10	0.66
Bolivia	23/134	79/28	−64/−156	44	0.48
	28/150	78/23	−71/−146	29	0.57

Parameters of the moment tensor: fault-plane solution (strike, dip, and rake values evaluated for both nodal planes) and percentage of the non-DC component, together with the corresponding variance reduction. Standard evaluation: The first line for each event involved retrieval by inverting the records, from which the effects of the second-degree moments (second line) were removed. For the evaluation of the variance see the footnote to Table 2. Frequency range for the MT determination: 0.02–0.04 Hz.

as much as 79% of CLVD), for the Solomon 2003 earthquake, we obtained a low non-DC (9%) in the MT from regional records. We applied the procedure of removing the spurious non-DC to this event as well to check its stability; the mechanism remained nearly unchanged, which indicates that the procedure works well. The remaining events (Kobe 1995, Izmit 1999, Tohoku aftershock 2011, and Bolivia 2005) exhibit a notable non-DC in both Global CMT and the MT from regional data. After extracting the SDM contribution from the data, the non-DC component is reduced significantly; it drops by 30% at least (excluding the Bolivia 2005 event, where it decreased by 15%; Table 5). The fault-plane solution is not changed much (i.e., the orientation of the DC remains stable; Fig. 10). At the same time, the match of the synthetics to the data is improved throughout the procedure, and substantially so for the Izmit and Kobe earthquakes (Table 5; see examples in Figs. 11–13). The only exception is the Tohoku aftershock. To explain the change, we performed a study of stability of the solution here and compared it with the others, which behave properly. We

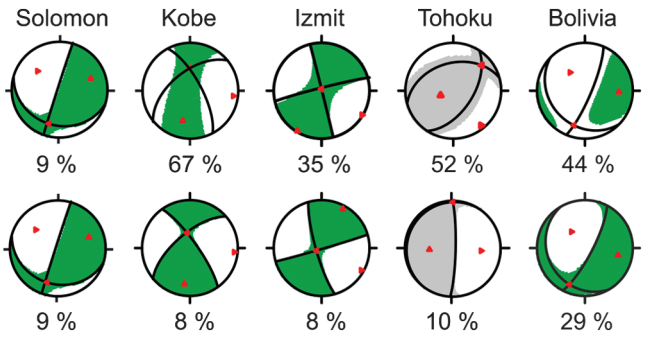

Figure 10. Removal of the spurious non-DC component due to source finiteness from the mechanism. Top: standard MT solution from the long-period regional data. Bottom: reprocessed MT solution from records after removing the SDM effects.

did a sensitivity study of the second-degree moments by perturbing the data randomly; we assumed a noise contamination of the Tohoku records, similar to that described for the Izmit data (see Second Degree Moments section). For Izmit, we investigated the distortion of the second-degree moments when contaminating the records, in turn, by noise reaching 20% and 30% of the maximum in the record and concluded that the former level is still acceptable while the latter harms the solution severely. Taking into account this behavior in the case of Izmit, we made the same test with the Tohoku data, assuming the lower level of contamination. While 20% noise was acceptable for Izmit, it destroyed the resolution in the case of Tohoku (Tables 4, 5; Fig. 8). We conclude that the solution for Tohoku is less stable, providing possibly biased second-degree moments and, consequently, a biased procedure of reconstruction of the standard MT as well. This case suggests that the stability of determination of the second-degree moments should be checked anyway, and the result of the mechanism "correction" assessed accordingly.

Discussion and Conclusion

The second-degree moment approach brings additional information to the standard MT: estimate of the geometry of the source zone expressed by the source ellipsoid, duration of the source process, temporal–spatial centroid, and vector of average velocity of the rupture propagation. Using this methodology, we studied five events possessing a noticeable non-DC component and for all of them obtained the SDM estimates. By modeling synthetic noise at different levels, in the setup of the Izmit 1999 earthquake it appears that 30% noise level (related to the peak amplitude within the record) already disables the SDM retrieval. In our exercise, the noise was simulated using a computer generator of pseudorandom numbers and filtered accordingly. Real noise is certainly different, but we assume that its particular characteristics are of

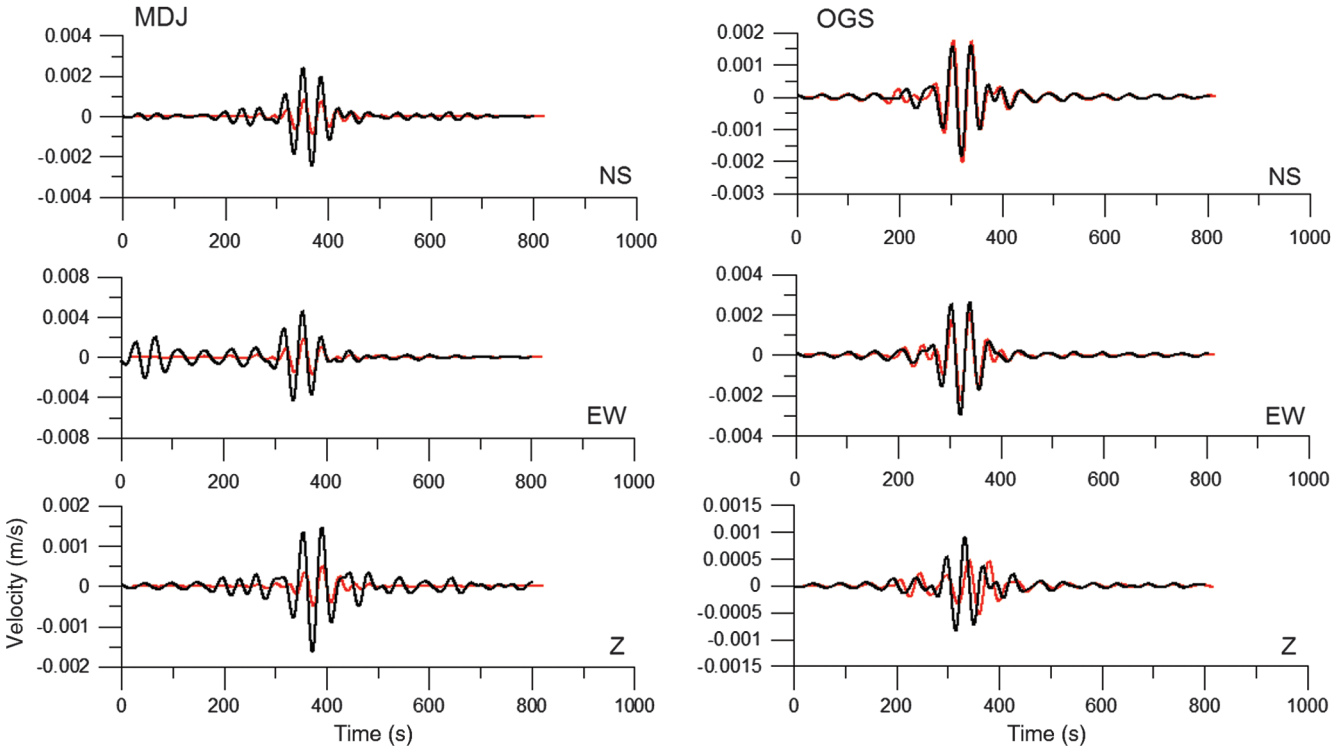

Figure 11. Observed records (black) at stations MDJ and OGS for the Kobe 1995 earthquake and synthetic seismograms (red) corresponding to the standard MT. Frequency range $f = 0.02$–0.04 Hz.

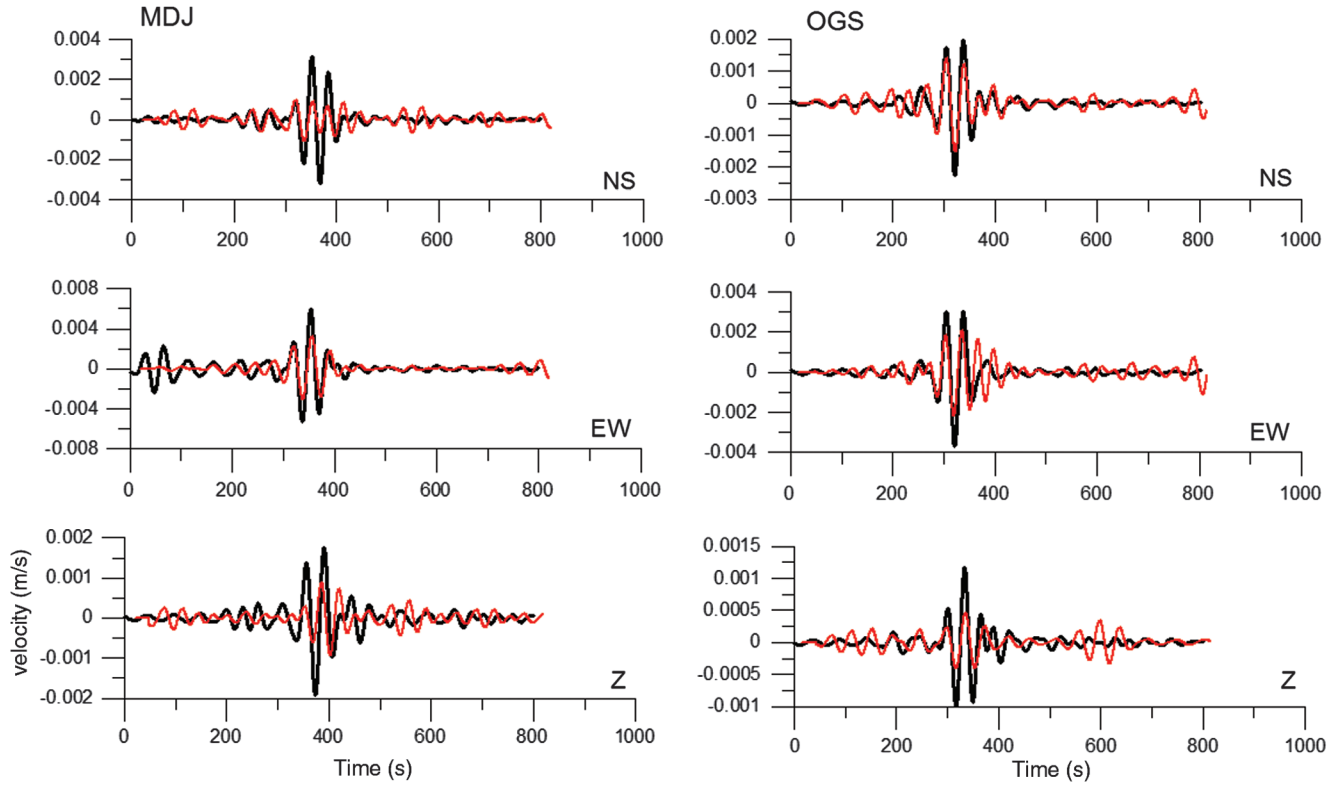

Figure 12. Observed records (black) and synthetic seismograms (red) from stations MDJ and OGS for the Kobe 1995 earthquake, corresponding to the MT up to degree 2. Frequency range $f = 0.02$–0.12 Hz.

a minor effect compared to the amplitude of the contamination.

Similar to the earthquake mechanism retrieval, major factors influencing determination of the SDM are the geometry of the observation and availability of a sufficiently accurate GF necessary in the inverse task. The requirement for the quality of the distribution of seismic stations providing the records to be inverted with respect to the earthquake focus is obvious: the finiteness of the focus is expressed first in the directivity of the seismic-wave radiation, which can be tracked only if observation from different azimuths is available. This is a big problem with regional data for the simple reason of geography of the continents and surrounding ocean areas. Although we tried to retrieve the maximum number of suitable records in each particular case from the Incorporated Research Institutions for Seismology (IRIS), resulting data sets are rather sparse. In the case of the Bolivia and Izmit earthquakes, the maximum gap in the azimuth is as high as about 180°; for the others it does not exceed 90°. Inaccuracy of the GF results from an error in the location of the hypocenter or from using a velocity–attenuation model, which may be a rough approximation only of the properties of the medium in the particular zone under study. We tested the effect of mislocation on the synthetic example in a previous paper (Adamová and Šílený, 2010), but the modeled error in the localization was rather small (1 and 2 km in horizontal and vertical coordinates, respectively, in the configuration of the Izmit 1999 earthquake observation). To be more realistic, we reconsidered the test but with the values 3 and 5 km. We obtained a solution that is comparable with the previous test; the error of the SDM parameters is similar (with the difference below 2%). Accuracy of the velocity–attenuation model is the crucial issue in both the MT and SDM retrieval; in the latter, accuracy is even more urgent as frequencies beyond the plateau must be processed. While even rough 1D models 32
are sufficient in the low frequencies exploited for the Global CMT, their application may be disputable for the inversion of regional records (typically between 0.02–0.1 Hz). Covellone and Savage (2012) demonstrated the bias of unconstrained MT obtained by a 1D velocity model: compared to the 3D solutions, there are more non-DC components there and their 33
percentage below about 20% should not be trusted to be a source effect. Therefore, detailed 3D models for particular zones of interest would be optimum, but, to our knowledge, they are mostly not available. Available regional models are 1D as a rule, and in many cases there is no alternative to using a global 1D model such as Iasp91. Then, only sufficiently large non-DC content exceeding about 20% must be considered in the suggested study of the connection non-DC 34
versus source finiteness. With little or no information on the accuracy of a global 1D model for the particular region, the error of the retrieved SDM cannot be estimated by a standard routine of error propagation from the medium into the source, but by crude resampling approaches only. We performed the jackknife test to explor the MT retrieval for the Kobe and Izmit earthquakes, and the results were satisfactorily robust. There are many more parameters to be determined with the SDM than in the MT; thus, with only few

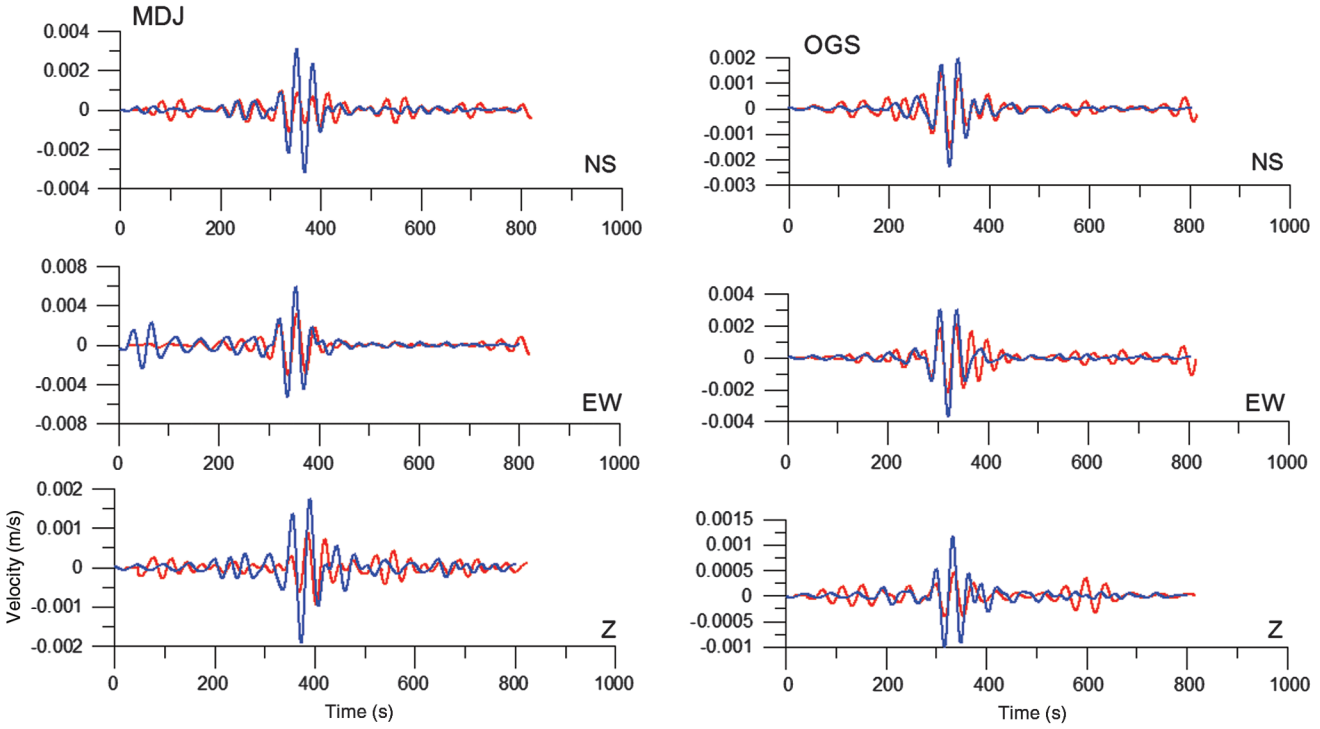

Figure 13. Observed records from stations MDJ and OGS, corrected for SDM effect (blue), and synthetic seismograms (red) for the Kobe 1995 earthquake. Inversion for standard MT after removing second-degree MT effects from the data. Frequency range $f = 0.02$–0.04 Hz.

records available for inversion, the jackknife is not reasonable. To gain insight into the part of the uncertainty of the SDM that is due to possible deterioration of the data by a noise, we performed an experiment of inverting for the SDM of records contaminated by two levels of a synthetic random noise, reaching 20% and 30% of the peak amplitude within the signal. The tolerable level is between these values: noise up to 20% still allows us to get a reasonable estimate of the SDM, while 30% is already too much.

An important indication of the soundness of results obtained with a particular method is their consistency with results yielded by another approach. We compared the SDM obtained for the Kobe and Izmit earthquakes with the slip distribution determined by Ide *et al.* (1996) and Clévédé *et al.* (2004), and found results largely in agreement with these studies. Particularly important is the comparison with results by Clévédé *et al.* (2004), as they determined the SDM from long-period teleseismic surface waves and evaluated them from various existing models of the slip distribution (i.e., they provide the SDM retrieved from data spanning a huge range of frequencies). Moreover, they designed the method of equivalent models (simplified models of slip distribution on the assumed fault) and tested the known slip distributions from the viewpoint of the equivalent model properties that can be checked mutually. Thanks to that, we can align our SDM into the sequence of the models already published.

The genuine aim of the paper was to explore how the effect of the source finiteness, which is neglected in the determination of the standard MT, can bias the retrieved mechanism. The SDM tool is suitable for the purpose. After determining the MT and SDM, we removed the SDM contribution from the data and recomputed the MT by using the data without the SDM effects. Processing regional records of five moderate to strong earthquakes in this way, we demonstrated that the large non-DC component obtained initially in the MT was probably the effect of the source finiteness, which remained in the data even after essential low-pass filtering. The suggested procedure substantially reduces the spurious non-DC component, which indicates that violation of the point-source assumption provides another possible source of spurious non-DC components, in addition to that due to velocity model error. It is, however, necessary to carefully check how confidently the SDM are determined and to correct the MT only if the SDM are retrieved well. Although we browsed the Global CMT catalog in the search for events with a large non-DC component, the subject of the study—the appearance of a spurious non-DC source component as a consequence of the source finiteness and design of the method for its removal—is relevant mostly to regional source inversions. Regional records with periods of tens of seconds are likely to be affected by the finiteness of the foci of moderate to strong events, while the effect is obviously small for periods of hundreds of seconds processed for the retrieval of Global CMT solutions.

Data and Resources

Seismograms used in this study were collected from the Incorporated Research Institutions for Seismology (IRIS) Data Management Center at www.iris.edu (last accessed January 2013). Some plots were made using Generic Mapping Tools (www.soest.hawaii.edu/gmt, last accessed January 2013; Wessel and Smith, 1998). We used the Finite-Source Rupture Model Database (SRCMOD) at http://www.seismo.ethz.ch/static/srcmod/ (last accessed January 2013).

Acknowledgments

The paper significantly profited from the constructive comments of Joe Fletcher and two anonymous reviewers. The Czech Republic Grant Agency supported the project under Grant Number P210/10/0296.

References

Adamová, P., and J. Šílený (2010). Non-double-couple earthquake mechanism as an artifact of the point-source approach applied to a finite-extent focus, *Bull. Seismol. Soc. Am.* **100,** 447–457.

Backus, G. E. (1977a). Interpreting the seismic glut moments of total degree two or less, *Geophys. J. Roy. Astron. Soc.* **51,** 1–25.

Backus, G. E. (1977b). Seismic source with observable glut moments of spatial degree two, *Geophys. J. Roy. Astron. Soc.* **51,** 27–45.

Bernardi, F., J. Braunmiller, U. Kradolfer, and D. Giardini (2004). Automatic regional moment tensor inversion in the European-Mediterranean region, *Geophys. J. Int.* **157,** 703–716.

Bouchon, M., and O. Coutant (1994). Calculation of synthetic seismograms in a laterally varying medium by the boundary element-discrete wavenumber method, *Bull. Seismol. Soc. Am.* **84,** 1869–1881.

Bulut, F., M. Bohnhoff, M. Aktar, and G. Dresen (2007). Characterization of aftershock-fault plane orientations of the 1999 İzmit (Turkey) earthquake using high-resolution aftershock locations, *Geophys. Res. Lett.* **34,** L20306.

Chen, P., T. H. Jordan, and L. Zhao (2010). Resolving fault plane ambiguity for small earthquakes, *Geophys. J. Int.* **181,** 493–501.

Clévédé, E., M.-P. Bouin, B. Bukchin, A. Mostinskiy, and G. Patau (2004). New constraints on the rupture process of the 1999 August 17 Izmit earthquake deduced from estimates of stress glut rate moments, *Geophys. J. Int.* **159,** 931–942.

Covellone, B. M., and B. Sabate (2012). A quantitative comparison between 1D and 3D source inversion methodologies: Application to the Middle East, *Bull. Seismol. Soc. Am.* **102,** no. 5, 2189–2199.

Doornbos, D. J. (1982). Seismic moment tensors and kinematic source parameters, *Geophys. J. Roy. Astron. Soc.* **69,** 235–251.

Ekström, G., A. M. Dziewoński, N. N. Maternovskaya, and M. Nettles (2005). Global seismicity of 2003: Centroid-moment-tensor solutions for 1087 earthquakes, *Phys. Earth Planet In.* **148,** 327–351.

Ferreira, A. M. G., and J. H. Woodhouse (2006). Long-period seismic source inversions using global tomographic models, *Geophys. J. Int.* **166,** 1178–1192.

Gusev, A. A., and V. M. Pavlov (1988). Determination of space-time structure of a deep earthquake source by means of power moments, *Tectonophysics* **152,** 319–334.

Henry, C., J. H. Woodhouse, and S. Das (2002). Stability of earthquake moment tensor inversions: Effect of the double-couple constraint, *Tectonophysics* **356,** 115–124.

Horálek, J., J. Šílený, and T. Fischer (2002). Moment tensors of the January 1997 earthquake swarm in NW Bohemia (Czech Republic): Double-couple vs. non-double-couple events, *Tectonophysics* **356,** 65–85.

Ide, S., M. Takeo, and Y. Yoshida (1996). Source process of the 1995 Kobe earthquake: Determination of spatio-temporal slip distribution by Bayesian modeling, *Bull. Seismol. Soc. Am.* **86,** 547–566.

Jost, M. L., T. Büßelberg, Ö. Jost, and H.-P. Harjes (1998). Source parameters of injection-induced microearthquakes at 9 km depth at the KTB deep drilling site, Germany, *Bull. Seismol. Soc. Am.* **88,** 815–832.

37 Julian, B. R., G. R. Foulger, F. C. Monastero, and S. Bjornstad (2010). Imaging hydraulic fractures in a geothermal reservoir, *Geophys. Res. Lett.* **37,** L07305.

Julian, B. R., A. D. Miller, and G. R. Foulger (1998). Non-double-couple earthquakes 1. Theory, *Rev. Geophys.* **36,** 525–549.

Kawasaki, I., and T. Tanimoto (1981). Radiation patterns of body waves due to the seismic dislocation occurring in an anisotropic source medium, *Bull. Seismol. Soc. Am.* **71,** 37–50.

Kennett, B. L. N., and E. R. Engdahl (1991). Traveltimes for global earthquake location and phase identification, *Geophys. J. Int.* **105,** 429–465.

Kuge, K., and H. Kawakatsu (1993). Significance of non-double couple components of deep and intermediate-depth earthquakes: Implications from moment tensor inversions of long-period seismic waves, *Phys. Earth Planet In.* **75,** 243–266.

Mann, P., and A. Taira (2004). Global tectonic significance of the Solomon Islands and Ontong Java Plateau convergent zone, *Tectonophysics* **389,** 137–190.

McGuire, J. J. (2004). Estimating finite source properties of small earthquake ruptures, *Bull. Seismol. Soc. Am.* **94,** 377–393.

McGuire, J. J., L. Zhao, and T. H. Jordan (2002). Predominance of unilateral rupture for a global catalog of large earthquakes, *Bull. Seismol. Soc. Am.* **92,** 3309–3317.

Miller, A. D., G. R. Foulger, and B. R. Julian (1998). Non-double-couple earthquakes 2. Observations, *Rev. Geophys.* **36,** 551–568.

Ortlepp, W. D. (1984). Rockbursts in South African gold mines: A phenomenological view, in *1st Int. Symp. Rockbursts and Seismicity in Mines*, N. C. Gay and E. H. Wainwright (Editors), Johannesburg, South Africa, 165–178.

Šílený, J. (2009). Resolution of non-double-couple-mechanisms: Simulation of hypocenter mislocation and velocity structure mismodeling, *Bull. Seismol. Soc. Am.* **99,** 2265–2272.

Šílený, J., and A. Milev (2008). Source mechanism of mining induced seismic events—resolution of double couple and non double couple models, *Tectonophysics* **456,** 3–15.

Šílený, J., D. P. Hill, L. Eisner, and F. H. Cornet (2009). Non-double-couple 38 mechanisms of microearthquakes induced by hydraulic fracturing, *J. Geophys. Res.* **114,** B08307.

Sipkin, S. A., and M. D. Zirbes (2004). Moment-tensor solutions estimated using optimal filter theory: Global seismicity, 2002, *Phys. Earth Planet In.* **145,** 203–217.

Sokos, E. N., and J. Zahradník (2008). ISOLA a Fortran code and a Matlab GUI to perform multiple-point source inversion of seismic data, *Comput. Geosci.* **34,** 967–977.

Stump, B. W., and L. R. Johnson (1982). Higher-degree moment tensors–the importance of source finiteness and rupture propagation on seismograms, *Geophys. J. Roy. Astron. Soc.* **69,** 721–743.

Vavryčuk, V. (2001). Inversion for parameters of tensile earthquakes, *J. Geophys. Res.* **106,** 16,339–16,355.

Vavryčuk, V. (2011). Detection of high-frequency tensile vibrations of a fault during shear rupturing: Observations from the 2008 West Bohemia swarm, *Geophys. J. Int.* **186,** 1404–1414.

Vavryčuk, V., M. Bohnhoff, Z. Jechumtálová, P. Kolář, and J. Šílený (2008). Non-double-couple mechanisms of microearthquakes induced during the 2000 injection experiment at the KTB site, Germany: A result of tensile faulting or anisotropy of a rock? *Tectonophysics* **456,** 74–93.

Wessel, P., and W. H. F. Smith (1998). New, improved version of the Generic Mapping Tool released, *Eos Trans. AGU* **79,** 579.

Yoshida, S., K. Koketsu, B. Shibazaki, T. Sagiya, T. Kato, and Y. Yoshida (1996). Joint inversion of near- and far-field waveforms and geodetic data for the rupture process of the 1995 Kobe earthquake, *J. Phys. Earth* **44,** 437–454.

Institute of Geophysics
Academy of Sciences
Department of Seismology
Boční II 1401
Prague 4, 14131
Czech Republic

Manuscript received 17 January 2013

Queries

1. AU: Please note: “Moment tensor” has been changed to “MT” in various locations throughout the article to accommodate journal style for abbreviation use.
2. AU: It is my understanding that the Global CMT is considered a database, not a seismological agency. Please check and provide revisions as needed.
3. AU: (1) Please provide revised wording for the sentence beginning with “The deviatoric constraint...”; the meaning is not clear for the information in parentheses. ALSO(2) Should “zero MT trace” be changed to “zero-degree MT trace”?
4. AU: The reference, Dufumier and Rivera (1997) is cited here but does not appear anywhere in the reference list. Please provide publication details for the reference. Else, delete this citation.
5. AU: I assumed that “It” referred to the CLVD; please review the edits to the sentence beginning with “In the catalogs...” to be sure your intended meaning was not changed.
6. AU: In the sentence beginning " It is important to note...," please confirm that intended meaning is preserved for the period range.
7. AU: In Introduction, you cite Covellone and Savage (2012), but in References only Covellone and Sabate (2012) appears. Which one is correct, or is either? Please determine the appropriate reference and make suitable correction(s) in the Introduction and/or References.
8. AU: In the sentence beginning " We describe seismic...," should "using replacment theorem" be changed to "using a replacement theorem" (meaning one of many replacement theorems)or "using the replacement theorem"?
9. AU: BSSA allows bold in equations only to indicate matrices, vectors, and tensors. Please provide a revised equation with only such terms set in bold.
10. AU: The subscript ij used in the definition that follows equation (1) does not match what is used in the equation itself. Please provide the necessary corrections to the math.
11. AU: Please check all date and time conversions to be sure they have been edited accurately.
12. AU: Should “Solomon earthquake” be changed to “Solomon Islands earthquake” throughout the article?
13. AU: Are you referring to the planet in “earth-flattening approximation”? If so, we will capitalize “Earth.”
14. AU: In the sentence beginning " For individual events...," please confirm that intended meaning is intact.
15. AU: Figures 3, 4, 10: As per the style, (top) and (bottom) should be replaced with part labels (a) and (b). Is it okay to change like this in caption and in figures? Please clarify.
16. AU: Please review the edit to the sentence beginning with “To assess the credibility..” to be certain your intended meaning has not been changed.
17. AU: In the sentence beginning "Second degree moments are the terms...," should ”expansion” be changed to ”equation”?
18. AU: In the sentence beginning " Within these frequency ranges...," please show all 14 parameters or explain how the listed items total up to 14.
19. AU: Please specify whether you wish reader to look at the bottom left or the top right (parts b and c) part of Figure 5 when you refer to the depth view.
20. AU: Please be more specific as to what agencies reported the CMT.
21. AU: Would it be correct to change “in the periods 50–100 s” to either (1) “in the 50–100 s period range” or (2) “in periods of 50–100 s”?
22. AU: Please note that the GPS and SAR have been abbreviated in their first use. Please clarify whether the definitions are correct.
23. AU: Beginning with “Then, by evaluating parameters...,” please review the rest of the paragraph to be sure your intended meaning has not been changed.
24. AU: Here, you cite Bouchon *et al.* (2002), but in References only Bouchon and Coutant (1994) appears. Which one is correct, or is either? Please determine the appropriate reference and make suitable correction(s) in the here and/or References.
25. AU: The reference, Delouis et al. (2000) is cited here twice but does not appear anywhere in the reference list. Please provide publication details for the reference. Else, delete this citation.
26. AU: Please change “right-hand column” and “left-hand column” of Figure 4 and to the appropriate column head names, because there are actually six columns of data in Table 4.
27. AU: Please review the sentence beginning with “Standard MT obtained...” and the sentence that follows to be sure that your intended meaning has not been changed.
28. AU: Please provide additional detail: both values are large enough to allow what?
29. AU: Please review the edit to the sentence beginning with “Contrary to the Global CMT solution...” to be sure your intended meaning has not been changed.

30. AU: Please review the sentence beginning with “We conclude” to be sure your meaning has been retained.
31. AU: In “By modeling synthetic noise at different levels,” the edit assumes you are referring to testing at the 20% and 30% levels; is this correct?
32. AU: Please review the edit of the sentence beginning with “While even rough 1D models” to be sure your meaning has not been changed.
33. AU: Replace “there” with “1D”?
34. AU: In the sentence beginning " Then, only sufficiently...," please confirm that my edit has not changed intended meaning.
35. AU: BSSA requires abbreviations be defined; I used the name from the listed website, though it does not really match the abbreviation “SRCMOD”. Is this what you intended?
36. AU: Please provide the page numbers, total page count, or doi number for Bulut et al.
37. AU: Please provide page numbers, total page count, or doi number for Julian et al.
38. AU: Please provide page range for this article. (B08307 is the issue number.)
39. AU: In the original (pre-edited) text for Figure 1, you wrote: Locations of the earthquakes investigated: Izmit earthquake 17/08/1999, MW 7.6, Solomon earthquake 12/06/2003, MW 6.2, Kobe earthquake 16/01/1995, MW 6.9, MW 6.5, Tohoku aftershock 7/04/2011 MW 7.1, Bolivia earthquake 17/11/2005 MW 6.8. I reconfigured to match BSSA style but did not know what to do with the extra magnitude (MW 6.9, MW 6.5), so I left it out. Please confirm that is ok, or reinsert (with additional description) where necessary.
40. AU: Would it be correct to change the x-axis label to VP?
41. AU: Here, you cite Bulut (2007), but in References only Bulut *et al.* (2007) appears. Which one is correct, or is either? Please determine the appropriate reference and make suitable correction(s) here and/or References.
42. AU: Please review all modifications to part labels in the Figure 5 caption and modify as needed.
43. AU: Please provide a revised Figure 5 that uses a more contrasting blue for the top left part of this figure.
44. AU: Please be as specific as possible what part(s) of the top right part of this figure are to be compared to the figure at top left. For example, should the reader only be looking at part (a) of the top right set of figures? parts (a)–(c)?
45. AU: Please review the changes made to the description of the top right group of images and provide corrections as needed.
46. AU: In the bottom right figure, the green star and green arrow appear to be overlapping to the point of obscuring the star. Please review and revise figure as needed so all essential parts of the figure are clearly visible.
47. AU: I added “axonometric projection" to the list of projections, assuming that such a projection is what is shown in the lower right block of the left grouping. Please indicate if this is not correct.
48. AU: Would it be correct to add “(arrows)” after “velocity vector”? (arrows in the right panels are not explained otherwise.)
49. AU: The reference, Yagi and Kikuchi (2000) is cited here but does not appear anywhere in the reference list. Please provide publication details for the reference. Else, delete this citation.
50. AU: The reference, Sekiguchi and Iwata (2002) is cited here but does not appear anywhere in the reference list. Please provide publication details for the reference. Else, delete this citation.
51. The reference, Cakir *et al.* (2003) is cited here but does not appear anywhere in the reference list. Please provide publication details for the reference. Else, delete this citation.
52. AU: (1) Please review all changes to the footnotes to be sure that information is properly placed with the respective columns, and (2) please provide column heads for the subcolumns labeled "Spatial Centroid" and "Average Velocity Vector." (Perhaps North, East, and Z?)
53. AU: In order to be included, every decimal must be followed by a number. Please provide the missing numbers or indicate that the decimals should be removed. In this table, see (1) Kobe row, column 2(2) Izmit row, column 4 (3) Solomon, column 6(4) Tohoku, column 6(5) Bolivia, column 6
54. AU: (1) Please review the footnotes to be sure they are properly assigned to the correct columns and have the correct content. ALSO (2) In order to be included, every decimal must be followed by a number. Please provide the missing numbers or indicate that the decimals should be removed.
55. AU: In order to be included, every decimal must be followed by a number. Please provide the missing numbers or indicate that the decimals should be removed.
56. AU: Please provide corrections as needed to the edit of the description of the standard evaluation.